Lovejoy, S., D. Schertzer, 1995: Multifractals and Rain. **New Uncertainty Concepts in Hydrology and Hydrological modelling**, Ed. A. W. Kundzewicz, 62-103, Cambridge press.

2 Multifractals and rain

S. LOVEJOY

Physics Department, McGill University, Montreal, Canada

D. SCHERTZER

Laboratoire de Météorologie Dynamique, C.N.R.S., Paris, France

ABSTRACT Scaling models and analyses of rain have now been around for over ten years, a period in which the corresponding scale invariant notions have seen rapid development. We review these developments concentrating on multifractals that are believed to provide the appropriate theoretical framework for scaling nonlinear dynamical systems. Although early scaling notions were geometric rather than dynamic, they contributed towards establishing and testing scaling ideas in rain and in determining the limits of scaling in both time and space. The problematic of passive scalar clouds and (continuous) turbulent cascades, provided them with a sound physical basis. Building on these advances, later analysis methods (particularly Double Trace Moment technique) made it possible to obtain robust estimates of the basic multifractal parameters. Continuous (and universal) cascades allow us to exploit these parameters to make dynamical models. We also discuss various applications of multifractals to rain including multifractal objective analysis, statistics of extreme values, multifractal modelling, space-time transformations, the multifractal radar observer's problem, stratification, and texture of rain.

INTRODUCTION

Stochastic models of rain, atmospheric scaling and multifractals

The atmosphere is probably the most familiar highly nonlinear dynamical system; the nonlinear terms are roughly $\approx 10^{12}$ (the Reynolds number) times larger than the linear (dissipation) terms, and structures vary over 9–10 orders of magnitude in space (≈ 1 mm to 10^4 km) and at least as much in time ($\approx 10^{-3}$ s on up). The nonlinearity involves many fields: rain is dynamically coupled with the velocity, temperature, radiation, humidity, liquid (and solid) water fields. Because it so palpably impinges on the human senses, it is undoubtedly subjectively experienced as the most extremely variable atmospheric field. For similar reasons, in terms of accuracy of measurements over the widest range of space and time scales, the associated radar ('effective') reflectivity field is likely to be the best measured turbulent field in geophysics or elsewhere.

While this extreme variability is undeniable, traditional modelling approaches have been limited by lack of knowledge of the nonlinear partial differential equations governing rain. Since the 1960s, these two circumstances have combined to lead to the development of stochastic[1] rain models[2]. In the 1980s, with the growing recognition of the fundamental importance of 'scaling' (especially associated with the fractal geometry of sets, Mandelbrot, 1983); scale invariant symmetries and fractals, it was natural to construct stochastic models that respected such symmetries (Lovejoy & Mandelbrot, 1985, Lovejoy & Schertzer, 1985). Unfortunately, the first scaling models were totally *ad hoc*, designed only to respect a purely statistical scaling symmetry (i.e., with no direct connection either with physics or phenomenology), and worse still, were restricted to a very simple kind of scaling

[1] Influenced by the rapid pace of developments in deterministic chaos, the idea was recently suggested (e.g. Tsonis & Elsner, 1989, Rodriguez-Iturbe *et al.*, 1989) that only a very small number of degrees of freedom were dynamically important, and that in rain deterministic rather than stochastic models would be appropriate. As argued by Osborne & Provenzale (1989), Ghilardi (1990) and Schertzer & Lovejoy (1991a) (section on stochastic chaos vs. deterministic chaos), such conclusions are based on overinterpretations of the data; in our view, there is no compelling reason for abandoning stochastic (large number of degrees of freedom) models. See also Visvanathan *et al.* (1991) for a discussion of stochastic behaviour of deterministic models.

[2] Early models include Cole (1964), Arajimo (1966) and Bras & Rodriguez-Iturbe (1976).

now known as 'simple' scaling[3]. This was all the more true since evidence had been accumulating since the 1960s suggesting that rather than being qualitatively distinct, the large and small scale regimes of the atmosphere were actually both part of a very wide single scaling regime. Rather than consisting of an isotropic two dimensional turbulent regime at large scales, and an isotropic three dimensional regime at small scales, the atmosphere is apparently scaling but anisotropic throughout[4].

In parallel with the development of these geometric 'monofractal' models, work in turbulent cascade processes and strange attractors showed that real dynamical systems were much more likely to be 'multifractal[5]' (Hentschel & Proccacia, 1983; Grassberger, 1983; Schertzer & Lovejoy, 1983, 1984, 1985b; Parisi & Frisch, 1985). They therefore require an infinite number of scaling exponents for their specification, a fact soon empirically confirmed in rain with radar data[6].

The multiscaling/multifractal problematic provided much more than just an improved empirical fit with the data. The bold proposal (Schertzer & Lovejoy, 1987a) that rain variability could be directly modelled as a turbulent cascade process for the first time provided the physical basis for stochastic rain modelling. This proposal was all the more attractive since such cascade processes were found to generically yield multifractals. In the same way that Gaussian noises frequently occur in linear (sums) of random variables, cascade processes generically produce special (universal) multifractals by nonlinear mixing of scaling noises. The existence of stable and attractive universality classes implies that the infinite number of multifractal dimensions can be described by just three basic exponents. This finding greatly simplifies analysis and simulation of multifractal fields.

Monofractal analyses, scaling and intermittency

In the following sections, we will argue that scaling systems will generally involve universal multifractals. This current understanding was the result of many years of research during which simpler (geometric monofractal) scaling analyses and models were developed and criticized. In order to understand these developments, we briefly review some early results.

The simplest scaling of relevance to rain is the following 'simple scaling[7]' or 'scaling of the increments': before the discovery of multifractals, it was thought to be quite generally associated with fractal fields. For the rainrate R, it can be defined as follows:

$$\Delta R(\lambda^{-1}\Delta x) \stackrel{d.}{=} \lambda^{-H}\Delta R(\Delta x) \quad (1)$$

where the small scale difference is $\Delta R(\lambda^{-1}\Delta x) = R(x_1 + \lambda^{-1}\Delta x) - R(x_1)$ and the large scale difference is $\Delta R(\Delta x) = R(x_2 + \Delta x) - R(x_2)$ where x_1, x_2 are arbitrary, λ is a reduction ratio, and H is the (unique) scaling parameter. The equality '$\stackrel{d.}{=}$' means equality in probability distributions viz. $a \stackrel{d.}{=} b$ if and only if $\Pr(a > q) = \Pr(b > q)$ for all q, where 'Pr' indicates 'probability'. The special case of equation 1 where the probability distributions are Gaussian is Brownian motion ($H = \frac{1}{2}$, increments are independent), and fractional Brownian motion ($H \neq \frac{1}{2}$, Kolmogorov, 1940; Mandelbrot & Van Ness 1968). Fractional Brownian motion was proposed as a streamflow model by Mandelbrot & Wallis (1969); the nontrivial exponent H was to account for the 'Hurst phenomenon' of long range dependence in streamflow (Hurst, 1951 empirically found $H \approx 0.7$ in many streamflow records over scales up to millenia).

In rain, Lovejoy (1981) hypothesized that simple scaling holds – although due to the extreme variability of rain – the probability distributions were expected to have algebraic ('fat') tails instead of ('thin') Gaussian tails[8]. Below, we show that such hyperbolic tails (associated with the divergence of the corresponding statistical moments) can be considered as multifractal phase transitions. Since then, Bak *et al.* (1987) have considered the combination of scaling with hyperbolic tails as the basic features of 'self-organized criticality' (S.O.C.) and Schertzer & Lovejoy (1994) have shown how multifractals generically lead to S.O.C. Probability distributions were used to test empirically both the simple scaling and the 'fatness' of the tails in space using Montreal radar rain data (with $\Delta x = 0.25, 0.5, 1$ km). Equation 1 was reasonably well followed (see Fig. 1), especially for the extreme tails, and

[3] Keddem & Chiu (1987) discuss an even simpler scaling which we called 'very simple' scaling, Lovejoy & Schertzer (1989), but it does not seem to be relevant to rain.

[4] For early discussion and reviews of scaling and its limits in the atmosphere, see Schertzer & Lovejoy (1985a), Lovejoy & Schertzer (1986a); for more recent discussion see many of the papers in the book *Nonlinear Variability in Geophysics; Scaling and Fractals*, (Schertzer & Lovejoy, 1991).

[5] This expression was coined somewhat later by Parisi & Frisch (1985). In a paper devoted in considerable part to defending the 'unicity' of fractal dimensions, Mandelbrot (1984), for the first time admitted the possibility of multiple fractal dimensions.

[6] Rain data provided the first determination of multifractal dimensions in any empirically measured field. Furthermore, the original analysis was done in one, two, three, four (x, y, z, t) and 1.5 dimensions (a simulated measuring network, see Fig. 5), showing the utility of radar rain reflectivities (Schertzer & Lovejoy, 1985b). Later, when similar analysis techniques were applied to other turbulent fields (the turbulent velocity field, Meneveau & Sreenivasan, 1987, Schmitt *et al.*, 1991), the data were only one dimensional (time series at a single point).

[7] This type of scaling was first introduced by Lamperti (1962) under the name 'semistable'. It was called 'self-similarity' by Mandelbrot & Van Ness (1968). However, this name turned out to be a misnomer since the actual functions were not self-similar but self-affine, and self similarity is a much wider concept anyway. We use the expression 'simple scaling', which contrasts it with the more general and interesting multiple scaling discussed later. For more on rain applications, see Waymire (1985).

[8] This terminology was introduced by Waymire (1985). Schertzer & Lovejoy (1985a) use the expression 'hyperbolic intermittency' for the 'fat' algebraic tails.

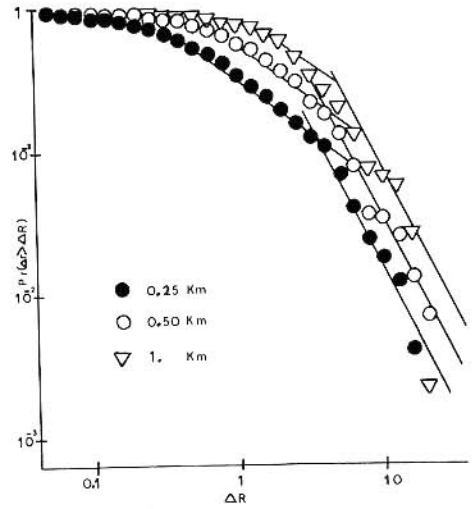

Fig. 1 The first direct empirical test of simple scaling. The probability ($\Pr(\Delta r > \Delta R)$ of a random (absolute) rain rate difference Δr, exceeding a fixed ΔR for spatial increments in $0.25 \times 0.25 \times 1$ km averaged rain rates. The curves shown are for $\Delta x = 0.25, 0.5, 1$ km respectively. Data are from the tropical Atlantic (GATE experiment, phase III) radar reflectivities from a single radar scan converted to rainrates using standard reflectivity/rain rate relations. The straight reference lines correspond to $q_D = 0.75, 2$ respectively, and indicates that the variance (the moment $q = 2$) barely converges. The roughly linear left–right shift between the curves indicates – at least for the extreme gradients – that simple scaling roughly holds with $H \approx 0.5$. From Lovejoy (1981).

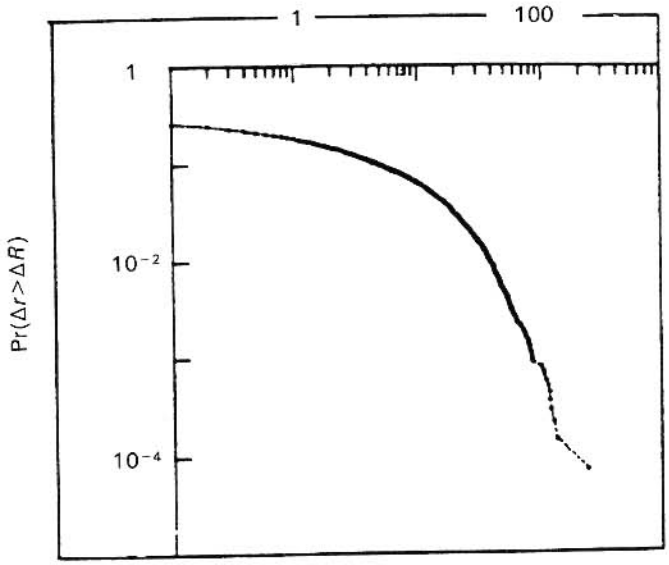

Fig. 2a The probability ($\Pr(\Delta r > \Delta R)$ of a random (absolute) rain rate difference Δr, exceeding a fixed ΔR for daily differences in daily rain accumulations at Nimes-Courbessac (France) from 1949–88 (14245 days). The tail is nearly straight with exponent $q_D \approx 3.5$. From Ladoy *et al.* (1991).

the value[9] of H was estimated as ≈ 0.5. In time, instead of using Eulerian differences, isolated storms were tracked, their total rain flux was determined every five minutes for 100 minutes. Here, simple scaling was again found to hold reasonably well (Montreal, Spain and tropical Atlantic data yielded similar results with value $H \approx 0.7$); in addition, the extreme tail of the distribution was roughly hyperbolic: $\Pr(\Delta r > \Delta R) \approx \Delta R^{-q_D}$ $(\Delta R >> 1)$ for the probability of a random rainfall fluctuation Δr exceeding a fixed value ΔR. The subscript D is necessary since the value of the exponent is expected to depend on the dimension of space over which averages are performed[10]. It was found[11] that $q_D \approx 1.7$, (with $D = 2$; the integration is over areas). For comparison, Fig. 2a (from Ladoy *et al.*, 1991) shows the probability distributions for daily rainfall accumulations from a station at Nimes from 1949–88, with $q_D \approx 3.5$ (see Ladoy *et al.* (1993) for an interpretation in terms of multifractal phase transitions). Similarly, Fig. 2b shows $q_D \approx 1.1$ and Fig. 2c shows $q_D \approx 3.0$ for radar rain reflectivities of rain, 2.4 for snow, and 3.9 for melting snow ('bright band')[12]. A related result is Fig. 2d, the probability distribution of raindrops with volumes in various Hawaiian rains (replotted from Blanchard, 1953). The tails are nearly hyperbolic with[13] $q_D \approx 1.9 \pm 0.5$. The long tails on these distributions point to the extremely variable, highly intermittent non-Gaussian nature of rain.

Perhaps the most systematic and voluminous study of high resolution (tipping bucket) raingage data to date is described in Segal (1979). He digitized 90000 tipping bucket records from 47 recording stations across Canada, each 5–15 years in length, seeking to obtain statistics on rare, high rain rate events that effect microwave transmission. After comparing regressions of a variety of functional forms (including the log-normal, see Fig. 2e and discussion in the next section) for one minute averaged rain rates greater than ≈ 3 mm/h he concluded that 'a power law relationship ... provided the best fit except in the low-intensity (drizzle) region', with (for seven of the stations for which the parameters were given), $q_D \approx 2.5 \pm 0.5$. Table 1 compares all the values cited above. It is still not clear whether the dispersion in values of q_D is due to the difficulty in obtaining accurate estimates (very large samples are needed), differences in the effective D of averag-

[9] In the same paper, a similar value of H was obtained via another method (R/S analysis) over the range 0.25–13 km.

[10] Note that in the original paper, the symbol α rather than q_D was used since α is the corresponding divergence exponent for Levy variables (the rain process was thought to be an additive, simple scaling Levy process).

[11] In Fig. 1, $q_D \approx 2$, although the evidence for this asymptotic behaviour is not conclusive. To our knowledge, other strictly comparable analyses do not exist. A related result was obtained by Zawadzki (1987) who found some some evidence for hyperbolic behaviour (with $q_D \approx 2$) in tipping bucket rain rain measurements rain with roughly the same exponent, although (as expected) the sample sized required to empirically see it was quite large. Table 1 summarizes related results.

[12] Further, we show that these fat tails cannot arise due to fluctuations in the reflectivities due to drop 'rearrangement'; the latter is a thin tailed (exponential) effect.

[13] This is significant for radar measurements of rain, since (among other things) standard theory requires $q_D > 2$ so that the variance converges.

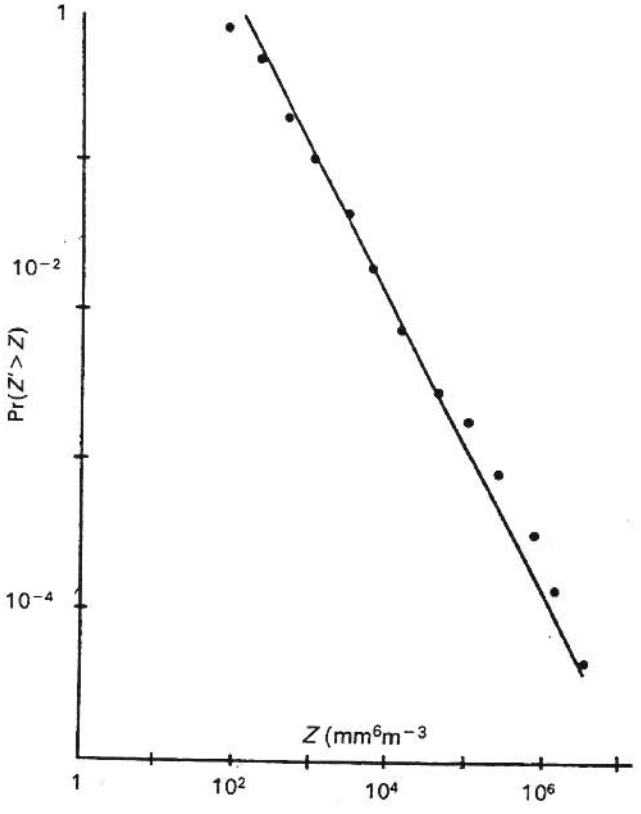

Fig. 2b The probability $Pr(Z' > Z)$ of a random radar rain reflectivity Z' exceeding a fixed threshold Z for 10 CAZLORs (Constant Altitude Z LOg Range maps), taken at the McGill weather radar, Montreal (data from 1984). The resolution varies over the map from ≈ 0.25 to 2.5 km at ranges 20 to 200 km. Each value is determined from the maximum of several consecutive pulses (the 'peak detection' method – necessary at the time (1984) due to limitations on the speed of digitizers). The reference line corresponds to $q_D = 1.06$. From Schertzer & Lovejoy (1987a).

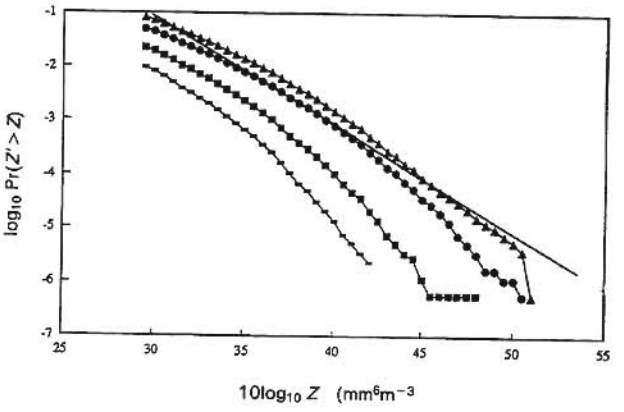

Fig. 2c The same as Fig. 2b except for a vertically pointing (nonscanning) radar at a pulse repetition rate of 1300 Hz, with each pulse return digitized, for a single Montreal storm (October 15, 1991) for 1380 seconds (1.8×10^6 points per histogram). The curves from top to bottom are bright band (melting snow and ice, 2.3 km altitude), rain (2.0, 2.15 km) and snow (2.45 km). The differences in reflectivities are largely explained by the low dielectric constant of ice compared to water, and by the large size of the water coated ice/snow particles. The asymptotic slopes yield estimates of $q_D \approx 2.4$ for snow, ≈ 3.9 for the bright band, and ≈ 3.0 for rain. The reference line corresponds to $q_D = 2$. From Duncan *et al.* (1992), Duncan, (1993).

ing, or due to true variations for different locations, climatological regimes[14] etc.

Other evidence for scaling was the area-perimeter[15] relation for radar rain and satellite cloud areas over the range 1 km^2 to $\approx 1.2 \times 10^6$ km^2, and the distribution of radar determined rain areas that was argued to be hyperbolic not log-normal[16]: $\Pr(A > a) \approx a^{-B}$ (with $B \approx 0.8$ over the range ≈ 1 to 10 km), for the probability of large areas A exceeding a fixed threshold a. A related result is the finding by Cahalan (1991) that over the range ≈ 80 m to ≈ 1 km, $B \approx 0.75$ for stratocumulus and intertropical convergence zone clouds.

The evidence suggesting that radar rain data could be approximated by simple scaling – although with highly non-Gaussian (hyperbolic) probability distributions[17] – was reviewed by Lovejoy & Mandelbrot (1985), where the 'Fractal Sums of Pulses' (FSP) process (an additive compound Poisson process involving pulses) was developed as a model. Although it had features common with other existing stochastic rain models such as those proposed by Waymire &

[14] These issues are discussed in the section on basic properties of multifractal fields; according to multifractal theory, a finite q_D is not necessary, indeed, there is evidence based on estimates of universality parameters that it may be very large (or even infinite) in time. It may well be that the dispersion of estimates for q_D are simply the result of undersampling a distribution with a much larger q_D; if we have an insufficient number of independent samples we really estimate the 'sampling moment' q_s; see equation 15a.

[15] See also Lovejoy (1982, 1983), Lovejoy *et al.* (1983), Lovejoy & Schertzer (1985b), Rhys & Waldvogel (1986), Come (1988) for more rain analyses of this type. For more recent empirical area-perimeter results, (for clouds) see Welch *et al.* (1988), Seze & Smith (1990), Cahalan (1991) and Yano & Takeuchi (1991). Other highly geometric (and, compared to statistical methods, indirect) type analyses are possible including analyses of fractal sets associated with graphs of rain series (Boucquillon & Moussa, 1991). Originally, area-perimeter exponents were interpreted as fractal dimensions of the perimeters. Since rain and clouds are in fact multifractals, a correction is necessary: for this as well as a detailed criticism of these geometric approaches to multifractals, see Lovejoy & Schertzer (1990a, Appendix A).

[16] The log-normal phenomenology of rain and cloud areas goes back to at least Lopez (1976, 1977a, b). Since lognormal distributions are long tailed – and except for the problem of 'dressing', correspond to universal multifractals – they are close to the theoretically expected distributions. In any event, they can only be distinguished empirically from hyperbolic distributions by carefully examining their tails corresponding to extremely rare large areas. The lognormal fits to rain area histograms could be profitably re-examined in this light.

[17] Such models exhibit what Mandelbrot & Wallis (1968) called the 'Noah' effect i.e. stochastic realizations of the corresponding processes involve extreme fluctuations the largest of which dominate the others. In multifractals, the effect is generalized to moments of fluctuations higher than the first. These authors also introduced the term 'Joseph' effect to denote the phenomenon of long range correlations; all multifractals exhibit this effect.

Table 1. *A comparison of various empirical estimates of the divergence of moments exponent* q_D

Data Type	Radar rain differences (space)	Radar rain differences (time)	Radar reflectivity	Vertical pointing radar reflectivity	Daily rain gauge accumulations	Tipping bucket gauges	Rain drop volumes	
Location	Tropical Atlantic	Tropical Atlantic	Montreal	Montreal	Nimes	Montreal	Western Canada	Hawaii
q_D	2	1.7	1.1	3.0 (rain) 2.4 (snow) 3.9 (bright band)	3.5	2	2.5 ± 0.5	1.9 ± 0.5
References	Lovejoy, 1981	Lovejoy, 1981; Lovejoy & Mandelbrot, 1985	Schertzer & Lovejoy, 1987a	Duncan *et al.*, 1992; Duncan, 1993	Ladoy *et al.*, 1991, 1993	Zawadzki, 1987	Segal, 1979	Blanchard 1953

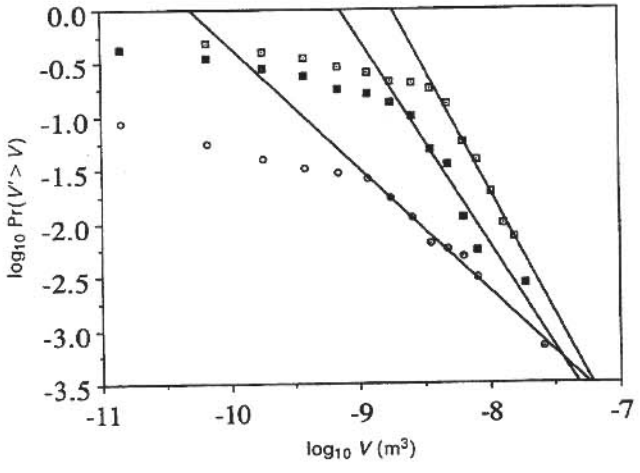

Fig. 2d Three rain drop distributions replotted from original data published in Blanchard (1953) from three different Hawaiian orographic rain events showing that the extreme tails have from top to bottom $q_D \approx 2.3$, 1.9, 1.1 in rains with rain rates 127 mm/h, 21 mm/h, 9 mm/h respectively.

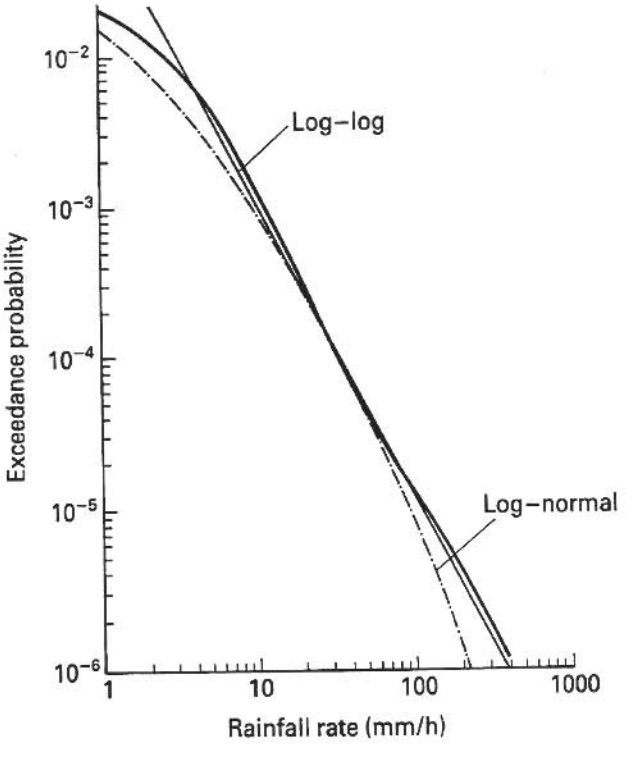

Fig. 2e An example (from 10 years of tipping bucket raingauge data at St. John, New Brunswick) of the extreme rainrate end of one minute resolution rainrate probability distributions from Segal (1979). The straight reference line corresponds to $q_D = 1.9$, the curved reference line is the best fit lognormal for comparison.

Gupta (1984) and Rodriguez-Iturbe *et al.* (1984), both its philosophy and properties are different. Instead of basing itself on an *ad hoc* division of the atmosphere into a hierarchy of qualitatively different regimes, each occuring at different scales, and each requiring a different set of modelling parameters[18], the FSP involved the linear superposition of structures whose relative size and frequency of occurence were related so that the resulting process lacked characteris-

[18] The better known of these scale dependent models the 'Waymire–Gupta–Rodriguez-Iturbe' (WGR) model involved over 10 empirically adjustable parameters; and even then only provided plausible statistical properties over a relatively narrow range of scales (see Rodriguez-Iturbe *et al.*, 1987, Eagleson *et al.*, 1987). Another 'nearly' scaling model (Bell, 1987) had similar problems.

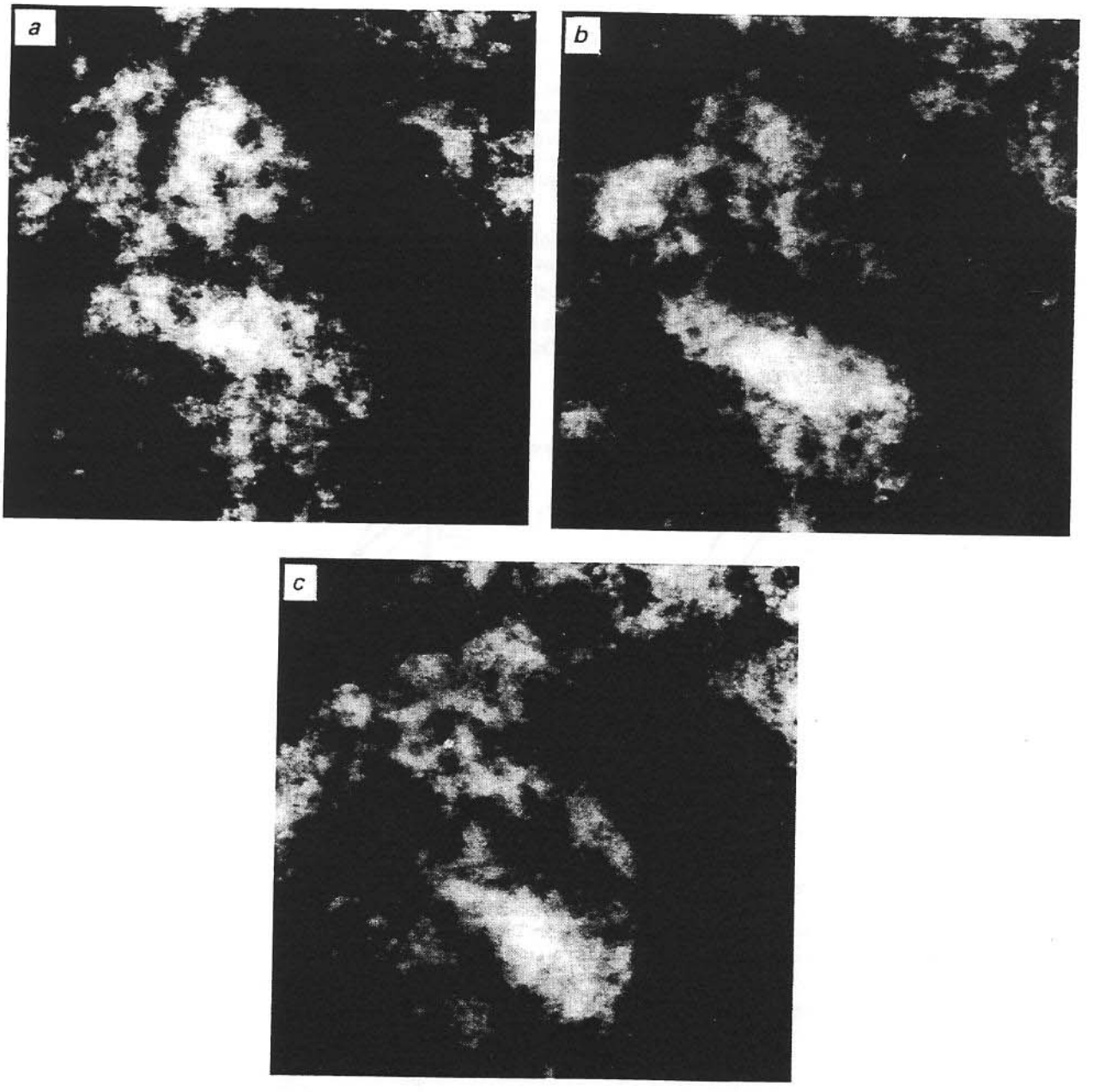

Fig. 3a–3c A single space-time FSP simulation of rain on an 800 × 800 grid showing three simulated fields seperated by 80 time units. The space/time transformation used was a statistical (and isotropic) version of Taylor's hypothesis of frozen turbulence. As expected, small structures live the shortest time, large ones longer, here (on average) linearly increasing with duration. The grey scale is proportional to the logarithm of the rain. From Lovejoy & Mandelbrot (1985).

tic scale[19]. It yielded simple scaling[20] with $q_D = H^{-1}$ (with $1 < q_D < 2, \frac{1}{2} < H < 1$). Two dimensional models on large grids were produced, and time series were modelled by making simulations in three dimensional (x, y, t) space[21]. By varying the shape of the 'pulses' from circles to annuli, more or less 'fragmented' or 'lacunar' rain fields could be produced. Using the same scaling parameters to model the concentration of liquid water, surprizingly realistic cloud fields were produced (see e.g. Figs. 3a, b, c for a temporal sequence).

[19] Similar models were discussed in Rosso & Burlando (1990).

[20] Lovejoy & Schertzer (1985a) proposed a variant on this model called the Scaling Sums of Pulses process (SCP) in which q_D, H could be varied separately. Another related model is (Wilson *et al.*, 1986), the Wave Intermittent Packet (WIP) model; in current parlance, the packets are essentially 'wavelets'.

[21] This relies on a generalization of Taylor's hypothesis of 'frozen turbulence'.

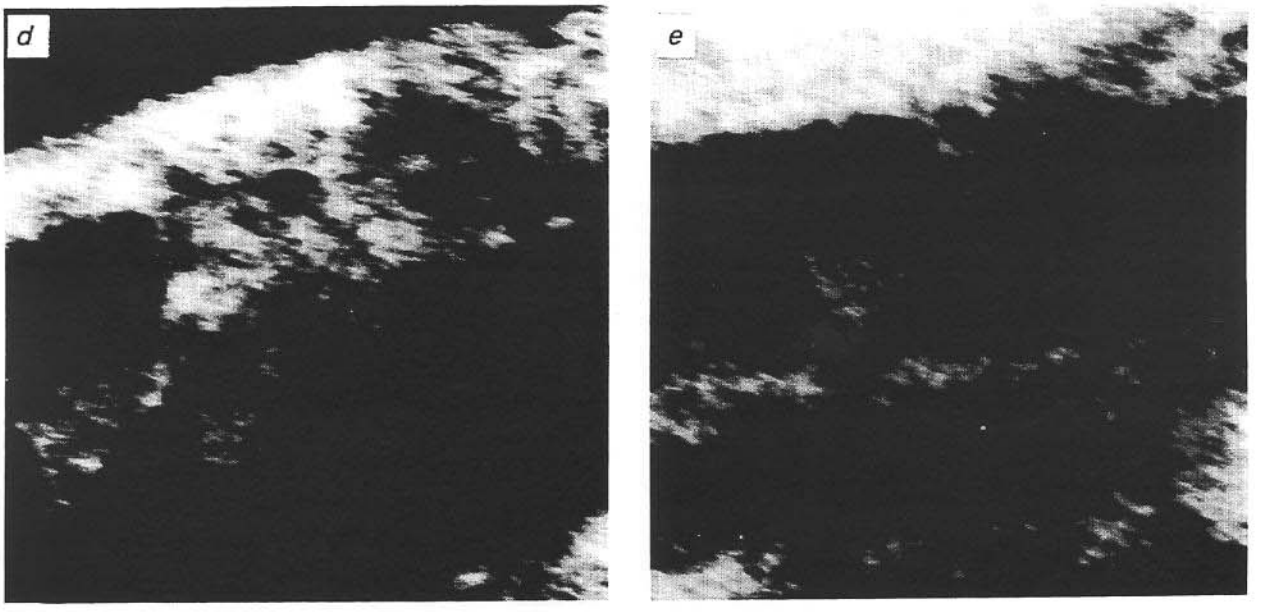

Fig. 3d, e Non self-similar (anisotropic scaling) FSP rain models on a 400 × 400 point grid, using linear Generalized Scale Invariance with generators with off-diagonal elements to yield differential rotation. This results in differences in orientation of structures as functions of scale which is clearly perceived as cloud 'texture'. From Lovejoy & Schertzer (1985a).

Realistic textures/cloud types also can be obtained by using 'Generalized Scale Invariance' – see Figs. 3d, e, as can vertical cross-sections with appropriate 'elliptical dimensions' (Figs. 3 f, g, h, i).

Another analysis method that can be used to investigate scaling is the energy spectrum $E(k)$. For statistically isotropic scaling fields[22] $E(k)$ will be of the power law form $k^{-\beta}$ where k is a wave vector modulus, and β is the spectral exponent. In time, the spectrum as a function of frequency ω will be of the same form but not necessarily with the same exponent. The most impressive single analysis of this sort to date is found in Duncan *et al.* (1992). These authors used a high resolution vertically pointing radar to perform a time series of 7×10^6 pulses at 1.3 kHz from a single pulse volume $30 \times 37 \times 37$m in size. For computational reasons, the total range $\approx 10^{-3}$–10^4 s was split up into two regions, with average spectra calculated in each (Fig. 4a, 4b). One notices two scaling regimes with $\beta \approx 1.66$ (roughly the same in each) corresponding to time periods $2 \times 10^{-3}\,\text{s} < t < 10^{-2}$, and $t > 3$ s. Duncan *et al.* (1992) and Duncan (1993) argue (with the help of multifractal models) that the breaks at 10^{-2} s, 3 s separating the flat 'spectral plateau' are both due to instrumental effects; they are simply the time scales associated with the spatial scales of the radar wavelength (3 cm), and the pulse volume[23] size (≈ 30 m). The rain itself is apparently scaling over almost the entire regime: only the high frequency ($t < 2 \times 10^{-3}$) regime is believed to be a real break associated with dissipation[24].

Other relevant temporal spectra are found in Ladoy et al. (1991) who examined daily raingauge accumulations, finding $\beta \approx 0.3$ (Fig. 4c) for periods of 1 day to 4 years at a station in Nimes (France). Fraedrich & Larnder (1993) find (Fig. 4d) the corresponding spectrum for a 45 year period for an average of 13 stations in Germany, showing roughly similar behaviour although for frequencies lower than $\approx (3\text{ years})^{-1}$ the spectrum rises more quickly[25]. The only relevant spatial spectra of which we are aware are shown in Figs. 4e and 4f from Tessier *et al.* (1993) using radar reflectivities, show $\beta \approx 0.3$ over the range 2–256 km in the tropical Atlantic but $\beta \approx 1.45$ in Montreal (over the range 150 m to 19.2 km; indicating the possibility of significant climatological differences[26]). Other relevant power law spectral analyses

[22] Self-similar fields – see section on generalized scale invariance.

[23] The corresponding velocities are $3\,\text{cm}/10^{-2}\,\text{s} = 3$ m/s, and $30\,\text{m}/3\,\text{s} \sim 10$ m/s respectively which are quite plausible fall speeds for rain. Further below we see that the velocity is expected to be a function of scale, so that the small difference in the two velocity values is not surprising.

[24] As expected, the exact breakpoint depends on the meteorological situation and precipitation type, although contrary to the standard theory of radar measurements, for all the cases studied, it is apparently smaller than the radar wavelength (3 cm here).

[25] Fig. 4d actually seems to have low and high frequency scaling regimes separated by a 'spectral plateau' of the sort found in temperature series by Lovejoy & Schertzer (1986b), Ladoy *et al.* (1986) and Ladoy *et al.* (1991). In this case, the difference with Fig. 4c could be due to differences in climatological regimes, and breaks delimiting the plateau might be time scales corresponding to structures of global spatial extent (see Lovejoy & Schertzer, 1986b for more discussion on this possibility).

[26] Another source of variation is the possibility of significant scatter of the estimated β from one scan to the next – this is expected since the asymptotic logarithmic probability distribution slopes (q_D or q_S) are frequently ~ 2, and the spectrum is a second order statistic.

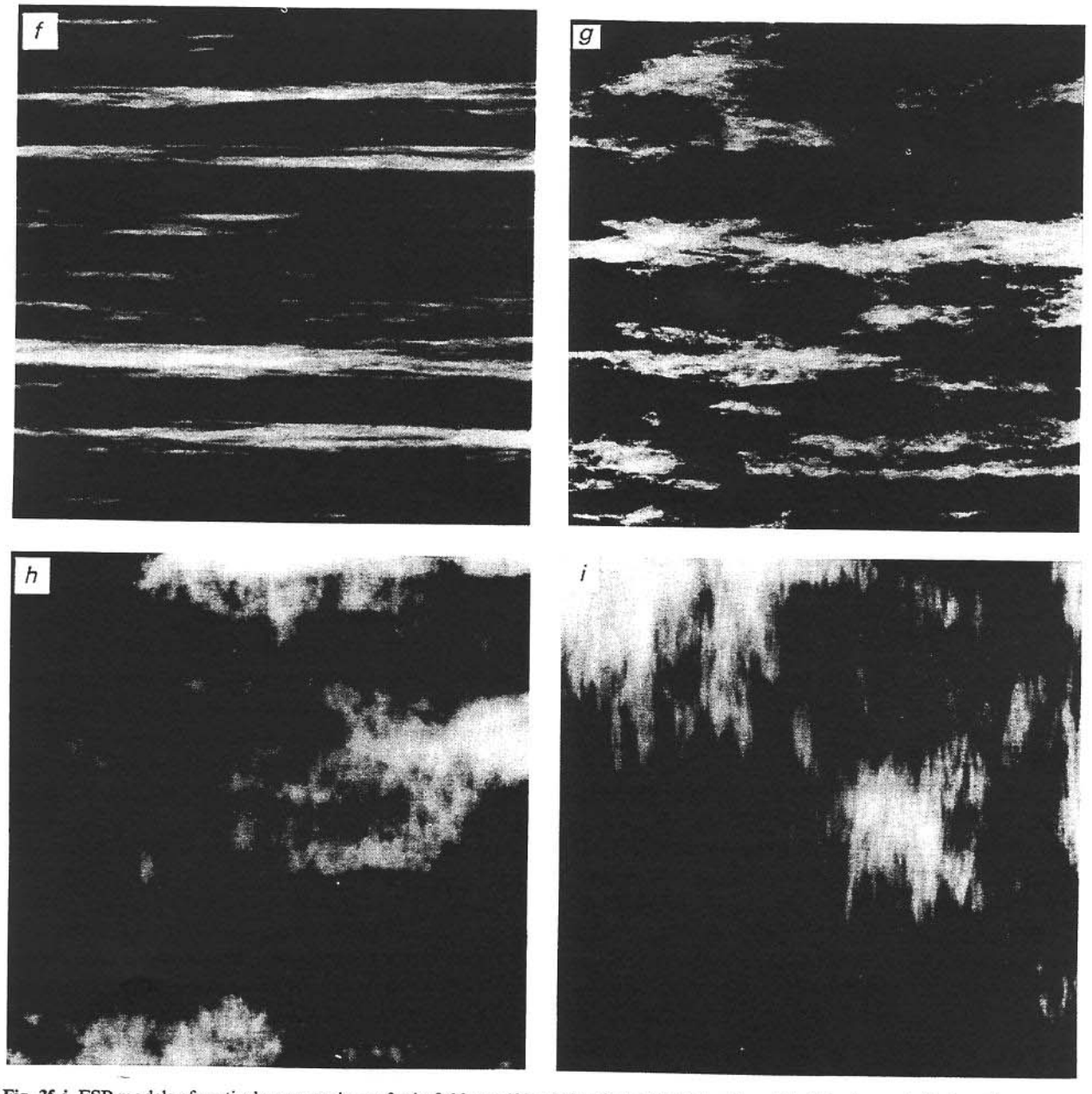

Fig. 3f–i FSP models of vertical cross sections of rain fields on 400 × 400 point grids. Going from f to i the isotropic ('sphero') scale increases from one pixel to 10, 100, 1000 (equivalent to 'zooming' in at random positions). In Fig. 3f, stratification dominates completely, as we zoom in, more and more vertical structure is visible, finally, at highest resolution (Fig. 3i), structures are vertically aligned, simulating convective rain 'shafts'. The elliptical dimension used for these cross-sections was 1.5. From Lovejoy & Schertzer (1985a).

are, Crane, 1990 (log radar reflectivity in space[27]), and Rodriguez-Iturbe *et al.*, 1989 (15 second averaged rain gage rain rates[28]).

[27] He obtains $\beta \sim 5/3$ over the range 1 minute to 1 hour. The scaling of the log reflectivities is not related in a simple way to the scaling of the reflectivities.

[28] From their Fig. 4, we estimate $\beta \sim 1.3$ over periods of ~ 1 minute to 2 hours. It is worth noting that gauge rain rates are frequently estimated from tipping buckets which mark equal accumulation times; this leads to a nontrivial bias in rainrate statistics, especially for the (very frequent) lower rain rates.

With the development of multifractals, it was realized that the apparent visual success of the FSP process masked a basic shortcoming: Lovejoy & Schertzer (1985a) criticized its monodimensional character, calling for the development of 'multidimensional'[29] alternatives. Nearly simultaneously, the first empirical multifractal analyses were performed using radar rain data (Schertzer & Lovejoy, 1985b, Fig. 5). An

[29] This cumbersome expression was a forerunner of the term 'multifractal'.

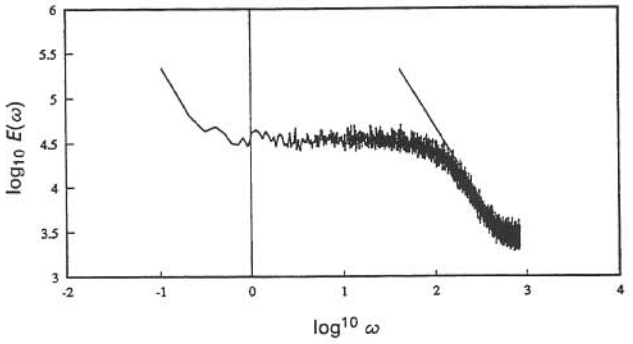

Fig. 4a Average power spectra $E(\omega)$ from 896 consecutive 8192 point sections of a time series from a vertically pointing, 3 cm wavelength radar at McGill taken from a single ($30 \times 37 \times 37$ m) pulse volume at 1 km altitude on Sept. 19, 1990 as a function of frequency w (in units of rad/s, from Duncan *et al.* (1992). The data was sampled at 1.3 kHz, so the entire $\approx 7 \times 10^6$ point data set spanned the range $\approx 10^{-3}$ to 10^4 s. The straight reference line shows an exponent $\beta = 1.66$.

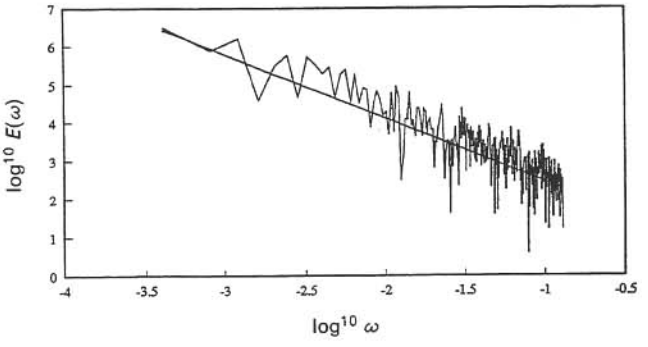

Fig. 4b Same as Fig. 4a except that the series was averaged over 512 consecutive points before the spectrum was taken. Here we obtain scaling over the entire range shown here (with the $\beta = 1.66$ line, same as in Fig. 4a, the beginning of this regime is ≈ 3 s, and is seen on Fig. 4a) shown for reference.

entire codimension function was necessary to specify the scaling of the reflectivities, not just the small number of exponents[30] (q_D, H) involved in simple scaling. The *ad hoc*, geometric FSP construction had to be replaced by a physically based multiscaling/multifractal model. There were two main obstacles to doing this. The first was the establishment of a sound connection between passive scalar concentrations and multifractal energy fluxes (via fractional integration, see below), and the second, was that then, multifractal cascades were discrete, i.e. they involved horrible artificial straight line structures; continuous cascades were needed. While the situation was apparently better as far as data analysis was concerned, it was soon to become evident that it too,

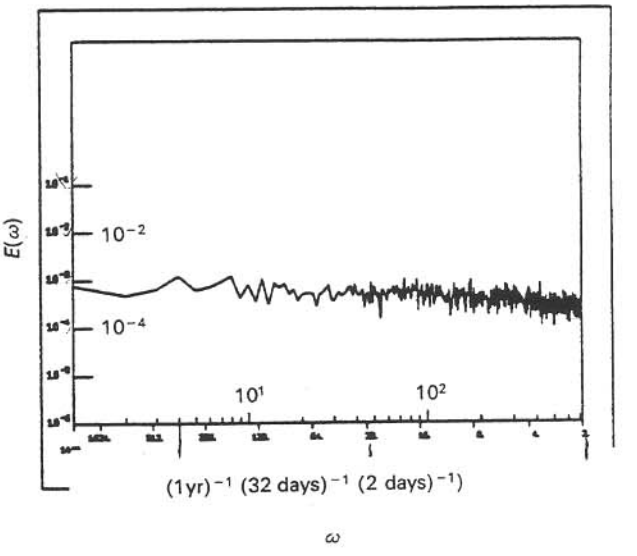

Fig. 4c The average of six consecutive 4 year spectra of the daily rainfall accumulations at Nimes-Courbessac. The annual peak is fairly weak, the scaling holds over most of the regime with slope $(= -\beta) \approx -0.3$. There is no clear evidence for the 'synoptic maximum' (i.e. a break at periods of a few weeks). From Ladoy *et al.* (1991).

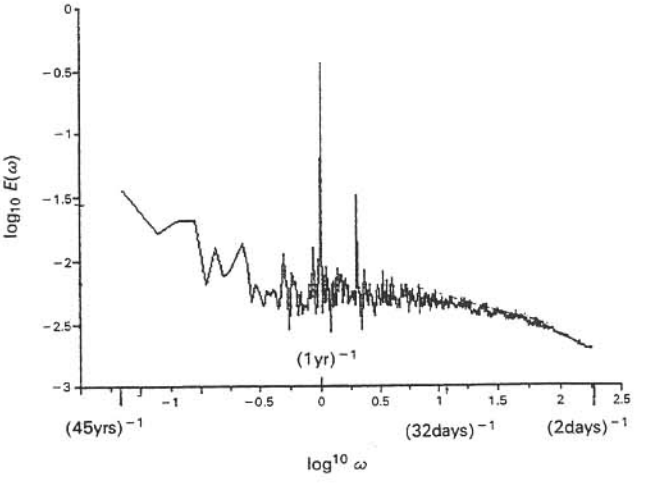

Fig. 4d Energy spectrum of daily rainfall accumulations over a 45 year period in Germany. The spectrum is an average of that obtained from 13 stations. The annual peak is much more pronounced than Fig. 4c, with evidence for a 'spectral plateau' from ≈ 20 days to ≈ 3 years. The overall spectral shape, including the low frequency rise ($\beta \approx 0.5$) is very similar to the temperature spectra analyzed in Lovejoy & Schertzer (1986b). The high frequency fall-off (also with $\beta \approx 0.5$) may be due to smoothing introduced by the spatial averaging (the 13 stations had correlated temperatures). At high frequencies, the power was averaged over logarithmically spaced frequency bins to decrease statistical scatter (Fraedrich & Larnder, 1993).

[30] In the multifractal models, we shall see that q_D, H are independent.

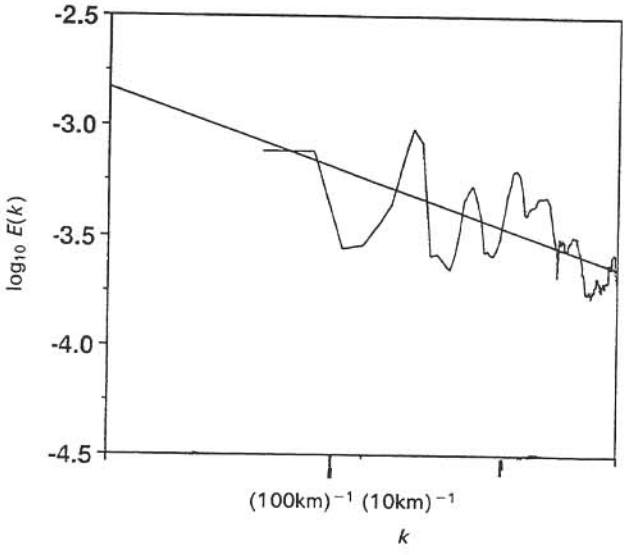

Fig. 4e Horizontal spectrum of tropical Atlantic (GATE experiment) radar reflectivities for 14 radar scans at 15 minute intervals, each scan with 360 radials (1°), 1 km downrange resolution. The (one dimensional) spectra were taken downrange (over 256 pulse volumes) and averaged over all the radials and scans. The reference line has $\beta = 0.3$. From Tessier *et al.* (1993).

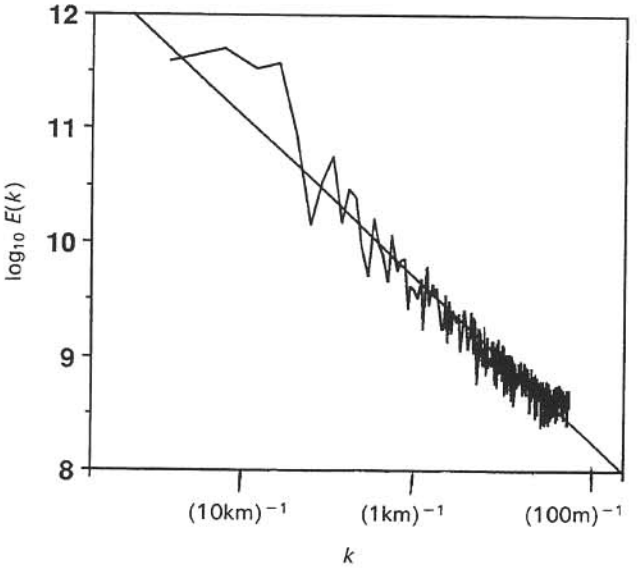

Fig. 4f Horizontal spectrum of McGill radar reflectivities for a 2.2° elevation radar scan with reflectivities averaged over 75 × 75 m grids (PPI). The isotropic two dimensional spectrum was taken over 256 × 256 grid points. The reference line has $\beta = 1.45$, (quite different from GATE). From Tessier *et al.* (1993).

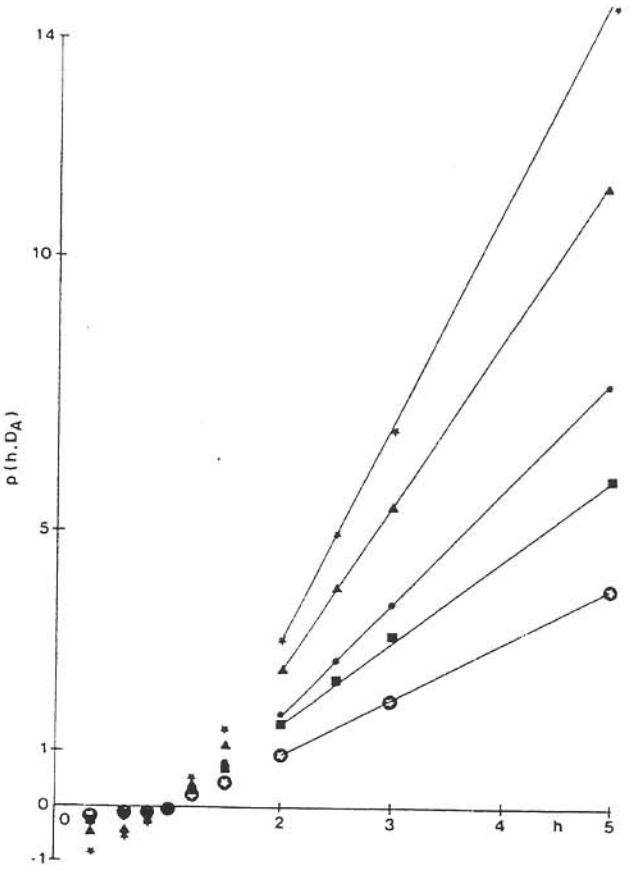

Fig. 5 The function $p(h, D_A)$ $(= K(q), h = q)$ for dressed radar reflectivities from 5 sets of radar CAZLORs at altitudes of 3, 4, 5 km, each set involving 14 scans taken at thirty minute intervals. There were 200 downrange elements, 375 azimuthal elements; the total data set involved $5 \times 3 \times 14 \times 200 \times 375 \approx 1.5 \times 107$ points. The data was dressed (averaged) over sets with various dimensions D_A: over the downrange only (bottom curve), downrange and cross range (third from bottom), downrange, cross-range and in altitude (second from top), space/time (top), as well as over a simulated measuring network, dimension 1.5 (second from the bottom). This curvature clearly shows the multiscaling, multifractal nature of rain. From Schertzer & Lovejoy (1985b).

involved nontrivial difficulties.... The remainder of this paper will concentrate on these developments.

PROPERTIES AND CLASSIFICATION OF MULTIFRACTALS

An explicit multifractal process, the α model

Multifractals arise when cascade processes concentrate energy, water, or other fluxes into smaller and smaller regions. To understand cascades intuitively and to see their relevance to rain, consider the daily rainfall accumulations

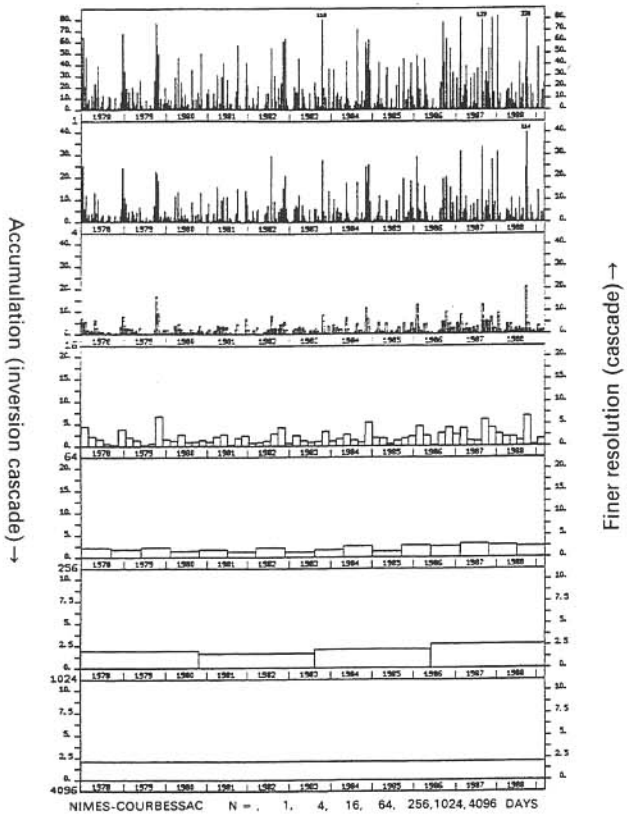

Fig. 6 The 'inverse cascade' produced by averaging daily rainfall from Nimes over longer and longer periods. Accumulation/averaging periods from top to bottom: 1, 4, 16, 64, 256, 1024, 4096 days, 11 years. From Ladoy *et al.* (1993).

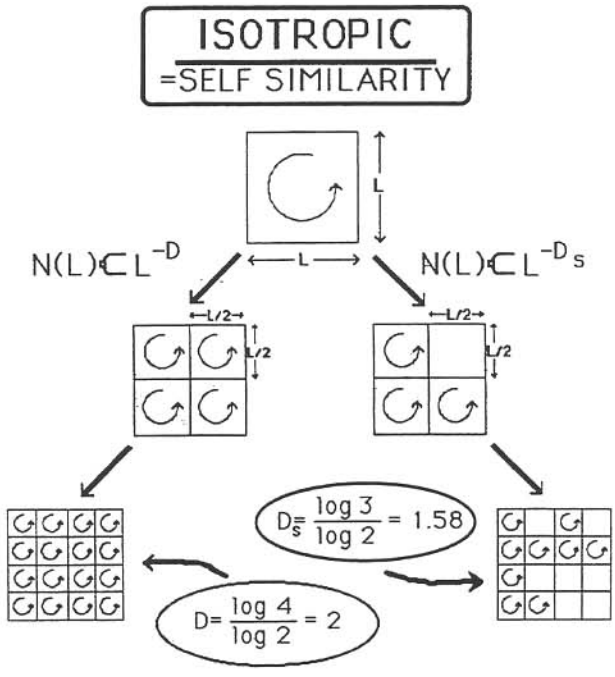

Fig. 7 A schematic diagram showing a two dimensional cascade process at different levels of its construction to smaller scales. Each eddy is broken up into four subeddies, transferring a part or all its energy flux to the sub-eddies. The left hand side shows a homogeneous cascade as originally proposed by Kolmogorov (1941); the nonlinearities simply redistribute energy flux density to smaller scales of motion, the overall density stays uniform. On the right hand side, the β model involving occasional dead eddies (here one in four) is shown, simulating intermittency; it already leads to a monofractal support. From Lovejoy & Schertzer (1986a).

for Nice shown in Fig. 6. Over the 11 year period (1978–88), we can see that several extreme events stand out; in particular, notice the record holder in October 1988 that had a 24 hour accumulation of 228 mm (compared to a mean of ≈ 1.5 mm)[31]. This extreme rainfall event is sufficiently violent that it stands out as the temporal resolution is degraded by averaging the series over four days (second row), 16 days (third row), 64 days (fourth row); even at 256 days (fifth row) its effect is still noticeable (see even ≈ 35 months (sixth row) or the entire 11 year period (bottom row)). We can see that the same type of behaviour is true (although to a lesser degree) of the less extreme 'spikes'. If the analysis sequence high resolution $\Rightarrow$ low resolution is inverted, we have a cascade that can be thought of as a dynamical production process by which rain water is concentrated from a low resolution 'climatological' average value into wet/dry years, wet/dry seasons, months, weeks, days etc. Since the lifetime of atmospheric structures including storms depends on their spatial scale[32], the actual cascade is a space/time process with analogous mechanisms concentrating water fluxes into smaller and smaller regions of space, yielding the observed high spatial variability.

As an example of the inverse low $\Rightarrow$ high resolution process that corresponds to the actual dynamics, consider a cascade produced by dividing the 11 year period with initial rainrate $R_1 = 1$ into sub-periods each of scale λ^{-1} where λ ($= 2$ here) is the scale ratio (see the schematic diagram Fig. 7, and simulation Fig. 8). The fraction of the rain flux concentrated from a long period (large interval) into one of its subintervals is given by independent random factors[33] (μR) given by the Bernoulli law shown in equation 2.

[31] This extreme behavior is quite typical; using tipping bucket gages, Hubert & Carbonnel (1989) have even determined in the Sahel that half of the yearly rainfall occurs in less than three hours!

[32] The time scale of structures of global extent seems to be of the order of two to three weeks; in temperature series, it is associated with a spectral break called the 'synoptic maximum'; see Koleshnikova & Monin (1965), Lovejoy & Schertzer (1986b). There is some evidence of this in Figs. 4d, see also Fig. 23c, d.

[33] These multiplicative 'increments' are denoted 'μ' in analogy with the 'Δ' used for the usual increments in additive processes.

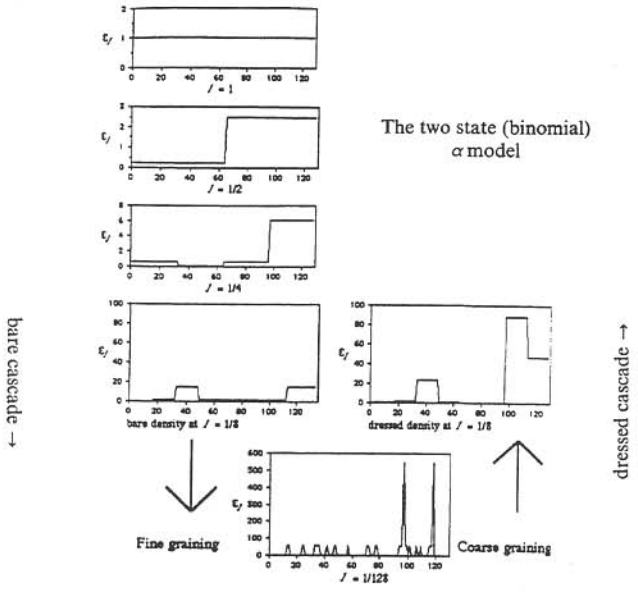

Fig. 8 A discrete (α model) cascade in one dimension. The construction of the 'bare' cascade is shown on the left (top to bottom), at each step, the unit interval is broken up into intervals half the size of the previous step and the energy flux density (vertical axis) is multiplied by a random factor. In the α model, there are only two possibilities – a boost or a decrease with probabilities chosen to respect ensemble conservation $\langle \varepsilon_l \rangle = 1$. As the scale ratio increases, the flux density is increasingly dominated by a few large spikes, the singularities. The right hand side shows the corresponding 'dressed' cascade obtained by averaging over the corresponding scale. The dressed cascade is more variable due to the high resolution modulations. From Schertzer & Lovejoy (1989a).

$$\Pr(\mu R = \lambda^{\gamma+}) = \lambda^{-c}, \qquad \Pr(\mu R = \lambda^{\gamma-}) = 1 - \lambda^{-c} \tag{2}$$

The parameters $\gamma+$, $\gamma-$, c are usually constrained so that the ensemble average $\langle \mu R \rangle = 1$, $\lambda^{\gamma+} > 1$ ($\gamma^+ > 0$) corresponds to strong (wet) intervals, $\lambda^{\gamma} < 1$ ($\gamma^- < 0$) to weak (dry) subintervals. This pedagogical model (Schertzer & Lovejoy, 1983, 1984; Levich & Tzvetkov, 1985; Bialas & Peschansky, 1986; Meneveau & Sreenivasan[34], 1991) was introduced and called the 'α model' because of the divergence of moment exponent[35] α it introduced (in the notation used here, the corresponding divergence parameter is q_D). The dead/alive β model[36] is recovered with $\gamma^- = -\infty$, $\gamma^+ = c$, c being the codimension of the support ($= D - D_S$, D is the dimension of space in which the cascade occurs). As the cascade proceeds, the pure orders of singularities γ^-, γ^+ yield an infinite hierarchy of mixed orders of singularities ($\gamma^- < \gamma < \gamma^+$), after steps these singularities are given by a binomial law:

$$\gamma = (n^+\gamma^+ + n^-\gamma^-)/n; \qquad n^+ + n^- = n$$

$$\Pr(n^+ = k) = \binom{k}{n} \lambda^{-ck}(1-\lambda^{-c})^{n-k}$$

$$\Pr(R_{\lambda^n} \geq (\lambda^n)^\gamma) \approx N_n(\gamma)/N_n \approx (\lambda^n)^{-c_n(\gamma)} \tag{3}$$

$N_n \approx (\lambda^n)^{-D}$ is the total number of intervals at scale λ^{-n}, D the dimension of space and $\binom{k}{n}$ indicates the number of combinations of n objects taken k at a time. In the large n limit, $c_n(\gamma) \approx c(\gamma)$, and we are lead (Schertzer & Lovejoy, 1987a, b) to the multiple scaling probability distribution law:

$$\Pr(R_{\lambda^n} \geq (\lambda^n)^\gamma) \approx (\lambda^n)^{-c_n(\gamma)} \tag{4}$$

Multifractal processes

The multifractal processes discussed here were first developed as phenomenological models of turbulent cascades, the α model being the simplest. They are designed to respect basic properties of the governing nonlinear dynamical ('Navier–Stokes') equations. The following three properties lead to a cascade phenomenology[37]: a) a scaling symmetry (invariance under dilations, 'zooms'), b) a quantity conserved by the cascade (energy fluxes from large to small scale), c) localness in Fourier space (the dynamics are most effective between neighbouring scales: direct transfer of energy from large to small scale structures is inefficient). Cascade models are relevant in the atmosphere in general and in rain and hydrology in particular since (as argued in Schertzer & Lovejoy, 1987a), although the full nonlinear partial differential equations governing the atmosphere will be more complex than those of hydrodynamic turbulence, they are nonetheless still likely to respect properties a, b, c. In other words we expect the complete dynamics to involve coupled cascades. There are now a whole series of phenomenological models: the 'pulse in pulse' model (Novikov & Stewart, 1964), the 'lognormal' model (Kolmogorov, 1962; Obukhov, 1962; Yaglom, 1966), 'weighted curdling' (Mandelbrot, 1974), the 'β model' (Frisch *et al.*, 1978), 'the α model' (Schertzer & Lovejoy, 1983b, 1985a), the 'random β model' (Benzi *et al.*, 1984), the 'p model'[38] (Meneveau & Sreenivasan, 1987) and the 'continuous' and 'universal' cascade models (Schertzer & Lovejoy, 1987a, b). It is now clear that scale invariant multiplicative processes generically yield multifractals and – due to the existence of stable and attractive multifractal generators – to universal multifractals in which many details of the dynamics are unimportant. These results are important in hydrology and geophysics since they show

[34] Although it was never intended to be more than pedagogical, these authors attempt a detailed comparison with turbulence data.

[35] The choice α for this exponent seemed natural at the time since it generalized the Lévy exponent α.

[36] This monofractal model was studied in various slightly different forms at different times (Novikov & Stewart, 1964; Mandelbrot, 1974; Frisch *et al.*, 1978), the parameter $\beta = \lambda^{-c}$ in the notation used here.

[37] First proposed by Richardson (1922) in his now celebrated poem.

[38] This is a microcanonical version of the α model.

that while geometrical fractals are sufficient to study many aspects of scaling sets, that multifractals (with their statistical exponents) provide the general framework for scaling fields (measures). In models of hydrodynamic turbulence, the energy flux ε from large to small scales is conserved (i.e. its ensemble average $\langle\varepsilon\rangle$ is independent of scale), therefore it is the basic cascade quantity. Directly observable fields such as the velocity shear (Δv_l) for two points separated by distance l are related to the energy flux via dimensional arguments:[39]

$$\Delta v_l \approx \varepsilon_l^{1/3} l^{1/3} \tag{5}$$

This equation should be understood statistically. A straightforward interpretation useful in modelling is to view the scaling $l^{1/3}$ as a power law filter ($k^{-1/3}$, fractional integral) of $\varepsilon_l^{1/3}$ (Schertzer & Lovejoy, 1987a; Wilson, 1991; Wilson *et al.*, 1991).

In contrast to the well studied case of hydrodynamic turbulence, the dynamical equations responsible for the distribution of rain and cloud radiances are not known;[40] the best we can do now is to speculate on the appropriate fundamental dynamical quantities analogous[41] to ε. Since *a priori*, there is no obvious reason the rainrate or cloud radiance fields themselves should be conservative, in analogy with turbulence, we introduce a fundamental field φ_l that has the conservation property $\langle\varphi_l\rangle$ = constant (independent of scale). The observable (nonconserved) rainfall (or cloud radiance) fluctuations (ΔR_l) is then given by:

$$\Delta R_l \approx \varphi_l^a l^H \tag{6}$$

Since we have yet no proper dynamical theory for rain, we do not know the appropriate fields φ_l nor the corresponding values of a. We shall see that changing a essentially corresponds to changing C_1 defined below. Therefore, the scaling parameter H has a straightforward interpretation: it specifies how far the measured field R is from the conserved field φ: $\langle|\Delta R_l|\rangle \approx l^H$. H therefore specifies the exponent of the power law filter (the order of fractional integration) required to obtain R from φ.

Basic properties of multifractal fields

We now focus our attention on the conserved quantity φ_l. Early scaling ideas were associated with additive (linear) processes, and unique scaling exponents H (which – only in these special cases) were related to unique fractal dimensions by simple formulae. The properties of φ_l were more straightforward, and were usually understood implicitly. We have already discussed 'simple scaling'. This is a special case of equation 6 in which φ_l is simply a scale invariant noise ($\langle\varphi_l^q\rangle$ are all constants, independent of scale).

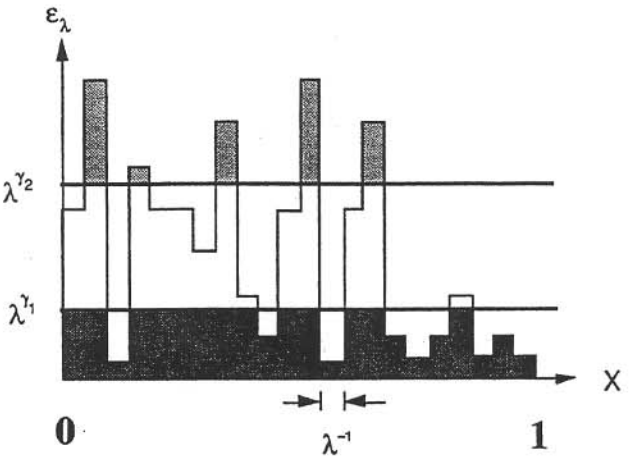

Fig. 9 A schematic diagram showing a multifractal energy flux density with smallest resolution λ^{-1}, and indicating the exceedance sets corresponding to two orders of singularities, γ_1, γ_2. From Tessier *et al.* (1993).

Turning our attention to (nonlinear) multiplicative processes we can consider some properties of φ that will generically result from cascades. We have already discussed the example of the α model, including the form of the probability distribution after n cascade steps. In fact, denoting the entire range of scales from the largest to smallest by λ, and considering the cascade of φ (rather than of R directly), we obtain the following general multifractal relation:

$$\Pr(\varphi_\lambda \geq \lambda^\gamma) \approx \lambda^{-c(\gamma)} \tag{7}$$

(equality is to within slowly varying functions of λ such as logs). $c(\gamma)$ is therefore the (statistical) scaling exponent of the probability distribution (see Fig. 9 for an illustration). However, when the process is observed on a low dimensional cut of dimension D (such as the $D=2$ dimensional simulation shown in Fig. 10) it can often be given a simple geometric interpretation. When $D > c(\gamma)$, we may introduce the (positive) dimension function $D(\gamma) = D - c(\gamma)$ which is the set with singularities γ.

This geometric interpretation can be useful in data analysis. For example, consider a data set consisting of N_s radar scans (assumed to be statistically independent realizations from the same statistical ensemble). A single D dimensional scan ($D=2$ in this example) will enable us to explore structures with dimension $D \geq D(\gamma) \geq 0$; structures with $c(\gamma) > D$ (which would correspond to impossible negative[42] values of

[39] Equation 5 is the physical space expression of the famous Kolmogorov $k^{-5/3}$ velocity spectrum.

[40] We exclude here the essentially *ad hoc* parametrizations employed in numerical cloud and weather models.

[41] These will be various conserved fluxes such as the humidity variance flux and bouyancy force variance flux.

[42] Mandelbrot (1984) introduced the expression 'latent' for these nonstandard dimensions. If the (intrinsic) codimensions are used, this artificial problem is entirely avoided.

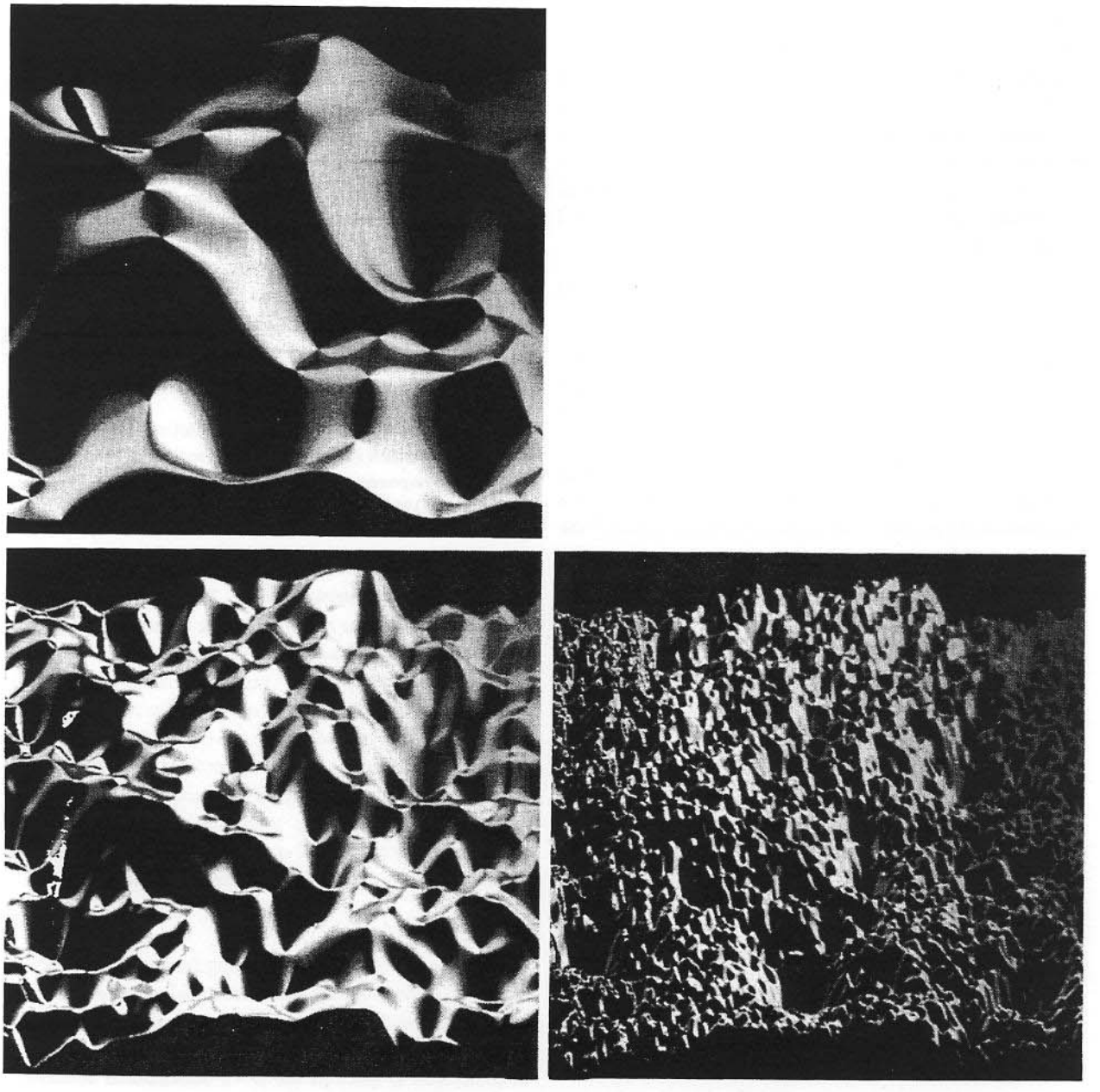

Fig. 10 Successive stages in the construction of a universal multifractal temperature field shown with resolution increasing by factors of four, counterclockwise from the upper left corner. The temperature is represented as a surface with false colours, incipient singularities (the high valued spikes) and associated 'Levy holes' are particularly evident in the low resolution image in the design. The parameters used for the simulation were those estimated from atmospheric measurements analysed in Schmitt *et al.* (1992), i.e. $\alpha = 1.3$, $C_1 = 0.5$, $H = \frac{1}{3}$. From Lovejoy & Schertzer (1991c).

$D(\gamma)$) will be too sparse to be observed (they will almost surely not be present on a given realization). This restriction on the accessible values of $c(\gamma)$ is shown in Fig. 11; to explore more of the probability space, we will require many scans. With N_s scans, the accessible range of singularities can readily be estimated. If each scan has a range of scales λ (= the ratio of the size of the picture to the smallest resolution = the number of 'pixels' on a side), then we can introduce the 'sampling dimension' (Schertzer & Lovejoy, 1989a; Lavallée, 1991; Lavallée *et al.*, 1991a): $D_s = \log N_s / \log \lambda$. It is not hard to see (Fig. 12) that the accessible range will be $\gamma < \gamma_s$, with $c(\gamma_\tau) = \Delta + \Delta_s$ (see Fig. 30 for a concrete illustration in rain).

$c(\gamma)$ has many other properties that are illustrated graphi-

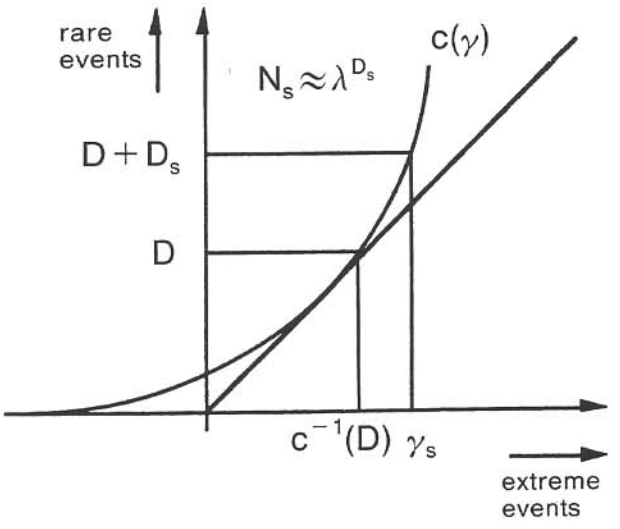

Fig. 11 A schematic diagram showing a typical codimension function for a conserved process ($H=0$). The lines $c(\gamma)=D$, $\gamma = C^{-1}(D)$ indicate the limits of the accessible range of singularities for a single realization, dimension D. The corresponding lines for $D+D_s$, where D_s is the sampling dimension, are also shown. As we analyse more and more samples, we explore a larger and larger fraction of the probability space of the process, hence finding more and more extreme (are rare) singularities. From Tessier *et al.* (1993).

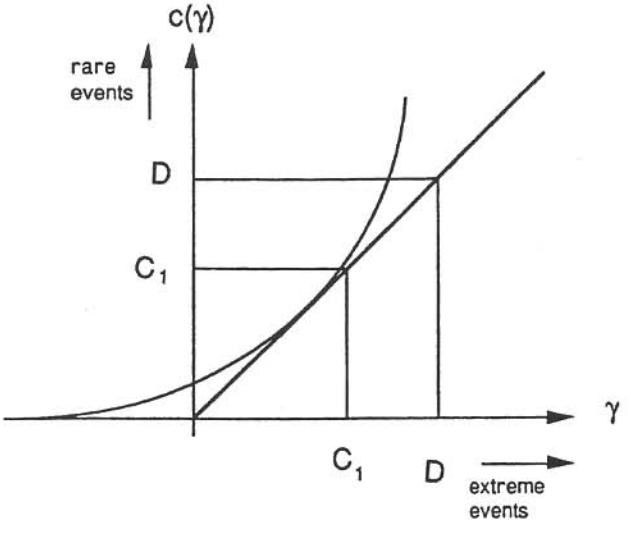

Fig. 12 Same as previous, but showing the fixed point $C_1 = c(C_1)$, (with $0 \le C_1 \le D$) the singularity corresponding to the mean of the process. The diagonal line is the bisectrix ($\gamma = c(\gamma)$). From Tessier *et al.* (1993).

cally. A fundamental property which is readily derived by considering statistical moments (below), is that it must be convex. It must also satisfy the fixed point relation $C_1 = c(C_1)$ as indicated in Fig. 12. C_1 is thus the codimension of the mean process; if the process is observed on a space of dimension D, it must satisfy $D \ge C_1$, otherwise, following the above, the

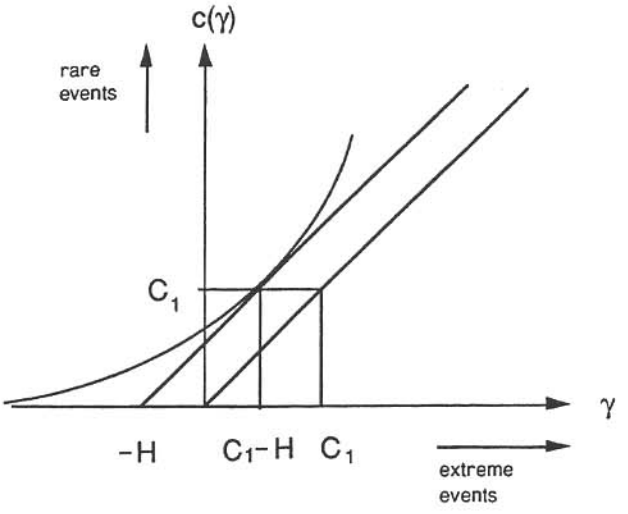

Fig. 13 Same as 11, but for a nonconserved process. All the singularities are shifted by $-H$. From Tessier *et al.* (1993).

mean will be so sparse that the process will (almost surely) be zero everywhere; it will be 'degenerate'. We can also consider the (nonconserved) ΔR_λ; it is obtained from φ_λ by multiplication by λ^{-H}, since $\varphi_\lambda = \lambda^\gamma$, we have $\Delta R_\lambda = \lambda^{\gamma - H}$; i.e. by the translation of singularities by $-H$ (see Fig. 13).

Rather than specifying the statistical properties via the scaling of probabilities $c(\gamma)$ can (equivalently) be specified by the scaling of the statistical moments[43]. Consider the qth order statistical moments $\langle \varphi_\lambda^q \rangle$. We can now define the multiple scaling exponent[44] $K(q)$:

$$\langle \varphi_\lambda^q \rangle = \lambda^{K(q)} \tag{8}$$

$K(q)$, $c(\gamma)$ are related by the following Legendre transformations (Parisi & Frisch, 1985):

$$K(q) = \max_\gamma (q\gamma - c(\gamma)); \; c(\gamma) = \max_q (q\gamma - K(q)) \tag{9}$$

which relate points on the $c(\gamma)$ function to tangencies on the $K(q)$ function and visa versa; $\gamma = K'(q)$, $q = c'(\gamma)$. For example, a quantity which will be useful below in estimating the multifractal parameters of radiances and reflectivities is the sampling moment q_s which is the maximum order moment that can be accurately estimated with a finite sample.

[43] Gupta & Waymire (1990) have introduced the idea of multiple scaling of random variables rather than fields/measures ('GW multiscaling'): in other words a multiple scaling without the notion of scales. In GW multiscaling there are no multifractals and there is no 'hard' behavior (see below).

[44] The turbulent codimension notation $c(\gamma)$ and $K(q)$ is related to the '$f(\alpha)$' dimension notation (Halsey *et al.*, 1986) by the following: $\alpha = (D - \gamma)$, $f(\alpha) = D - c(\gamma)$, $\tau(q) = (q-1)D - K(q)$. Because the dimension notation fundamentally depends on the dimension of the observing space D; it cannot be used in stochastic processes such as those of interest here where we deal with infinite dimensional probability spaces, $D \Rightarrow \infty$. The dimension notation is useful for multifractal probability measures; in turbulence, we deal with spatial measures ε which do not reduce to probability measures.

Table 2. *Classification of multifractals according to their extreme singularities*

Type of multifractal	Types of singularities present	Localized?	Conservation per realization?	Convergence of all moments?
Geometric	calm	yes	yes	yes
Microcanonical	calm	no	yes	yes
Canonical	calm, wild, hard	no	no	usually no

Recalling that the maximum accessible order of singularity was $\gamma_s = c^{-1}(D+D_s)$, we obtain: $q_s = c'(\gamma_s)$. The functions for the corresponding nonconserved fields ($H \neq 0$) are obtained by $\gamma \Rightarrow \gamma - H$, $K(q) \Rightarrow K(q) - Hq$.

The classification of multifractals: nonlocal, wild and hard multifractals, multifractal phase transitions

We now discuss various different types of multifractals. To this end, we must first make a distinction between the 'bare' and 'dressed' multifractal properties (Schertzer & Lovejoy, 1987a, b). The 'bare' properties are those which have been discussed above, they correspond to the construction of the process over a finite range of scales λ. In contrast, the 'dressed' quantities (see the right hand side of Fig. 8) are obtained by integrating (averaging) a completed cascade over the corresponding scale. Experimentally measured quantities are generally 'dressed' since geophysical sensors typically have resolutions which are much lower than the smallest structures in the fields they are measuring (which in the atmosphere, is typically of the order of 1 mm or less). The dressed quantities will generally display an extreme, 'hard' behavior involving divergence of high order statistical moments. Specifically, for spatial averages over observing sets with dimension D there is a critical order moment q_D (and corresponding order of singularity $\gamma_D = K'(q_D)$) such that:

$$\langle \varphi_\lambda^q \rangle = \infty \qquad q \geq q_D \tag{10}$$

where q_D is given by the following equation:

$$K(q_D) = (q_D - 1)\, D \tag{11}$$

The associated qualitative change of behaviour at q_D (or γ_D) can be considered a multifractal phase transition (Schertzer *et al.*, 1993). Unfortunately, these general multiplicative processes with their corresponding hard behaviour have received relatively little attention in the literature; it is much more usual to introduce various constraints which have the effect of severely limiting the occurence of extreme events. While these restrictions lead to simplifications in the theoretical treatment which are justified when studying strange attractors, they are too restrictive to be appropriate in geophysics; one must be wary of the simplistic data analysis techniques they have spawned. Since this underestimation of the diversity of multifractal behaviour persists in the literature, we now briefly summarize the properties of both 'geometrical' and 'microcanonical' multifractals.

To understand the corresponding different types of multifractal process, recall that we have considered 'canonical' multifractals subject only to the weak constraint of conservation of φ only over the entire statistical ensemble, individual realizations will not be conserved. If on the contrary, we impose the much stronger constraint of conservation on each realization, then large fluctuations are suppressed and we obtain a 'microcanonical' process. Specifically, we find that 'wild' singularities with $\gamma > D$ are supressed. Both canonical and microcanonical multifractals are stochastic processes, they are defined on (infinite dimensional) probability spaces: each realization in a space of dimension D must be viewed as low-dimensional cuts.

Just as microcanonical processes are calmer than canonical processes, another type of multifractal; 'geometric' multifractals (Parisi & Frisch, 1985) can be defined which are even calmer. Geometric multifractals involve no probability space, nor stochastic process; they are defined purely geometrically as a superposition of completely localized (point) singularities each distributed over fractal sets. As mentioned earlier, since such sets must have positive dimensions, their singularities are restricted so that $c(\gamma) \leq D$. Schertzer *et al.* (1991) and Schertzer & Lovejoy (1992) discuss this classification of multifractals in much more detail; their properties are summarized in Table 2.

Universal multifractals

The above discussion is quite general and at this level, it has the unpleasant consequence that an infinite number of scaling parameters (the entire $c(\gamma)$, $K(q)$ functions) will be required to fully specify the multiple scaling of our field. Fortunately, real physical processes will typically involve both nonlinear 'mixing' (Schertzer *et al.*, 1991) of different multifractal processes, as well as a 'densification' (Schertzer & Lovejoy, 1987a, b) of the process leading to the dynamical excitation of intermediate scales. Rather than just the dis-

crete scales (factors of 2) indicated in Figs. 7 and 8, there is the continuum indicated in 10. Either mixing or densification are sufficient[45] so that we obtain the following (bare[46]) universal[47] multifractal functions[48]:

$$c(\gamma - H) = C_1[\gamma/(C_1\alpha') + 1/\alpha']\alpha'; \quad \alpha \neq 1 \tag{12}$$
$$c(\gamma - H) = C_1 \exp[(\gamma/C_1) - 1] \quad \alpha = 1$$

$$K(q) - qH = \begin{cases} \dfrac{C_1}{\alpha - 1}(q^\alpha - q) & \alpha \neq 1 \\ C_1\, q \log(q) & \alpha = 1 \end{cases} \quad (\text{for } \alpha < 2, q \geq 0)$$

$$\frac{1}{\alpha} + \frac{1}{\alpha'} = 1 \tag{13}$$

The multifractality parameter α is the Lévy index and indicates the class to which the probability distribution belongs[49]. There are actually 5 qualitatively different cases. The case $\alpha = 2$ corresponds to multifractals with Gaussian generators[50], the case $1 < \alpha \leq 2$ corresponds to multifractal processes with Lévy generators and unbounded singularities, $\alpha = 1$ corresponds to multifractals with Cauchy generators. These three cases are all 'unconditionally hard' multifractals, since for any D, divergence of moments will occur for large enough q (q_D is always finite). When $0 < \alpha < 1$ we have multifractal processes with Lévy generators and bounded singularities. By integrating (smoothing) such multifractals over an observing set with large enough dimension D it is possible to tame all the divergences yielding 'soft' behavior, these multifractals are only conditionally 'hard'. Finally[51] $\alpha = 0$ corresponds to the monofractal 'β model'. Universal multifractals have been empirically found in both turbulent temperature and wind data (Schertzer *et al.*, 1991a; Schmitt *et al.*, 1992; Kida, 1991). They have also have recently found applications in high energy physics (Brax & Pechanski, 1991; Ratti, 1991; Ratti *et al.*, 1994), oceanography (Lavallée *et al.*, 1991b), topography (Lavallée *et al.*, 1993), as well as the low frequency component of the human voice (Larnder *et al.*, 1992). The first empirical estimates[52] of C_1, α in cloud radiances[53] are discussed in Lovejoy & Schertzer, 1990 (see also Gabriel *et al.*, 1988 for the first test of universality in an empirical data set[54]).

It is interesting to note here that the probability distributions associated with the various (bare) universality classes are respectively lognormal ($\alpha = 2$), and log-Lévy ($\alpha < 2$). The latter are in turn approximately log-normal since, with the exception of their extreme tails, Lévy distributions are themselves nearly normal (this 'tail' is pushed to lower and lower probability levels as $\alpha \to 2$). The multifractal nature of rain is therefore quite in accord with the widespread hydrological, meteorological (and generally geophysical) lognormal phenomenology. Of particular relevance here are numerous studies that have claimed that rainrates, cloud and radar echo sizes, heights and lifetimes, as well as total rain output from storms over their lifetimes are either log-normal or 'truncated log-normal' distributions (Biondini, 1976; Lopez, 1976, 1977a; Drufuca, 1977; Houze & Cheng, 1977; Konrad, 1978; Warner & Austin, 1978 etc.). Furthermore, the cascade models that generate them are actually just concrete implementations of vague laws of 'proportionate effects' (see Lopez, 1977a, b for an invocation of this law in the rain context). Shifting our attention to the dressed quantites, the above statement still holds for (nonextreme) fluctuations (up to γ_D, q_D), but will (drastically) underestimate the frequency of occurence of extreme events ($\gamma > \gamma_D$, $q > q_D$).

Using the universal multifractal formulae above, some of the results discussed earlier may be expressed in simpler form. Formulae which will prove useful below are for the sampling order moment q_s (the maximum order moment that can be reliably estimated with a finite sample), and q_D, the critical order for divergence:

$$q_s = [(D + D_s)/C_1]^{1/\alpha} \tag{14a}$$
$$(\alpha - 1)/C_1[(q_D^\alpha - q_D)/(q_D - 1)] = D \tag{14b}$$

For $q > q_c = \min(q_s, q_D)$, $K(q)$ will be linear, for $\gamma > \gamma_D$ $c(\gamma)$ will also be linear:

[45] This applies only to canonical multifractals; there seems to be no corresponding universality for geometric or microcanonical multifractals.

[46] The corresponding dressed functions are the same only for $\gamma < \gamma_D$, and $q < q_D$; for finite sample sizes, they becoming linear for larger γ, q.

[47] The problem of universality was for some time obscured by the exclusive study of (nonuniversal) discrete cascades in which the limits of more and more random variables and smaller and smaller scale structures were confounded (both limits occured simultaneously as the number of discrete steps approached infinity). On the contrary, universality results when more and more random variables are involved within a fixed and finite range of scales. The limit of the range of scales approaching infinity (the small scale limit) is taken only later. An example of the widespread anti-universality predjudice is the recent statement by Mandelbrot (1989): '... in the strict sense there is no universality whatsoever ... this fact about multifractals is very significant in their theory and must be recognized ...' (*op cit*, p. 16).

[48] These formulae (with $H = 0$) first appeared in Schertzer & Lovejoy (1987a, Appendix C). Recently, in the special case $H = 0$, Kida (1991), Brax & Peschanski (1991) have obtained equivalent formulae using different notations. They use the expressions 'log stable' and 'log Lévy' multifractals respectively. These terms are somewhat inaccurate since due to the dressing problem, the distributions will only be approximately log stable or log Lévy.

[49] Similar looking formulae (but for random variables, not multifractal measures) can be obtained in GW multiple scaling, Gupta & Waymire (1990).

[50] This is nearly the same as the lognormal multiscaling model of turbulence proposed by Kolmogorov (1962), Obhukhov (1962), except that the latter missed the essential point about the divergence of high order moments, thinking in terms of pointwise processes.

[51] A more detailed discussion about these fives cases and in particular about the generators of the Lévy variables can be found in Schertzer *et al.*, 1988; Fan 1989; and Schertzer & Lovejoy 1989a; see also Lovejoy & Schertzer (1990a, b, 1991a, b) for some applications and review.

[52] Recent (greatly improved) analyses indicate that the original estimates of α were not too accurate. See Tessier *et al.*, 1992, and below.

[53] For theoretical discussion of multifractal clouds and their associated radiance fields, see Lovejoy *et al.* (1990), Gabriel *et al.* (1990), Davis *et al.* (1990, 1991a, b).

[54] Only the hypothesis $\alpha = 2$ was tested.

$$K(q)=q\gamma_{d,s}-c(\gamma_{d,s}) \qquad q>q_c \tag{15a}$$

$$c(\gamma)=\gamma q_D-K(q_D) \qquad \gamma>\gamma_D \tag{15b}$$

where $\gamma_{d,s}$ is the highest order dressed singularity present in the sample.

MULTIFRACTAL ANALYSES OF RAIN

Trace moment analyses

Soon after the discovery of multifractals, it was realized that radar rain data would provide ideal testing grounds for multifractal theories as well as data analysis techniques[55]. A whole series of new multifractal analysis techniques (trace moments, functional box-counting, elliptical dimensional sampling), were developed and tested for the first time on rain data. In this section we first discuss what might be viewed as first generation multifractal analysis techniques: methods that can be applied (with various limitations) to general multifractals. These methods are the multifractal analogues of the nonparametric methods of standard statistics. Further we indicate how a second generation of techniques can be be developed which explicitly exploit the existence of universality classes. These are the analogues of parametric statistics, and just as parametric statistical methods have more statistical power than nonparametric methods, the specific (universal) multifractal analysis techniques (when applicable) will lead to much more accurate multifractal characterizations. All these techniques are essentially experimental in the sense that no proper goodness of fit statistics are known; at the moment, confidence in the results of analyses can be obtained primarily by comparing the results of different and complementary methods as well as by extensively testing the analysis on numerical simulations.

The first multifractal rain analyses were performed on radar volume scans of rain from the McGill radar weather observatory[56] (Schertzer & Lovejoy, 1985b, 1987a, see Figs. 5, 15). Volume scans are made every 5 minutes, at 200 ranges (r) and 375 azimuthal (θ) and 13 elevation angles. In the trace moment analysis described here, data were resampled in the vertical onto constant altitude projections ('CAZLORs') at 3 levels (3, 4, 5 km altitudes, z) at 30 minute intervals in time. The analysis was performed using the data to estimate the trace moments. In this technique, the data are systematically degraded in resolution, average reflectivities being calculated over grids whose resolution is successively doubled, the resulting spatial averages are then raised to a series of powers q and the result averaged over each image, and then over many realizations.

To give a formal definition, consider the conserved ($H=0$)

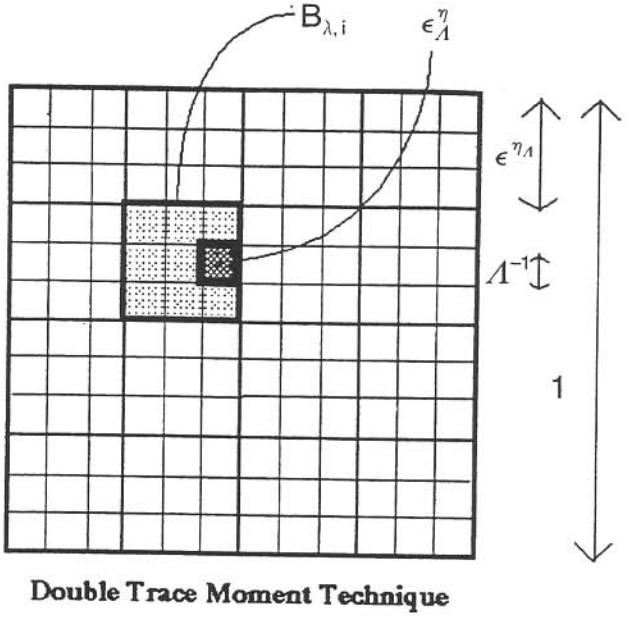

Fig. 14 A schematic diagram illustrating the different averaging scales used in the double trace moment technique, the single trace moment is obtained by taking $\eta=1$. The idea is straightforward; at the highest available resolution (λ') various powers (η) are taken. They are then degraded to an intermediate resolution (λ) by averaging, finally the qth power of the result is averaged over all the data sets. From Tessier *et al.*, 1993.

multifractal flux density at (fine) resolution Λ' (the ratio of the outer (largest) scale of interest to the smallest scale of homogeneity). The (dressed) flux over an observing set (B_λ, this corresponds to the j-th low resolution 'pixel') with dimension D, (lower) resolution λ ($\lambda<\Lambda'$) is simply an integral over the density:

$$\Pi_\Lambda(B_{\lambda,i})=\int_{B_{\lambda,i}} \varphi_\lambda \, d^D x \tag{16}$$

We may now define the qth order 'Trace moments' (Schertzer & Lovejoy[57], 1987a) by summing $\Pi_\Lambda^q(B_{\lambda,i})$ over each individual realization[58] (each satellite picture, covering the region A has λ^D disjoint covering sets B_λ which are summed over in equation 16, see the schematic illustration, Fig. 14), and then ensemble averaging over all the realizations:

$$\mathrm{Tr}_\lambda(\varphi_\Lambda^\eta)^q=\left\langle \sum_i \Pi_\Lambda^q(B_{\lambda,i}) \right\rangle \approx \lambda^{K(q)-(q-1)D} \tag{17}$$

This formula will break down for moments $q>q_D$, and (when finite samples are used to estimate the ensemble average) when $q>q_s$. Although it allows the determination of $K(q)$ (at least for small enough q), and hence in principle the

[55] Schertzer & Lovejoy (1989b) and Lovejoy & Schertzer (1990b) develop this idea and argue that it is true of many other geophysical fields.

[56] For an analogous analysis of tropical Atlantic radar data see Gupta & Waymire (1990).

[57] Although the formalism above was developed here, essentially the same method was empirically applied to rain in Schertzer & Lovejoy (1985b).

[58] Without the ensemble averaging, we have a partition function, appropriate for analyzing strange attractors.

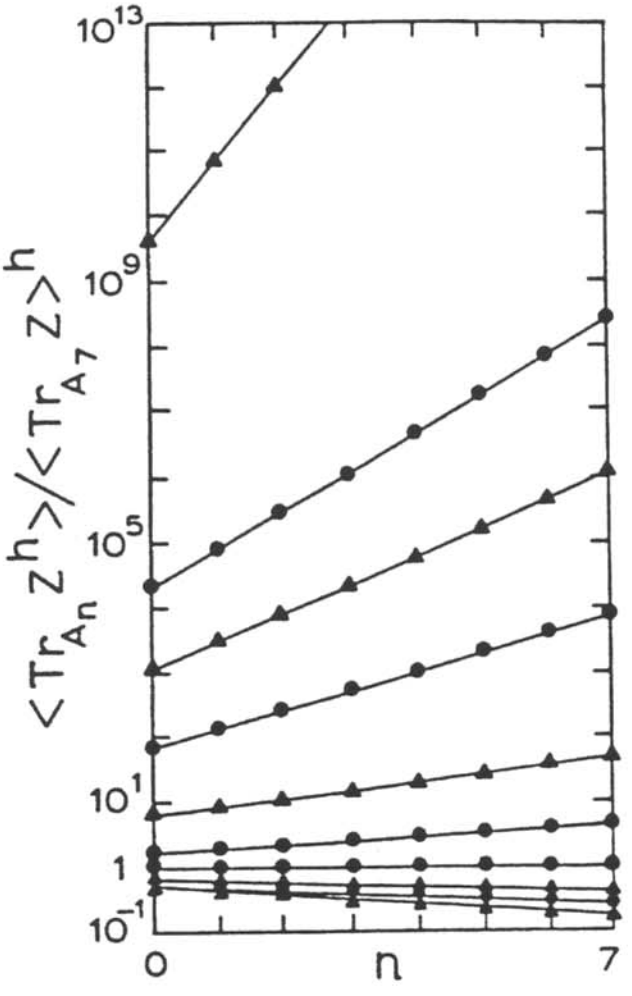

Fig. 15a The hth trace moments (in the notation in the text, $q=h$) estimated from 70 CAZLORs in the horizontal, averaging over a straight line (A is the set of downrange elements used in the averaging), the data is the 3 km altitude subset of that used in Fig. 5. The resolution is $\lambda=2^n$. Lines from top to bottom are for the following values of h: 5, 3, 2.5, 2, 1.5, 1.2, 1., 0.8, 0.6, 0.3. Note that the scaling is extremely accurately followed. From Schertzer & Lovejoy (1987a).

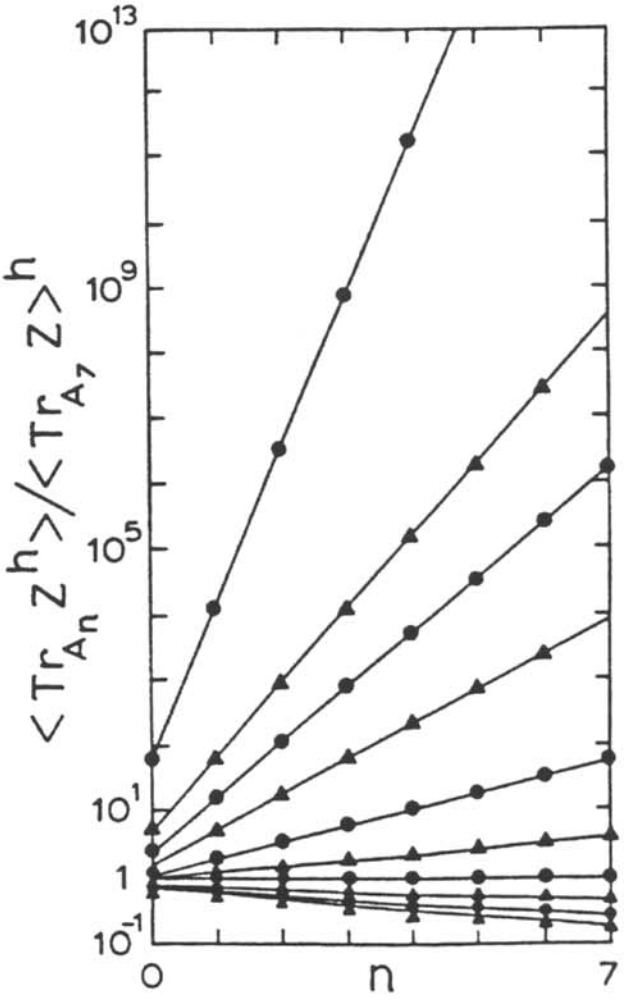

Fig. 15b Same as 15a but for averaging in the horizontal, A is a plane. From Schertzer & Lovejoy (1987a).

determination of C_1, α (via equation 14) this method will involve ill-conditioned nonlinear regressions ($K(q)$ vs. q).

Fig. 15 shows the result using 70 realizations, clearly showing that the multiple scaling is very well respected. The resolution can be degraded along ranges ($D=1$), (r,Θ) simultaneously ($D=2$), (r,Θ,z) or (r,Θ,z,t) simultaneously ($D=3,4$ respectively). Fig. 5 shows the resulting exponents including a 1.5 dimensional case obtained by using simulated fractal measuring networks[59]. The exponents are nearly independent of dimension for low order moments (q), but for $q \geq 1.1$ become increasingly separated, asymptotically tending to straight lines with slopes $\approx D$ for large q. It was argued (Schertzer & Lovejoy, 1987a) that this behaviour could be simply explained since for that data set $q_D \approx 1.1$ (Fig. 2b). Some recent results on the 'pseudo-scaling' (Schertzer & Lovejoy 1983a, 1984) obtained when $q > q_D$ and the relation of this to multifractal 'phase transitions' is discussed in Schertzer *et al.* (1991b).

More recently (Lovejoy & Schertzer, 1991a) trace moments were used to investigate the multiple scaling of rain at scales much smaller than the minimum (≈ 1 km) of the above radar analysis. One of the analyses (Pham & Miville, 1986) was performed on data obtained by rapidly (≈ 1 s) exposing large pieces (128×128 cm) of chemically treated blotting paper to rain, estimating the position and size of the drops. Fig. 16a shows the result of one such exposure, and Fig. 17 shows the resulting trace moment analysis and Fig. 18 the scaling exponent estimates for scales ≥ 8 cm. This analysis indicates that at least down to this scale, rain is multiscaling. The break observed at ≈ 8 cm could be due to

[59] This was close to the dimension estimated for typical gage networks; a better estimate (Lovejoy *et al.*, 1986) is 1.75.

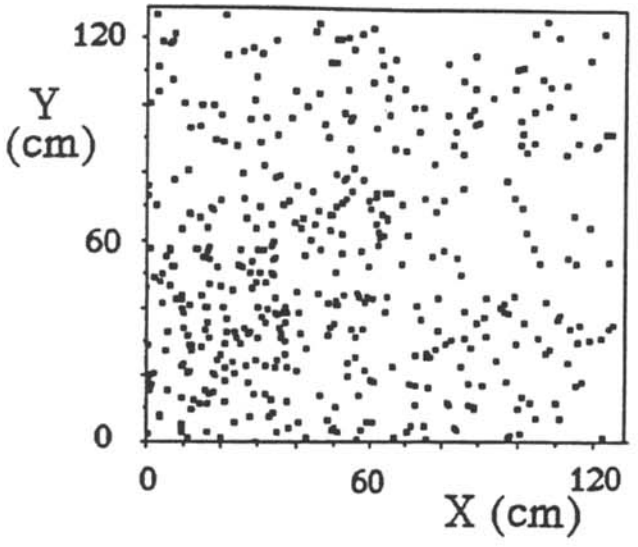

Fig. 16a Each point represents the centre of a raindrop for the 128 × 128 cm piece of chemically treated blotting paper discussed in the text. There are 452 points, the exposure was about 1 s. From Lovejoy & Schertzer (1990c).

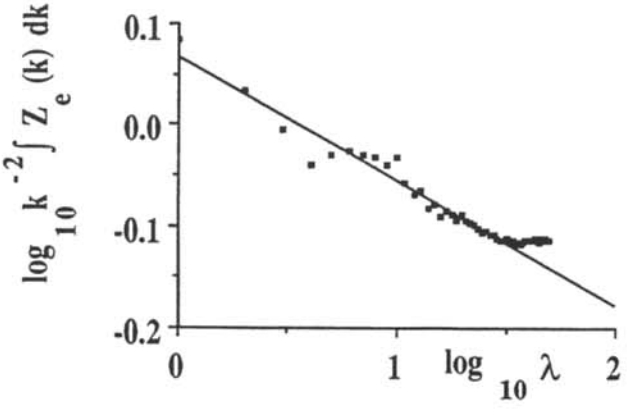

Fig. 16b Plot showing k^{-2} times the integrated energy spectrum of the radar reflectivity of the distribution in Fig. 16a plotted against $\lambda = k/k_0$ where k is the wave number, k_0 corresponds to the largest scale ($k_0 = |k_0| = 2\pi/128$. The straight line (slope -0.12) indicates a scaling power law spectrum (Gaussian white noise yields a slope 0) up to $\lambda \approx 30$ which corresponds to ≈ 4 cm. From Lovejoy & Schertzer (1991a).

finite sample effects (a single exposure was used with only 452 drops), or the break could be more fundamental; related to the inner scale at which rain can no longer be treated as a field[60], where its particulate nature must be considered[61]. Fig. 16b shows the Fourier energy density integrated over circles, confirming the breakdown by the flattening of the spectrum

[60] However, the spectrum in Fig. 4a suggests an inner dissipation scale of the order of millimeters.

[61] The proper mathematical framework is mathematical measures, associating with each drop a position r_i, and volume V_i.

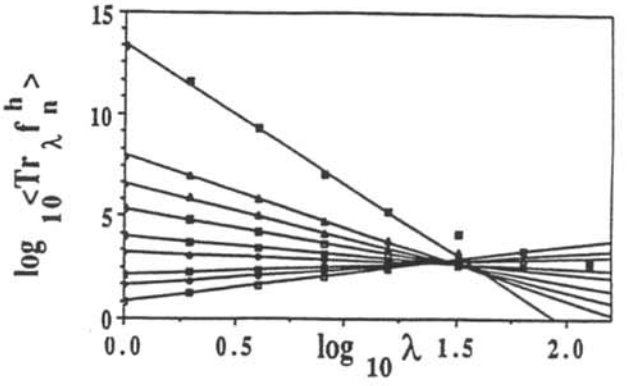

Fig. 17 A log-log plot of $\langle \mathrm{Tr}_\lambda f_n^q \rangle = \lambda - K_D(q)$ vs. λ where f_n is the number of drops per unit area at resolution λ (= the scale ratio). (The h in the figure is the same as the q used here – this is also true for Figs. 18, 19). Note that the largest scale ($\lambda = 1$) was 128 cm and that convergence to power laws occurs only for lengths ≥ 4 cm. The curves, top to bottom, are for $q = 5, 3, 2.5, 2, 1.5, 1.2, 0.8, 0.6, 0.3$. From Lovejoy & Schertzer (1991a).

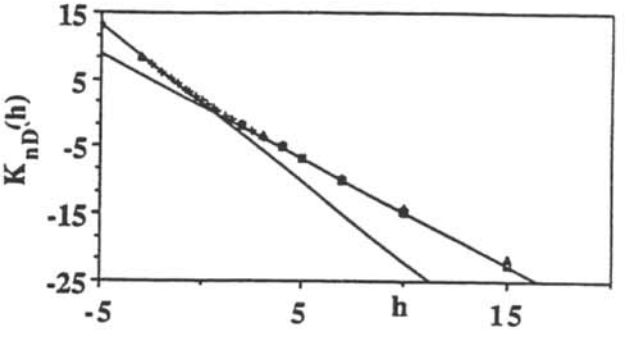

Fig. 18 $-K_{nD}(q) = K(q) - (q-1)D$ estimated from (top to bottom) a manually analysed 1293 drop case ($q > 0$ only; $q = h$), the 452 drop (digital) case, and a 339 drop manually analysed case ($q > 0$). The straight lines are asymptotic fits to the negative and positive large (absolute) q regions for the 452 drop case. The large q slope gives $\gamma_{d,s} = 0.44$ (the largest singularity present). From Lovejoy & Schertzer (1991a).

for scales less than about 4 cm. To our knowledge, this is the first attempt to study spatial heterogeneity at the individual drop level; existing empirical studies of the distribution of the drops are numerous, but consider only their relative sizes; spatial homogeneity is simply assumed on faith. Much more research at the individual drop level will be necessary to properly understand the multifractal structure of rain. We may anticipate that the results will be important in applications: Lovejoy & Schertzer (1990a) already indicate how even monofractal approximations lead to important corrections to standard radar estimates. Two low budget feasibility studies at McGill[62] point to the difficulty in accurately

[62] The blotting paper, lidar and other feasibility studies were all performed as third year physics lab projects from 1986 to present.

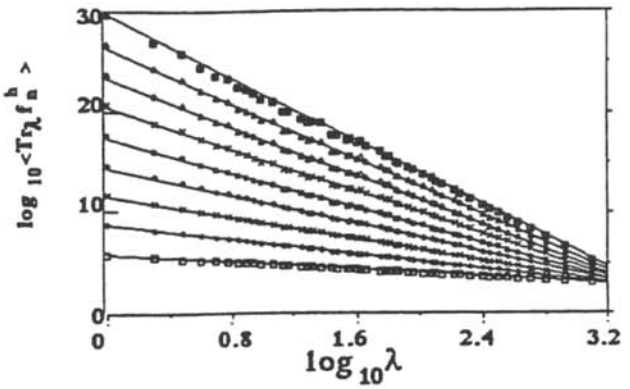

Fig. 19a Trace moment analysis for the time domain (5000 pulses $t_0 = 500$ s) for those range corrected returns that exceeded the average (this is an estimate of the drop number density f_n; it assumes either zero or one drop per pulse volume). Curves from top to bottom are for $q = 10, 9, 8, 7, 6, 5, 4, 3, 2$ respectively. Note that the scaling is extremely accurately followed. From Lovejoy & Schertzer (1991a).

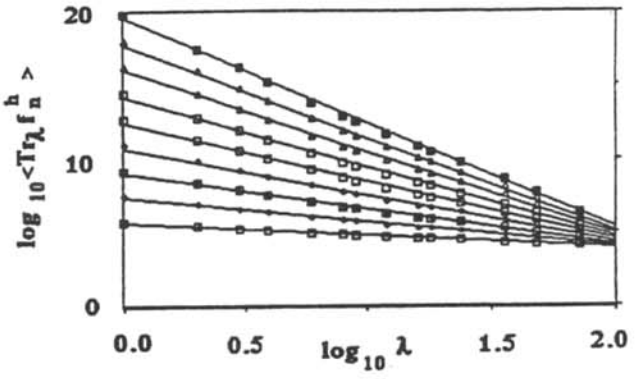

Fig. 19b Trace moment analysis for downrange domain (each pulse return is divided into 180 pulselength sections, 3 m apart, hence the largest scale is $L_0 = 540$) for those range corrected returns that exceeded the average. Curves from top to bottom same as for Fig. 19a. Note that the scaling is extremely accurately followed. From Lovejoy & Schertzer (1991a).

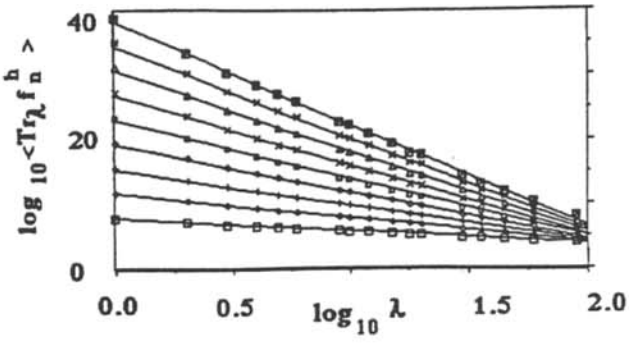

Fig. 19c Trace moment analysis for the (x, t) domain (180 pulses, 0.1s apart in time, space resolution 3 m) for those range corrected returns that exceeded the average. Curves from top to bottom same as for Fig. 19a. Note that the scaling is extremely accurately followed. This data set is the same as that shown in Fig. 19b except that analysis was performed on 'squares' in (x, t) space rather than by intervals (downrange) only. By comparing the slopes in 19a, b, c, the elliptical dimension of (x, t) space can be estimated. From Lovejoy & Schertzer (1991a).

obtaining spatial information about large numbers of drops: stereophotography of a ≈ 1 m^3 region (Bochi Kebe & Howes, 1990), and photography of rain illuminated by sheets of laser light (to obtain horizontal rain intersections with rain, Harris & Lewis, 1991) both indicate that the relevant measurements will be quite difficult, primarily due to the very small cross-sections (at visible wavelengths) of the rain drops which makes their detection quite difficult[63].

To extend these results to slightly larger scales, high powered lidars (Weisnagel & Powell, 1987) were used to detect the optical backscattering from very small volumes[64] the sensitivity was such that individual drops 1 mm in diameter could be detected at ≈ 10 km distances. The YAG laser used had a pulse repetition frequency of 10 Hz, data were logged over 180 downrange bins, several thousand in time. Often, especially in light rain, pulse volumes were empty, and they rarely contained a large number of drops. Shorter pulse length lasers should be able to probe down to the individual drop level (this may indeed be the most promising approach for further studies). Fig. 19a, b, c shows the resulting trace moment analyses (space, time, space/time), showing not only the surprising accuracy with which the (multiple) scaling is respected, but also the possibility of using this approach for studying the space/time transformations associated with rain. A different approach currently being studied at McGill is to use stereo photography with high powered flash lamps.

Functional box-counting

Since the discovery of multifractal universality classes in 1986–7, a primary goal has been to test the (multi)scaling and to estimate the basic parameters H, C_1, α in rain over wide ranges of scale. While the trace moment analyses discussed above clearly established the multiple scaling nature of rain, they suffer from a number of limitations which make them difficult to use to estimate the universal parameters. These

[63] The cross-section is however significantly enhanced for both forward and back scattering.

[64] The pulse lengths were 3 m and the widths varied from 0.3 mm to 30 cm at distances of 10 and 1000 m respectively. The associated pulse volumes were thus in the range 10^{-6} to 10^{-2} m^3: 10^{15} to 10^{11} times smaller than typical radar volumes.

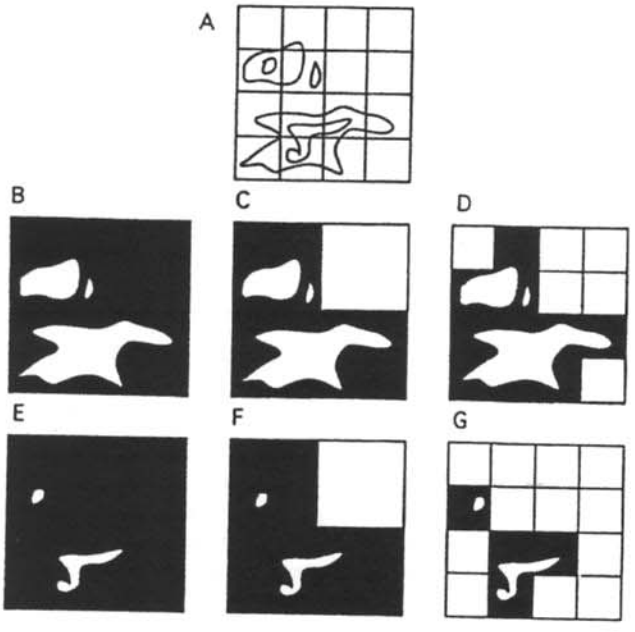

Fig. 20 Functional box-counting analysis of the field $f(r)$. In A the field is shown with two isolines that have threshold values $T_2 > T_1$; the box size is unity. In B, C, and D, we cover areas whose value exceeds T_1 by boxes that decrease in size by factors of 2. In E, F and G the same degradation in resolution is applied to the set exceeding threshold T_2.

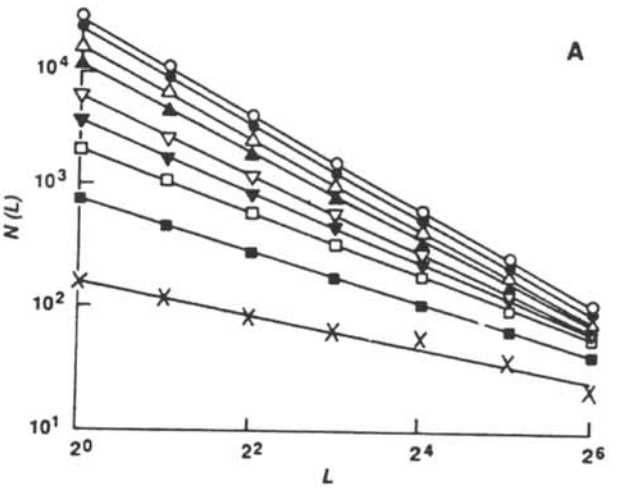

Fig. 21a A plot of $N(L)$ versus L for a single radar scan with nine radar reflectivity thresholds increasing (top to bottom) by factors of ≈ 2.5, analyzed with horizontal boxes increasing by factors of 2 in linear scale. The negative slope (dimension) decreased from 1.24 to 0.40. From Lovejoy *et al.* (1987).

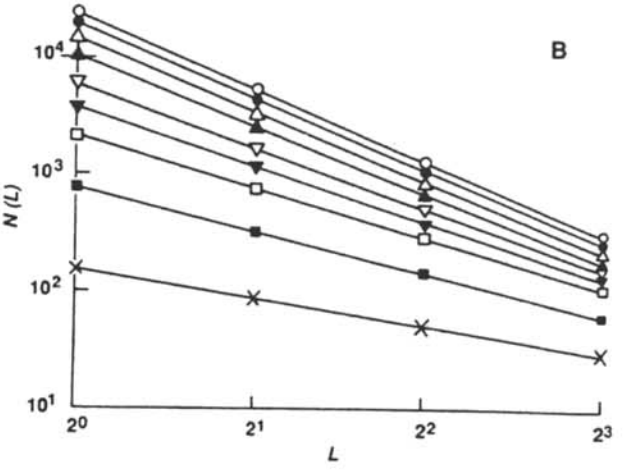

Fig. 21b Same volume scan as Fig. 21a except that the boxes used are cubical and yielded values of dimension that decreased from 2.18 to 0.81 for the same thresholds. Only eight vertical levels were available. See text for discussion of the vertical anisotropy, and 'elliptical box counting'. From Lovejoy *et al.* (1987).

limitations are summarized and studied in detail in Lavallée *et al.*, 1991a, Lavallée, 1991; they are a) the divergence of moments which leads to 'spurious' or 'pseudo-scaling', b) finite sample size. Both effects will lead to asymptotically straightline exponents (as observed in both Figs. 1 and 18); corresponding to multifractal phase transitions. In order to overcome these difficulties, other methods which avoid the use of statistical moments were developed. The first of these was 'functional box counting' (Lovejoy *et al.*, 1987). This method is straightforward: the empirical fields are first converted into finite resolution sets by using a series of thresholds; the sets of interest being defined by the regions exceeding the threshold (T), see the schematic illustration Fig. 20. In the second step, the resolution of these sets is degraded systematically by covering the sets with boxes of increasing size (the standard 'box-counting' procedure for analysing strange attractors). The dimension as a function of threshold is then obtained as the (negative) logarithmic slope of the number of boxes $N_T(L)$ as a function of the log of the box size (L). Fig. 21a, b shows the result when this method is applied to radar rain data, Fig. 22 when it is applied to the associated cloud fields (from satellite data). Again, the (multiple) scaling is well respected.

Hubert & Carbonel (1988, 1989, 1991) have used functional box-counting to study rainfall time series from Burkina Faso raingauges, finding that the multiscaling extends from one day to at least a year. For example they found that the fractal dimension of wet days was ≈ 0.8 which meant that local rule of thumb knowledge of the climate (7 wet months/year) could be extended down to at least a day since $\log 7/\log 12 \approx 0.8$.

Other related applications of functional box counting in rain can be found in Olsson *et al.* (1990), satellite cloud pictures in (Gabriel *et al.*, 1988; Baryshnikova *et al.*, 1989; Detwiller, 1990), and *in situ* measurements of cloud liquid water (Duroure & Guillemet, 1990). Although functional box-counting has the advantage of avoiding the use of statistical moments, it has the basic problem that it is not easy

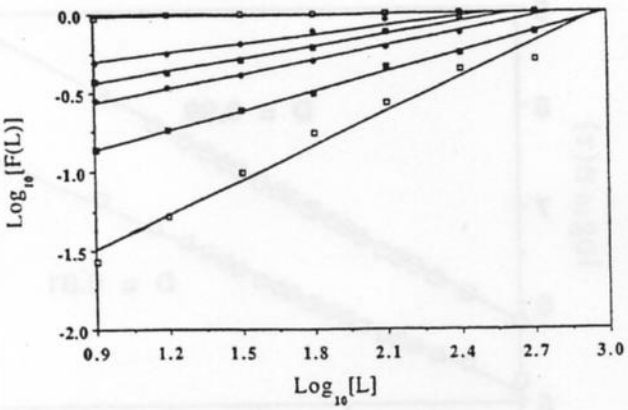

Fig. 22a A plot of the fraction $F_T(L)$ of cloud pictures exceeding a threshold T, for six radiance thresholds with L increasing for 8 to 512 km, at visible wavelengths. From a GOES (geostationary) satellite picture over the Montreal region (summer with mostly cloud cover). The minimum digital count is 24 (ground), maximum is 52 (bright cloud) corresponding to a brightness ratio of $(52/24)^2 \approx 4.7$. The fraction is estimated by using box counting to degrade the resolution of exceedance sets, and then calculating the fraction of all the boxes available at resolution L: $F_T(L) = N_T(L)/L^{-2}$. The straight lines indicate that over the range (which includes most of the meso-scale), that the scaling is accurately followed. From Gabriel *et al.* (1988).

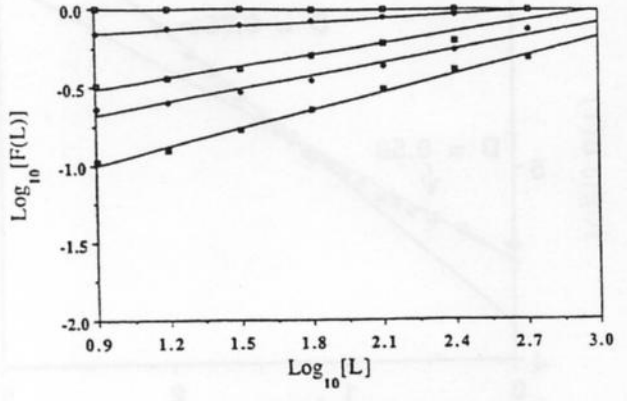

Fig. 22b Same as Fig. 22a except for the corresponding infrared image. The straight lines correspond to effective black body temperatures of (top to bottom) 17, 9, 2, −5, −23 °C respectively. Here the lowest radiances (proportional to the fourth power of the temperature) comes from the sparsest (highest) cloud tops.

to relate the threshold to the order of singularity[65] γ. Another related problem is its tendency to 'saturate' in certain situations because all the boxes larger than a given scale can be filled, a problem likely associated with statistical nonconservation ($H \neq 0$). Finally, the method does not take into account whether a given box is filled by more than one pixel (it is an all or nothing estimator). For a critique of this method, see Lovejoy & Schertzer, 1990a (Appendix A), and Lavallée (1991).

Direct application of functional box-counting requires gridded data. We now describe a variant which is useful for highly inhomogeneous raingage network data (indeed, as shown in Lovejoy *et al.* (1986), they are more nearly uniform over a fractal than over a surface[66]). Define the 'exceedance stations' as all the stations whose rain rate exceed a given threshold, and then calculate the number of pairs of exceedance stations that are closer than a distance[67] l (this is proportional to the average number of exceedance stations in a circle radius l). The resulting scaling exponent is called the 'correlation dimension'; it will less than or equal to[68] the corresponding fractal (box-counting) dimension. Fig. 23a shows[69] the result when the method is applied to daily rain accumulations for 1983 (roughly 8000 stations were used), for various exceedances levels up to 150 mm/day. Although the statistics become poor at the high thresholds, the lines are fairly straight indicating that the scaling is well respected (over the range $\approx$3 km–5000 km). Note that the zero level exceedance line is also included; this has a nontrivial fractal dimension ($\approx$1.78 here) due to the fractal nature of the network.

This method of improving statistics by examining pairs of points can also be applied to time series. Tessier (1993) has used this method to effectively study the scaling of increasingly wet stations using the same global daily rainfall data set. Fig. 23b shows that the value 0.8 for wet/dry days (using a threshold of 0.1 mm/day) seems to be global (rather than specific to the Sahel, Hubert & Carbonnel 1988). However, Fig. 23c, d indicate that a definite scale break occurs at $\approx$3 weeks for higher thresholds, consistent with the existence of a 'synoptic maximum' (see Fig. 4d; i.e. a break whose duration corresponds to the lifetime of global sized rain events).

The probability distribution/multiple scaling technique (pdms)

A more successful way of estimating $c(\gamma)$ is to directly exploit the scaling of the probability distributions of the multifractals as indicated in equation 7. Methods which directly exploit this equation were developed and baptized 'prob-

[65] This can be done approximately via the relation $T \sim L^{-\gamma}$, but the normalization (which is required to nondimensionalize this relation and determine the proportionality constant), is nontrivial, and cannot be completely determined at a single averaging resolution.

[66] In fact it is even better to treat the density of stations as a multifractal.

[67] To account for the curvature of the earth, the following measure of distance should be used:

$$l = r\sqrt{(8(1-\cos\theta/2))},$$

where r is the radius of the earth, θ is the angle subtended at the centre of the earth by the two stations (Lovejoy *et al.*, 1986).

[68] In practice, the difference is usually small.

[69] We thank C. Hooge for help with this analysis.

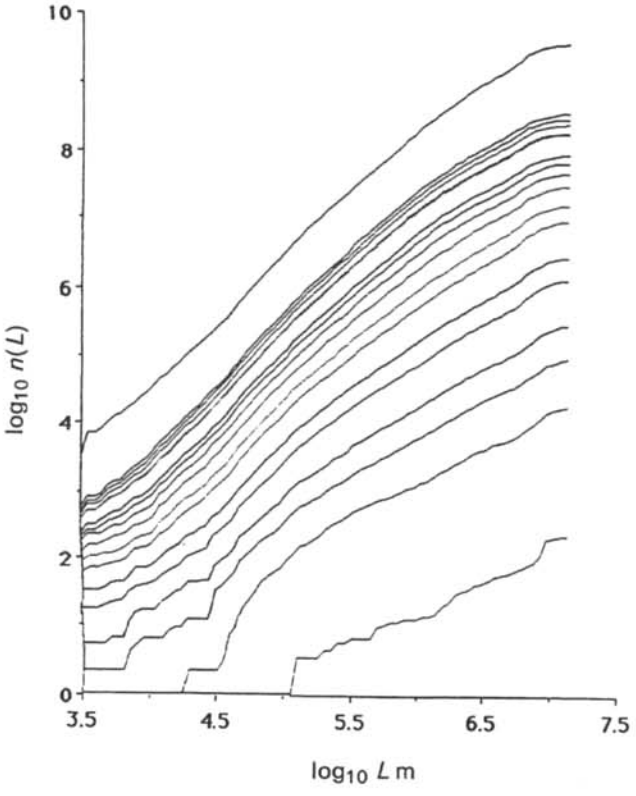

Fig. 23a The correlation function (the average number of exceedance stations in a circle) $n(L)$ as a function of radius (L), for various thresholds. From top to bottom, the thresholds (in mm for daily accumulations) are 0, 0.1, 0.2, 0.4, 0.8, 1.6, 2.5, 3.2, 5.0, 6.4, 10.0, 12.8, 17.5, 20.0, 25.0, 40.0, 52.5, 76.0, 150.0. Note that at least some of the deviations from straight line (scaling) are due to the imperfect scaling of the network itself (top line).

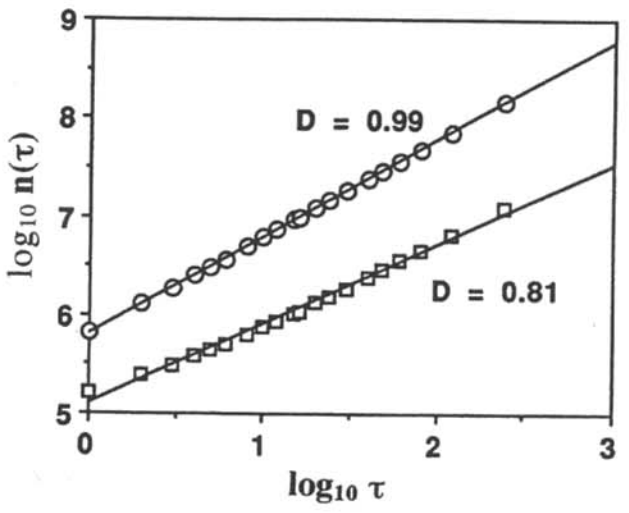

Fig. 23b The number $n(\tau)$ of exceedance pairs for daily accumulations in time τ (for a year), accumulated over all 8000 stations. Since many stations frequently had missing data, it was first confirmed (top curve) that the pattern of missing data was not itself fractal (the slope is consistent with a dimension 1 on the time axis, hence nonfractal data outages). The line below is only for those stations whose accumulation was above the minimum detectable level 0.1 mm/day. From Tessier (1993).

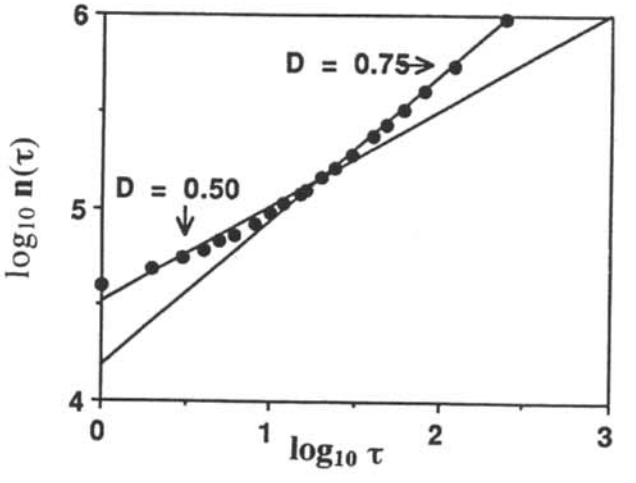

Fig. 23c Same as Fig. 23b except for a threshold of 1.28 cm/day, showing a clear break at about three weeks (the 'synoptic maximum'). From Tessier (1993).

ability distribution/multiple scaling' techniques (PDMS) in Lavallée *et al.* (1991a), Lavallée (1991). They are distinguished from other histogram based techniques (e.g. Paladin & Vulpiani, 1987; Atmanspacher *et al.*, 1989) in that they overcome the nontrivial problem of the (slowly varying) proportionality constants in equation 7 by examining the histograms over a range of scales rather than at a single scale. The drawback of these methods is that they are quite sensitive to the correct normalization of the field: the ensemble average of the large scale spatial average must satisfy $\langle R_1 \rangle = 1$ (i.e. in rain, the large scale, climatological rate must be used). An early implementation in rain is given in Seed (1989) (see e.g. Fig. 24) who studied radar reflectivities of four separate convective storms in Montreal. However, the statistical estimation of H, C_1, a from $c(\gamma)$ is a poorly conditioned nonlinear regressions and leads to low accuracies in the estimates. Nonetheless, Seed found α in the range 0.3–0.6 and C_1 in the range 0.6–1.0. Although he averaged in space, he pooled statistics into histograms involving many (~ 144) consecutive 5 minute PPIs. His estimates are in fact close to the more accurately estimated temporal parameters found here.

Another application of PDMS to rain is described in Tessier *et al.* (1994), where it is applied to the global meteorological network (Fig. 25) used to estimate global rain.

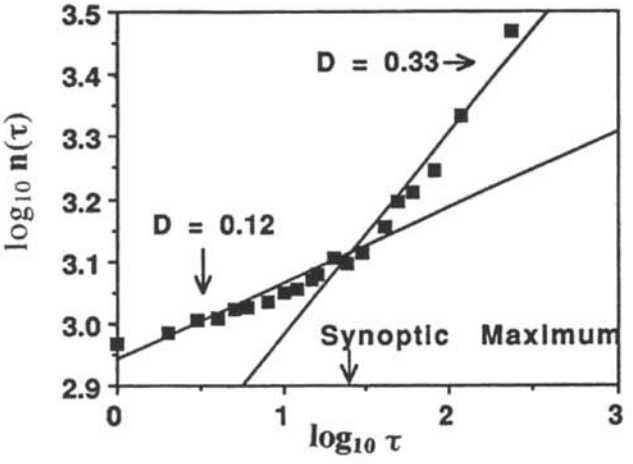

Fig. 23d Same as 23c except for a (very high) threshold of 10.24 cm/day, showing the same break at about three weeks and much lower dimensions. From Tessier (1993).

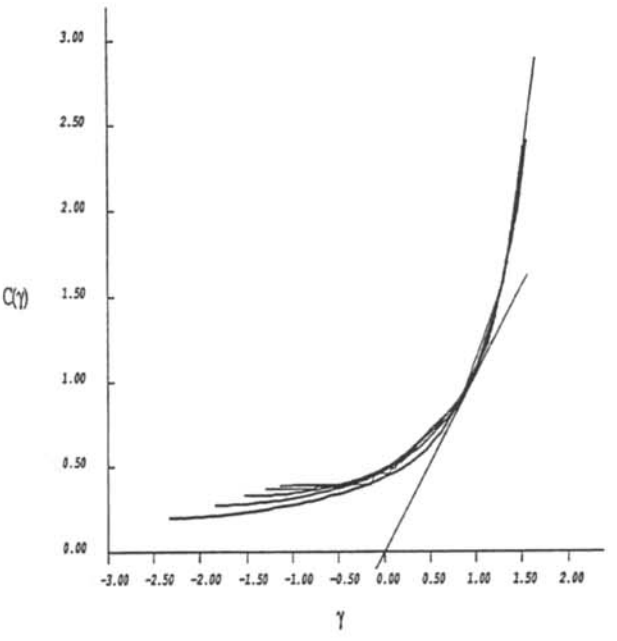

Fig. 24 An early implementation of the PDMS technique on radar reflectivities during a summer storm in Montreal (August 14th, 1988), using 144 consecutive CAPPIs (Constant Altitude Plan Position Indicators, i.e. constant altitude reflectivity maps), at five minute intervals. The codimension function was estimated at scales of 2, 4, 8, 16, 32 and 64 km from the corresponding probability distributions (of spatially degraded reflectivities) using the following approximation: $c(\gamma) \approx -\log(Z_\lambda)/\log\lambda$ (i.e. setting the proportionality coefficient in equation 7 equal to unity). The resulting estimates for each of 6 resolutions is shown, along with a smooth curve obtained by nonlinear regression using the theoretical (universal) formula equation 12. The universal parameters can be graphically estimated using the construction line (the bisectrix $x=y$) shown, which exploits the fact that for a conserved multifractal ($H=0$), $c(C_1)=C_1$, $c'(C_1)=1$, i.e. the bisectrix will be tangent to $c(\gamma)$ at the point C_1 (see Figs. 12, 13). From the graph we immediately deduce that $H \approx 0$, (from equation 12, $H \neq 0$ leads to a left/right shift of $c(\gamma)$ with respect to the bisectrix), $C_1 \approx 0.9$, and from some other point on the curve (e.g. the value of $c(0)$) we deduce $\alpha \approx 0.55$. From Seed (1989).

Direct estimates of universality parameters: double trace moments

Above, we reviewed the results of multifractal analysis techniques which in principle could be applied to arbitrary multifractals. They enjoyed the apparent advantage of making no assumptions about the type of multifractal being analyzed. In practice however, the techniques are overly ambitious: for a finite (and usually small) number of samples of a process, they attempt to deduce an entire exponent function, with the result that there is considerable uncertainty in the resulting estimates of $c(\gamma)$ or $K(q)$. With the realization that physically observable multifractals are likely to belong to universality classes, it is natural to develop specific methods to directly estimate the universality parameters (H, C_1, α). These parameters can then be used to determine $c(\gamma)$, $K(q)$ from equations 12–13.

The double trace moment (DTM) technique (Lavallée, 1991; Lavallée *et al.*, 1991d) directly exploits universality by generalizing the trace moment; it introduces a second moment η by transforming the high resolution field $\varphi_{\lambda'} \Rightarrow \varphi_{\lambda'}^{\eta}$. This transforms the flux Π into an 'η flux'

$$\Pi_\lambda^{(\eta)}(B_\lambda) = \int_{B_\lambda} \varphi_\lambda^\eta \, d^D x, \text{ see (16)} \tag{18}$$

The double trace moment can then be defined as:

$$\mathrm{Tr}_\lambda(\varphi_\lambda^{(\eta)})^q = \left\langle \sum_i [\Pi_\lambda^{(\eta)}(B_{\lambda,i})]^q \right\rangle \approx \lambda^{K(q,\eta)-(q-1)D} \tag{19}$$

where we have introduced the (double) exponent $K(q,\eta)$, which reduces to the usual exponent when $\eta = 1$: $K(q,1) = K(q)$ (the sum is over all disjoint boxes indexed by i). Note that the basic implementation of the DTM is quite straightforward[70]; the field at the highest available resolution is raised to the power q, the result is iteratively degraded in resolution and the qth moment averaged over the field and the ensemble of samples available – see Fig. 14 for a schematic illustration.

The entire transformation from single to double trace moments (i.e. taking η powers and then integrating) can be summarized in the following formulae (where the prime indicates transformed, double trace quantities, not differentiation):

[70] Note that, if $H>0$ the data will require some 'prewhitening' before the application of the DTM, i.e. power law filtering to yield a conserved field.

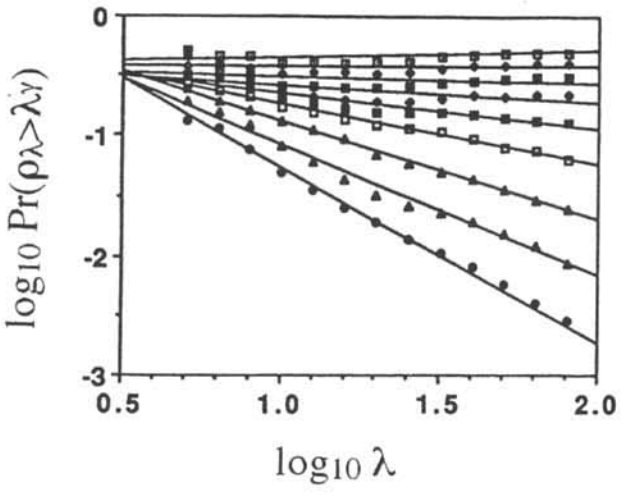

Fig. 25 Probability Distribution/Multiple Scaling analysis of the NMC network (Fig. 26), $\log_{10} \Pr(\rho_\lambda > \lambda^\gamma)$ vs. $\log_{10}\lambda$ for γ increasing in 0.1 intervals from 0 (top) to 0.8 (bottom line), the absolute slopes give $c(\gamma)$, ρ_λ is the station density at resolution λ. $\log_{10}\lambda = 0$ corresponds to the largest scale (here ≈ 15000 km), the (multiple) scaling is well followed up to $\log_{10}\lambda \approx 2$ (≈ 150 km); for smaller scales, the finite number of stations leads to a break in the scaling. Using nonlinear regressions, the universal parameters were estimates as $\alpha \cong 0.8$, $C_1 \approx 0.5$. From Tessier *et al.* (1994).

$$\gamma \Rightarrow \gamma' = \eta\gamma - K(\eta) \tag{20a}$$

$$c(\gamma) \Rightarrow c'(\gamma') = c(\gamma) \tag{20b}$$

$$q \Rightarrow q' = q/\eta \tag{20c}$$

$$K(q) \Rightarrow K'(q') = K(q,\eta) = K(\eta q') - q'K(\eta) \tag{20d}$$

Note the subtlety in the above: due to the integration in equations 18–19, we are dealing with dressed rather than bare quantities, hence the dressed singularities (equation 20a) transform with an extra term $(-K(\eta))$; necessary since the dressing operation enforces conservation of the η flux.

The real advantage of the DTM technique becomes apparent when it is applied to universal multifractals (Lavallée,1991) since we obtain the following transformations of C_1:

$$C_1 = \left.\frac{dK}{dq}\right|_{q=1} \Rightarrow C_1' = \left.\frac{dK'}{dq'}\right|_{q'=1} = C_1\eta^\alpha \tag{21}$$

Therefore, $K'(q') = K(q,\eta)$ has a particularly simple dependence on η:

$$K(q,\eta) = \eta^\alpha K(q) \tag{22}$$

α can therefore be estimated on a simple plot of $\log K(q,\eta)$ vs. $\log \eta$ for fixed q. By varying q, we improve our statistical accuracy. Finally, note that since equation 20d is only valid when the relevant statistical moments converge, and the sample size is sufficiently large to accurately estimate the scaling exponents, whenever $\max(q\eta, q) > \min(q_\alpha, q_D)$ the above relation will break down; $K(q,\eta)$ will become independent of η. We shall see that effective exploitation of the above involves a 'bootstrap' procedure in which the well estimated low q, η exponents are used to estimate α, C_1, and then equations 14a, b can be used to predict the range of reliable estimates.

In comparison with existing multifractal analysis methods, the DTM technique has two advantages. First, the estimated scaling exponent $K(q,\eta)$ is independent not only of the normalization at the largest scales, but also of the change $\gamma \Rightarrow \gamma + b$ corresponding to a translation in γ space – in the bare quantities[71]. The second is that when a multiplicative change of γ is made ($\gamma \Rightarrow a\gamma$) then relation for $K(q,\eta) \rightarrow K(q, a-\eta) = a^\alpha K(q,\eta)$ (when a corresponds to a contraction in the γ space, but is also equivalent to the integration of the fields φ_A at an unknown power a by the experimental apparatus). This implies that the determination of α will also be independent of the power a to which the process is raised. In other words the universality has been exploited to give a method to determine α which is invariant under the general transformation $\gamma \Rightarrow a\gamma + b$!

Estimating H

We have seen that in multiplicative processes, it is convenient to isolate an underlying conserved quantity which has basic physical significance; in turbulence it was the energy flux to smaller scales, in rainfall we denoted it by φ, and related it to the rain fluctuations via equation 3. In terms of the scaling, conservation means $\langle \varphi_\lambda \rangle$ = constant (independent of λ), hence $K(1) = 0$. If we consider the energy spectrum of φ_λ, it is of the form $k^{-\beta}$ with[72] $\beta = 1 - K(2)$, i.e. the spectrum is always less steep than a $1/f$ noise[73].

The reason for dwelling on this is that it illustrates a basic point common to most geophysical fields viz, their spectra often have $\beta > 1$, hence they cannot be conservative processes, they must be[74] (fractionally) differentiated by order $-H$ (the spectra must be power law filtered by k^H) to become conservative. Lavallée (1991) analyzed simulations of conserved processes fractionally integrated and differentiated by varying amounts. As long as he differentiated (filtered by k^H with $H > 0$) using the DTM technique, he obtained stable and accurate estimates of both C_1 and α; however when he fractionally integrated ($H < 0$), he only recovered α. C_1 was

[71] This is also true of single trace moments or partition function approaches.

[72] This formula is a consequence of the fact that the energy spectrum is the Fourier transform of the autocorrelation function which is a second order moment.

[73] The difference is often not great since $K(2)$ is usually small: $= C_1(2^\alpha - 2)/(\alpha - 1)$, and $0 \le \alpha \le 2$.

[74] See Schertzer & Lovejoy (1991, Appendix B.2) for more discussion of fractional derivatives and integrals.

not accurately determined[75]. From the C_1, α estimated this way, we can determine $K(2)$ from equation 11 and hence[76], writing β for the spectral slope of the observed process, the order of fractional integration required to go from the conserved process to the nonconserved (observed) process is given by:

$$H=\frac{\beta-1+K(2)}{2}=\frac{\beta-1}{2}+\frac{C_1(2^\alpha-2)}{2(\alpha-1)} \tag{23}$$

In many data analyses, it is possible to avoid the use of Fourier space. In $1-D$ we have already recalled that replacing the time series by its differences is approximately the same as multiplying by k in Fourier space[77]. To generalize this to two (or more) dimensions, one possibility is to use a finite difference Laplacian. This multiplies by $|k|^2$ in Fourier space, hence the spectrum by $|k|^4$; although this is quite drastic we have found that it apparently works fairly well. A method involving less smoothing which also works well, is to replace the field by the modulus of the local finite difference gradient operator.

As a final comment, it is possible to directly estimate H via (first order) structure functions (the scaling of absolute differences). However, current direct methods are designed for time series analysis, the optimum extension for fields in two or higher dimensions is not clear. Other methods such as the probability distribution and R/S analysis methods used in Lovejoy (1981) when applied to multifractals yield results which are not directly related to the multifractal parameters; the value $H\approx 0.5$ quoted earlier (which assumed simple scaling) needs careful reconsideration.

ESTIMATES OF UNIVERSAL MULTIFRACTAL EXPONENTS IN RAIN —

Analyses of rain gage network in space and multifractal objective analysis

A basic problem with *in situ* geophysical measurements – such as those from rain networks – is that the networks are typically sparse, they have 'holes' at all scales. An early method for dealing with this problem involved characterizing the sparseness by fractal dimensions, for example, Lovejoy *et al.* (1986) found a fractal dimension of ~ 1.75 in the ≈ 10000 station network reporting to the World Meteorological Organization indicating that 'holes' do indeed occur over a wide range of scales. Using (generalized) intersection theorems and ordinary trace moments, Montariol & Giraud (1986), Giraud *et al.* (1986), Marquet & Piriou (1987) and Ladoy *et al.* (1987) showed how corrections to network infered rain statistics could be made by subtracting appropriate network codimensions from the corresponding measured rain codimensions. Below, we examine the daily rainfall accumulations observed by raingages at synoptic weather stations[78] covering the earth for the year 1983 (Fig. 26).

Fig. 26 Position of the stations reporting daily rainfall accumulations in 1983 that have been used in our analysis.

Actually, it is better to treat the density of stations as a multifractal measure (rather than the stations themselves as a fractal set, see Fig. 25), and then to statistically correct for the multifractal nature of the network density. In what follows we summarize the results of Tessier *et al.* (1994). Consider that the measuring stations have a multifractal density ρ_λ when measured at resolution λ. This is found (see Fig. 25) to be a reasonable approximation to the density field over the range $\sim 5.0\times 10^3$ km to $\sim 1.5\times 10^2$ km (the lower limit arises because there were only ~ 8000 stations which is quite small for this type of analysis).

Over the multifractal range, the station density may be estimated in a variety of ways, for example by counting the number N_λ of stations in a circle of radius λ^{-1} (taking the size of the earth = 1), and then[79] $\rho_\lambda\approx N_\lambda\lambda^2$. Consider now the product measure $M_\lambda=\rho_\lambda R_\lambda$. In the i^{th} circle $B_{\lambda,i}$, it can be estimated as follows:

$$\lambda^2\sum_{j\in B_{\lambda,i}} R_j\cong\lambda^2 N_{\lambda,i}R_{\lambda,i}=M_{\lambda,i}=\rho_{\lambda,i}R_{\lambda,i} \tag{24}$$

where the sum is over the measured rain rates (indexed by j) of the stations in the ith circle. If we now suppose statistical independence of ρ, R, by taking qth powers and ensemble averaging we immediately obtain:

$$K_R(q)=K_M(q)-K_\rho(q) \tag{25}$$

[75] This indicates that as long as the spectrum is less steep than the underlying conserved process ($\beta<1-K(2)$), that we can recover C_1.

[76] In the case of turbulence, it is not necessary to infer the relation since it is given by dimensional analysis from known dynamical quantities. In rain, we don't know the corresponding dynamical (partial differential) equations, nor their conserved quantities, so that this type of empirical inference is unavoidable.

[77] Because of the finite differencing, this will not be exactly true at the highest frequencies corresponding to the resolution the series.

[78] This data set was archived at the National Meteorological Center (NMC) of NOAA; it is not exactly the same as the WMO set.

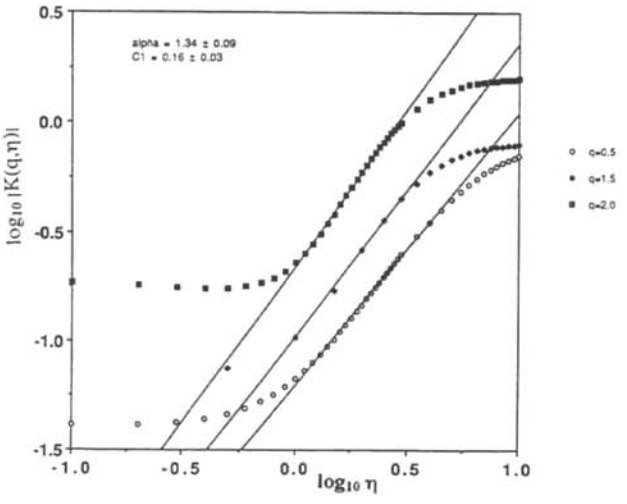

Fig. 27 $\log(|K(q,\eta)|)$ versus $\log(\eta)$ for daily rainfall accumulations on a global network after the corrections explained in the text. The regression lines (for $q=0.5$, 1.5, 2, bottom to top respectively) give a value of $\alpha=1.35\pm0.1$ and $C_1=0.16\pm0.05$. From Tessier *et al.* (1993).

Tessier *et al.* (1993) indicate how to generalize this result to double trace moments ($K(q,\eta)$); the principle is the same, subtract the measured K_M, from the network[80] K_ρ: $K_R(q,\eta) = K_M(q,\eta) - K_\rho(q,1)$. From such an analysis we obtain $\alpha = 1.35\pm0.1$ and $C_1=0.16\pm0.5$ as may be seen on Fig. 27 where we have plotted $\log|K(q,\eta)|$ vs $\log\eta$ for $q=0.5$, 1.5, 2. We see that for large values of η the curve $K(q,\eta)$ becomes flat, here due to limited sample size, whereas at low values of η, it also becomes flat due to the sensitivity of the low order moments to noise and/or the presence of a minimum order of singularity.

The classical radar observer's problem for multifractal reflectivity fields and estimates of C_1, α from radar

Up to now, we have discussed various fractal and multifractal analyses of radar rain reflectivity data, carefully distinguishing this from the rain rate. The exact relationship between the radar reflectivity and the rain rate (R) is an unsolved problem going back to the 1940s. Standard (non-scaling) theory already leads to power law relations between the two and we have already mentioned the monofractal (Lovejoy & Schertzer, 1990c) corrections that can be used to improve the latter. In this section we summarize some recent theoretical results (Lovejoy & Schertzer, 1990a) on this 'classical'[81] multifractal 'observer's problem'.

In its classical form (Marshall & Hitschfeld, 1953, Wallace, 1953), the observer's problem makes assumptions of subsensor homogeneity (specifically that the rain drops have uniform (Poisson) statistics over scales smaller than the radar 'pulse volume': typically about 1 km^3). The variability in observed 'effective'[82] radar reflectivity factor Z_{eff} is then considered to arise from two sources. The first is the natural variability of interest characterized by the 'reflectivity factor' Z (proportional to the variance of the drop volumes). The second arises as a result of the random positions of each of the drops within the pulse volume. Under certain assumptions about the homogeneity of the field and on the form of the drop size distribution (finite variance, $q_D>2$), Z can be related to the rain rate, total volume of liquid water, or other parameters of interest[83].

Figs. 2a, b, c, d, Fig. 4a, b and Figs. 16a, b already point to the inadequacy of the assumptions of homogeneity (even at subwavelength scales); even the assumption of finite variance is not trivially respected. In spite of this, based on these assumptions, much work has been done to devise sampling and averaging strategies to obtain Z from Z_{eff}. In this section, we indicate that even with these subsensor homogeneity assumptions, that correction can still arise if we allow for a multifractal Z field from the largest scales down to the radar scale; hence even in the standard theory, we must still account for multifractal effects. Introducing the natural log of the range in scales[84] ($\zeta=\ln\lambda$) and the measured codimension function $c_{\text{eff}}(\gamma)$ (for Z_{eff}) we seek to relate this to the underlying $c(\gamma)$ (for Z). The basic result of Lovejoy & Schertzer (1990a) is:

$$\Delta c(\gamma) = c(\gamma) - c_{\text{eff}}(\gamma) = \frac{c'(\gamma)[\ln c'(\gamma) - 1]}{\zeta} + O\left(\frac{1}{\zeta^2}\right) \qquad (26)$$

hence for λ large enough, $c_{\text{eff}}(\gamma) \Rightarrow c(\gamma)$: in the limit where the natural variability builds up over a sufficiently wide range of scales (i.e. that the radar resolution is much smaller than the outer scale of the rain producing processes), the two are equal[85]. In other words, in this limit the natural variability is so strong that it completely dominates that arising from random fluctuations due to drop phases. This answers the

[79] Ignoring factors of π; this will be a good approximation when $N_\lambda \gg 1$.

[80] The double trace moment is with respect to the measure $\rho d^D x$, rather than the usual $d^D x$; hence the $K_\rho(q,1)$ rather than $K_\rho(q,\eta)$. $K_\rho(q,1)$ is easy to estimate since $K_\rho(q,1) = K_M(q,0)$.

[81] 'Classical' because we assume subresolution homogeneity; the multifractals are (unrealistically) assumed to be cutoff at this scale.

[82] In this subsection we denote the 'effective reflectivity factor' by Z_{eff}, and the 'reflectivity factor' by Z; in the rest of the paper, for convenience, we drop the subscript 'eff'; Z denotes the measured 'effective' quantity, we do not require the (unobserved, theoretical) 'reflectivity factor'.

[83] The fact that individual radar echoes have long tails (e.g. Figs. 2b, c) and that the drops are highly non uniformly distributed means that in reality, Z can only be statistically estimated from Z_{eff} – ultimately it will probably be simpler to statistically relate the Z_{eff} directly to the rain rate; use of the unmeasureable Z will be unnecessary.

[84] Taking a typical radar resolution of 1 km, and an external scale for the rain processes at 1000 to 10000 km, we find ζ in the range $\ln(1000)$ to $\ln(10000) \sim 7$–9.

[85] Using data from Seed (1989), Lovejoy & Schertzer (1990a) estimated that the largest correction to $c(\gamma)$ is ~ 0.14.

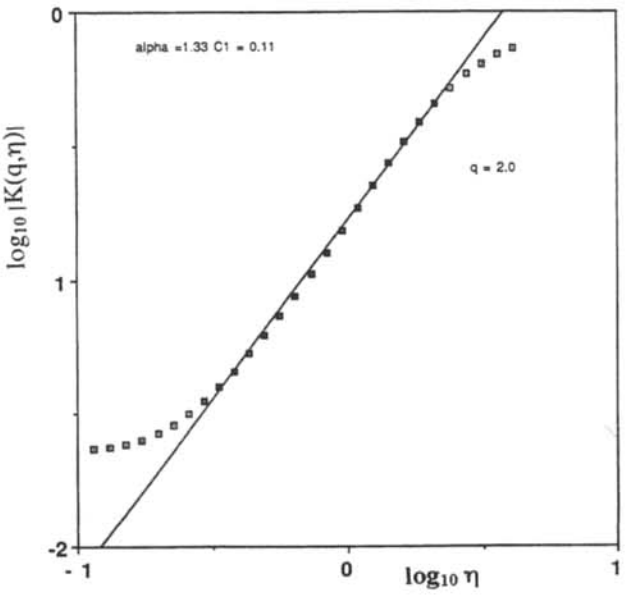

Fig. 28a $\log(|K(q,\eta)|)$ versus $\log(\eta)$ for the gradient of vertically pointing radar reflectivities in the vertical direction (128 elevations at 21 m intervals), for $q=2$, statistics accumulated over 8192 consecutive pulses at 2 second intervals. The straight line indicates $\alpha=1.35$, $C_1=0.11$. From Tessier *et al.* (1993).

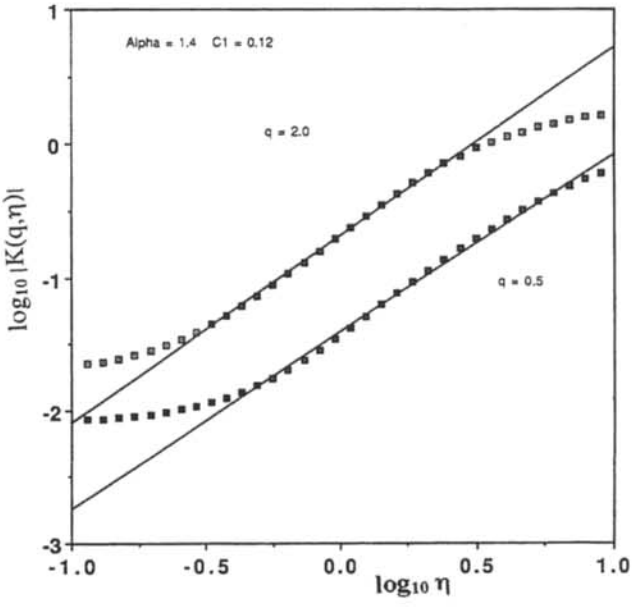

Fig. 28b $\log(|K(q,\eta)|)$ versus $\log(\eta)$ for the gradient of the horizontal radar reflectivities (same data as in Fig. 4f) at 75 m resolution. The bottom curve is for $q=0.5$ and the top for $q=2.0$. The straight line indicate $\alpha=1.40$, $C_1=0.12$. From Tessier *et al.* (1993).

question raised by Zawadzki (1987) as to which variability is strongest.

We now seek to explore the relation between the reflectivity factors and rain rates. Limiting ourselves to studying the implications of the usual semi-empirical relations, (based again on subresolution homogeneity) we find the simplest statistical relation between Z and R is a power law i.e. $Z \propto R^a$. Such power laws are frequently invoked in rain (e.g. the well known semi-empirical Marshall–Palmer (1948) law has exponent $a=1.6$). Writing $Z=\lambda^{\gamma_Z}$ and $R=\lambda^{\gamma_R}$ this is equivalent to the linear transformation of singularities: $\gamma_z=a\gamma_R$ where γ_z is the singularity in Z and γ_R is the corresponding singularity in R. We have already seen (equation 20 with $\eta=a$) that under such transformations, $\alpha \Rightarrow \alpha$, $C_1 \Rightarrow C_1 a^\alpha$.

Fig. 28a shows the results for vertical pointing radar reflectivities yielding $\alpha_z \approx 1.35$ and $C_{1z} \approx 0.11$ (vertical direction) and Fig. 28b for a horizontal pointing radar yielding $\alpha_z \approx 1.40$ and $C_{1z} \approx 0.12$ (horizontal direction) showing remarkable agreement with α for network rain, and between the vertical and horizontal directions. To estimate H, we may use the horizontal estimate of β (≈ 1.45, Fig. 4f), to yield $H_{Zhor} \approx 0.32$, and in the vertical, using the estimate $\beta \cong 2.3$ (Tessier *et al.*, 1991a), we obtain $H_{Zhor} \approx 0.73$. The agreement between the values of α is particularly significant considering the apparently very different natures of the data sets involved. The C_1 estimates are comparable, although

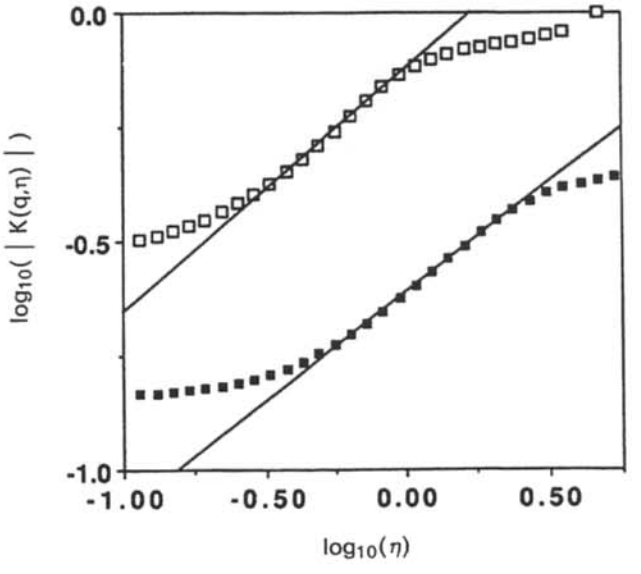

Fig. 28c $\log(|K(q,\eta)|)$ versus $\log(\eta)$ for the gradient of vertically pointing radar reflectivities in time (8192 consecutive pulses at 2 second intervals) and statistics accumulated for 128 elevations at 21 m intervals (same data set as Fig. 28a). The straight line indicates $\alpha=0.50$, $C_1=0.60$. From Tessier *et al.* (1993).

Table 3. *A comparison of various gauge and radar estimates of α, C_1, H over various space scales and directions. Particularly significant is the agreement between the a estimates from such disparate sources. The errors in α are estimated to be about ± 0.1, in C_1, ± 0.05. The value of H is poorly estimated. The value $\alpha \approx 1.35$, $C_1 \approx 0.15$ is the same as that obtained by Tessier* et al. *(1991a) for visible and infra red cloud radiances. It is also very near that found by Schmitt et al. (1991) for turbulent temperatures*

Data type	Radar reflectivity, Montreal	Gauge, daily accumulations	Radar reflectivity, Montreal
Domain	horizontal space	horizontal space	vertical space
Data type	radar reflectivity	daily gauge accumulations	radar reflectivity
Range of scales	75 m to 19.2 km	$\approx$150 km to global	21 m–2.5 km
α	1.40	1.35	1.35
C_1	0.12	0.16	0.11
H	0.32	0.2 ± 0.3	0.73
References:	Tessier *et al.* 1993	Tessier 1993	Tessier *et al.* 1993

Table 4. *A comparison of various gauge and radar estimates of α, C_1 over various time and space scales. All parameters were estimated from the DTM technique with the exception of the Seed (1989) study. Note that the C_1 value for reflectivities are not expected to be the same as for the gauge rain rates*

Data type	Gauge, daily accumulations	Gauge, daily accumulations	Gauge, daily accumulations	Gauges, daily accumulations	Radar reflectivity	Radar reflectivity
Location	Global network	Reunion island	Nimes	Germany	Montreal	Montreal
Sample characteristics	1000 stations, 1–64 days	1 station, 30 years, scales 1–64 days	1 station, 30 years, scales 1–64 days	1 station, 45 years, scales 1–32 days	4 storms, 144 PPIs each 1 km resolution every 5 minutes	1 storm, vertically pointing radar 20 m resolution, every 2 s for $5\frac{1}{2}$ hours
α	0.5	0.5	0.5	0.6	0.3–0.6	0.5
C_1	0.6	0.2	0.6	0.5	0.6–1.2	0.6
References	Tessier *et al.* 1993	Hubert *et al.* 1993	Ladoy *et al.* 1993	Larnder & Fraedrich*	Seed 1989	Tessier *et al.* 1993

Note:
* = Private communication.

differences[86] are to be expected if only because of the Z–R relation, and the horizontal/vertical anisotropy[87]. This is the first empirical agreement between any fundamental statistical rain gauge and reflectivity parameters and gives us confidence in the value obtained. Table 3 shows an overall comparison of these spatial estimates.

Double Trace Moments and the statistics of rain in time

The scaling of rain in space coupled with the scaling of the dynamic (wind) field leads to temporal scaling. Theoretically, the appropriate framework for treating the problem is via scaling space/time transformations and Generalized Scale Invariance; this is discussed in the next section, here we summarize various recent empirical results. Table 4 is a summary of six independent analyses from four different locations, different data types, ranges of scale and analysis methods, studies indicating a remarkable consistency[88] in estimates of α, C_1, especially α. Considering only the gauge estimates, we obtain $\alpha \approx 0.5 \pm 0.1$, $C_1 \approx 0.5 \pm 0.1$. Unfortunately, at present the temporal value of H is not well known. A rough estimate can be obtained from the high frequency end of Fig. 4d: $\beta \approx 0.5$. If we use the corresponding values of α, C_1 we obtain[89] (using equation 23), $H \approx 0.1 \pm 0.1$, i.e. it is

[86] Differences could also arise because of the limited sample sizes used in the various studies, and because C_1 may in fact vary climatologically: the theoretical arguments for the universality of C_1 are less convincing than for α.

[87] From the values quoted above, it seems that the most obvious effect of anisotropy is to modify the values of H.

[88] The theoretical arguments leading to the expectation of a universal C_1 are much weaker than those for a universal α.

[89] Using the mean of the individual H values also yields $H \approx 0.1 \pm 0.1$.

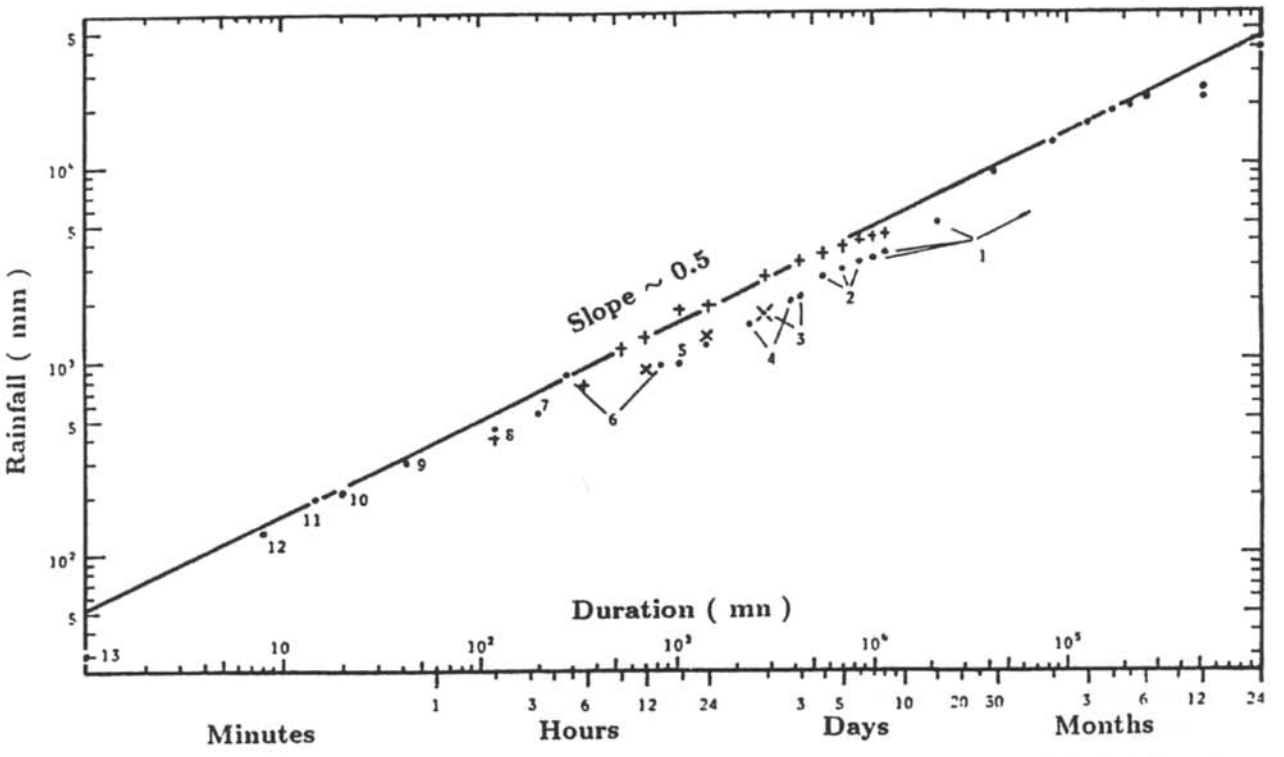

Fig. 29 The world's record point rainfall values, 1 – Cherrapunji, India; 2 – Silver Hill Plantation, Jamaica; 3 – Funkiko, Taiwan; 4 – Baguio, Philippine Is.; 5 – Thrall, Texas; 6 – Smethport, Pa; 7 – D'Hani, Texas; 8 – Rockport, W.Va; 9 – Holt, Mo.; 10 – Cutea de Arges, Romania; 11 – Plumb Point, Jamaica; 12 – Fussen, Bavaria; 13 – Unionville, Md.; values from Jennings (1950). (+) La Reunion, France; (x) Paishih, Taiwan; values from Paulhus (1965).

possible that in time, rain is a conserved process ($H=0$). In comparison, we may apply the double trace moment technique to time series from the vertical pointing radar data discussed in the previous sub-section (Fig. 28c), finding $\alpha \approx 0.50$, $C_1 \approx 0.60$. The spectral slope yielded $\beta \approx 1.1$, hence we obtain $H \approx 0.4$ for the effective reflectivity.

EXTREME RAINFALL EVENTS

One of the attractive features of multifractal models of rain is that they naturally generate violent extreme events. In this subsection, we show that they are apparently of the same type as those which actually occur. The following is a summary of recent work by Hubert *et al.* (1993).

To begin with, consider a multifractal rainfall time series with maximum order of singularity γ_{max}. This maximum may arise through a variety of mechanisms: it could be due to geometrical or microcanonical constraint, the result of a cascade with bounded singularities, or – of relevance here (Table 3) – associated with universal multifractals with $0 \leq \alpha < 1$ (see equation 12). In any case even if the process itself has unbounded orders of singularity (as in the universal multifractals with $1 \leq \alpha < 2$), in any finite sample there will always be a maximum order of singularity present γ_s. Whichever way it arises, for any fixed averaging period (resolution), this maximum order of singularity places an upper bound on the extreme values that will be observed. To see this, consider the maximum rain accumulation A_τ ($=\tau R_\tau$) over time τ ($=\lambda^{-1}$):

$$A_\tau \approx \tau^{1-\gamma_{max}} \tag{27}$$

We therefore will expect log–log plots of maximum accumulations A_τ versus duration τ to be straight, Fig. 29 (from Rémémeras & Hubert, 1990) shows a typical result showing the maximum recorded point rainfall depths for different durations going from minutes to several years. These measurements easily fit straight line with slope equal to about 0.5 (hence $\gamma_{max} \approx 0.5$).

If we consider the empirically observed C_1 and α values for the temporal rain process we can readily explain this remarkable alignment. Recall from Table 3, (gauge results only) that $\alpha \approx 0.5 \pm 0.1$, $C_1 \approx 0.4 \pm 0.1$ from series of quite disparate origins. Since $0 \leq \alpha < 1$, the following maximum order of singularity γ_0 of the process is obtained (equaton 12):

$$\gamma_0 = \frac{C_1}{1-\alpha} + H \tag{28}$$

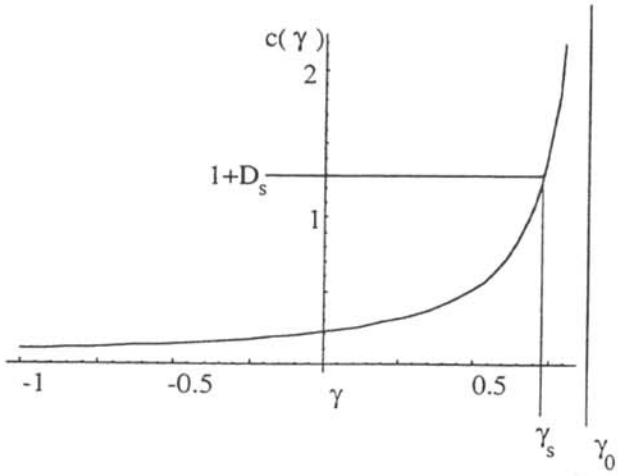

Fig. 30 The $c(\gamma)$ curve corresponding to the estimated parameters $\alpha \approx 0.51 \pm 0.05$, $C_1 \approx 0.44 \pm 0.16$, with γ_s for $N_s = \lambda^{D_s}$ samples, and γ_0 ($= \gamma_s$ for an infinite number of samples; $D_s = N_s = \infty$). From Hubert *et al.* (1993).

Using the above estimate of α, C_1, (with $H = 0$) we obtain $\gamma_0 \approx 0.8 \pm 0.2$. This maximum corresponds to the stochastic generating process, for any finite sample, the actual limit will be determined by $\gamma_s = \gamma_{max} = c^{-1}(D + D_s)$, see Fig. 30 for the corresponding illustration). However, when $\alpha < 1$, the difference $\gamma_s - \gamma_0$ is typically small:

$$\gamma_0 \left(1 - \alpha \left(\frac{C_1}{D}\right)^{-\frac{1}{\alpha}}\right) \leq \gamma_s \leq \gamma_0 \qquad (29)$$

with the upper limit (implying $\gamma_s \to \gamma_0$) occuring when $D_s \to \infty$ (an infinite number of samples), and the lower limit applying for single samples ($D_s = 0$). Using the above gauge values in Table 3 for C_1, α, we obtain with $D_s = 0$, $\gamma \approx 0.7 \pm 0.2$, whereas for an infinite number of independent rain series, $\gamma \approx 0.9 \pm 0.3$. In both cases, the predicted slopes ($1 - \gamma \approx 0.3 \pm 0.2$, 0.1 ± 0.3 respectively) are close to those observed in Fig. 29 (≈ 0.5).

These results help to reconcile two opposing views on extreme precipitation, the 'extreme maximum precipitation' (PMP) and probability approaches (based on frequency analyses) since it simultaneously clarifies the role of the accumulation period and sample size in determining the observed maxima. It also provides a solid theoretical ground for the derivation of rate-duration-frequency curves.

GENERALIZED SCALE INVARIANCE, STRATIFICATION AND SPACE TIME TRANSFORMATIONS

Vertical stratification of rain

We have considered the simplest scaling system involving no prefered orientation; isotropic (self-similar) scaling whose

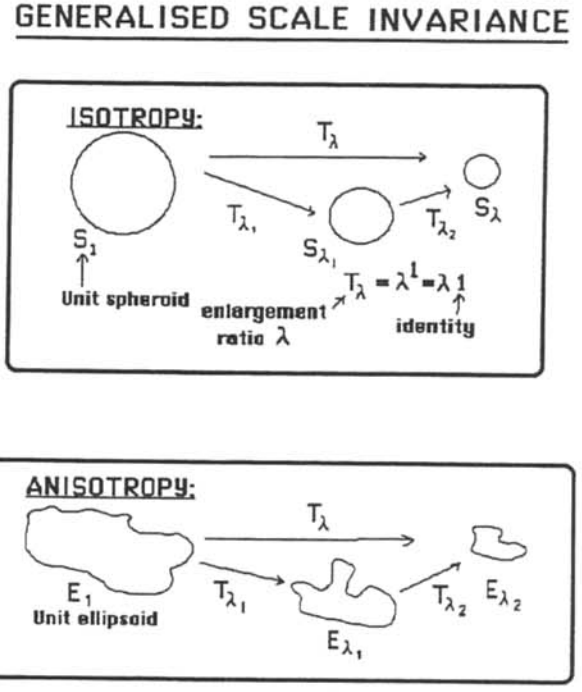

Fig. 31 A schematic diagram illustrating Generalized Scale Invariance. The top box indicates the familiar self-similar scale invariance involving ordinary 'zooms', with scale changing operator $\mathbf{T}_\lambda = \lambda^{-\mathbf{G}}$ with $\mathbf{G}$ the identity. The bottom box illustrates the more general case, the main requirement on $\mathbf{T}_\lambda$ is that it satisfy group properties. From Schertzer & Lovejoy (1989b).

theory has been developed over a considerable period of time, particularly in fluid turbulence. However, the atmosphere is not a simple fluid system, nor is it isotropic; gravity leads to differential stratification, the Coriolis force to differential rotation and radiative and microphysical processes lead to further complications. However even when the exact dynamical equations are unknown it can still be argued that at least over certain ranges, these phenomena are likely to be symmetric with respect to scale changing operations. This view is all the more plausible when it is realized that the requisite scale changes to transform the large scale to the small scale can be very general.

To see this, introduce a scale changing operator $\mathbf{T}_\lambda$ defined by: $\mathbf{T}_\lambda B_1 = B_\lambda$, where B_1 will be a large scale averaging set, B_λ, the corresponding set 'reduced' by factor λ. For example, considering multifractals, 'self-similar' measures will satisfy equations 7 or 9 with $\mathbf{T}_\lambda = \lambda^{-1} = \lambda^{-1}\mathbf{I}$ where $\mathbf{I}$ is the identity matrix i.e. $\mathbf{T}_\lambda$ is a simple reduction by factor λ. However, much more general scaling transformations are possible; detailed analysis shows that practically the only restriction on $\mathbf{T}_\lambda$ is that it has group properties, viz.: $\mathbf{T}_\lambda = \lambda^{-\mathbf{G}}$ where $\mathbf{G}$ is the generator of the group of scale changing operations (this formalism is called 'generalized scale invariance' or GSI, (Schertzer & Lovejoy 1983b, 1985a, b, 1987a, b, 1989a,

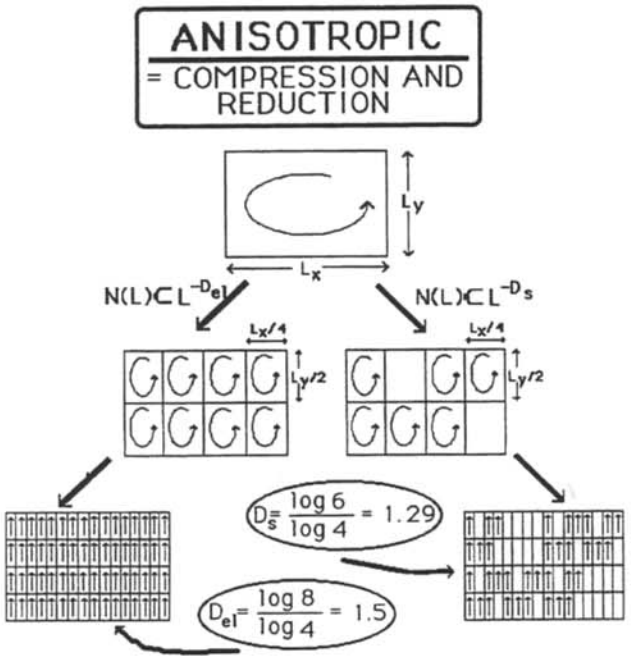

Fig. 32 A schematic diagram analogous to Fig. 7, but showing an anisotropic cascade, here with

$$\mathbf{G} = \begin{bmatrix} 1 & 0 \\ 0 & 1/2 \end{bmatrix}.$$

At large scales eddies are flattened in the horizontal (like Hadley and Ferrel cells), whereas at small scales, they are more vertically aligned (like convective cells). The cross-sectional area clearly decreases with the 3/2 power of the horizontal scale; the elliptical dimension is 3/2. Left and right hand sides again show (stratified) homogeneous and (stratified) β model turbulence. From Lovejoy & Schertzer (1986a).

1991b), see Fig. 31 for a schematic illustration). For example 'self-affine' measures involve reductions coupled with compression along one (or more) axes; **G** is again a diagonal matrix but with not all diagonal elements equal to one (see Fig. 32 for a schematic of such a cascade, Fig. 33a for the corresponding balls). If **G** is still a matrix ('linear GSI') but has off-diagonal elements, then $\mathbf{T}_\lambda$ might compress an initial circle B_1 into an ellipsoid as well as rotate the result (see Fig. 33b). Linear and nonlinear GSI has already been used to model galaxies, clouds and rain (for examples of the corresponding balls B_λ, see Fig. 33c, d for examples with rotation (also Fig. 37), see Fig. 3d,e, for stratification only, see Fig. 3f, g, h, i). Empirically, the trace of **G** (called the 'elliptical dimension' d_{el} of the system) has been estimated in both rain and wind fields to have the values 2.22 and 2.55 respectively, indicating that the fields are neither isotropic ($d_{el} = 3$), nor completely stratified ($d_{el} = 2$), but are rather in between, becoming more and more stratified at larger and larger scales.

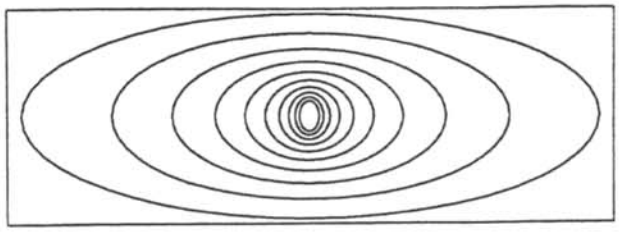

Fig. 33a The series of balls B_λ for a example of linear GSI with only diagonal elements (a 'self-affine' transformation) showing the stratification of structures that result. From Schertzer & Lovejoy (1989b).

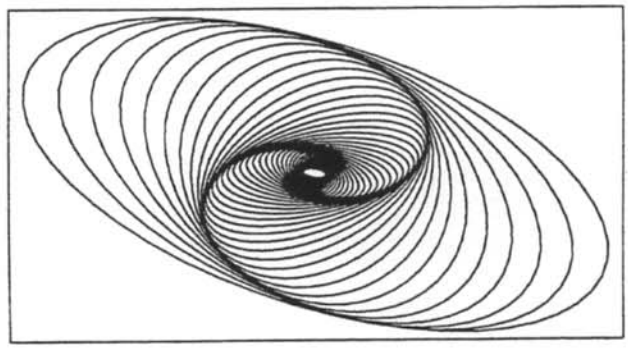

Fig. 33b Same as Fig. 33a, but with off diagonal elements showing the rotation and stratification of structures that result. From Schertzer & Lovejoy (1989b).

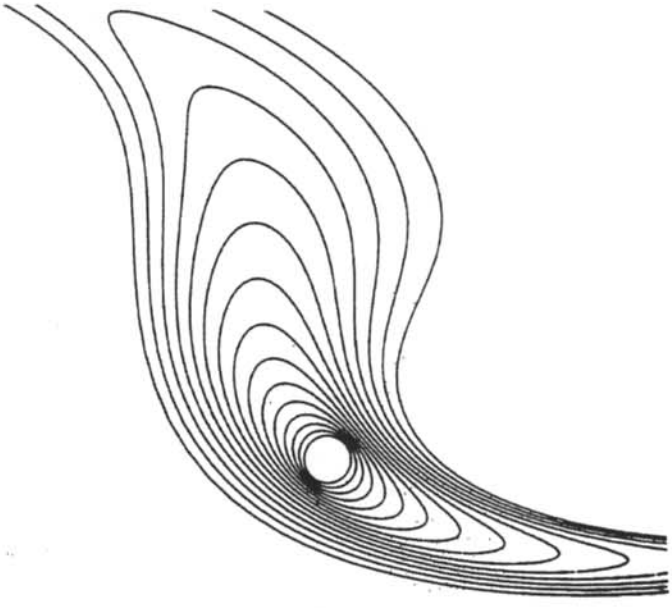

Fig. 33c Same as Fig. 33a, but for a nonlinear but deterministic generator **G**. From Schertzer & Lovejoy (1989b).

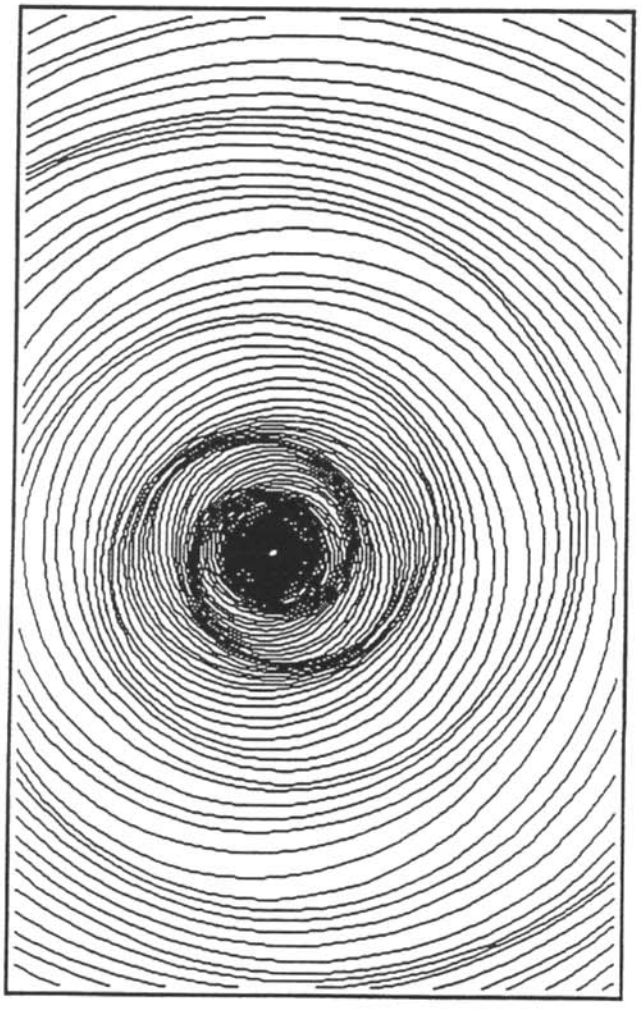

Fig. 33d Same as Fig. 33a, but for a nonlinear but stochastic generator **G**. From Schertzer & Lovejoy (1991a).

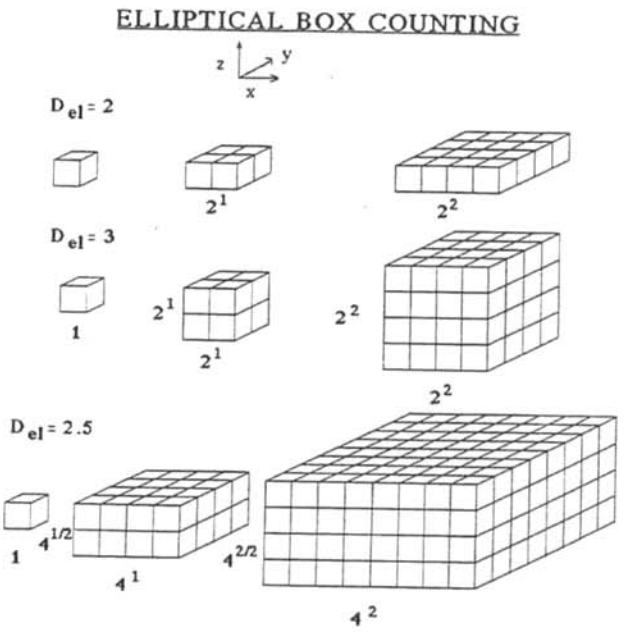

Fig. 34 The variation on usual (isotropic) box counting that can be used to estimate del when the direction but not magnitude of the stratification is known; this method applied to radar reflectivities (Figs. 13a, b) yielded $d_{el} \approx 2.22 \pm 0.07$ (Lovejoy *et al.*, 1987). This figure is from Schertzer & Lovejoy (1989b).

The method that was used to estimate d_{el} in rain was 'elliptical dimensional sampling' (Lovejoy *et al.*, 1987), the basic idea is shown in Fig. 34; the corresponding functional box-counting indicates quite different dimensions in (x, y, z) and (x, y) space, (Figs. 21a, b). There now exists a much improved Fourier space based method for studying scaling anisotropy and estimating linear approximations to **G** called the 'Monte Carlo Differential Rotation' technique (Pflug *et al.*, 1991a, b, see Figs. 35a, b and 37 for examples). It has now been successfully tested on satellite cloud radiances; tests on radar rain data are in progress.

Space-time transformations in rain and the prediction problem

In both geophysical and laboratory flows, it is generally far easier to obtain high temporal resolution velocity data at one or only a few points than to obtain detailed spatial information at a given instant. It is therefore tempting to relate time and space properties by assuming that the flow pattern is frozen and is simply blown past the sensors at a fixed velocity without appreciable evolution, and to directly use the time series information to deduce the spatial structure. This 'Taylor's hypothesis of frozen turbulence' (Taylor, 1938) can often be justified because in many experimental set ups, the flow pattern is caused by external forcing at a well defined velocity typically much larger than the fluctuations under study. However, in geophysical systems (in particular in the atmosphere and ocean) where no external forcing velocity exists, the hypothesis has often been justified by appeal to a 'meso-scale' gap separating large scale motions (two dimensional turbulence associated with 'weather') and small scale three dimensional turbulence (viewed as a kind of 'noise' superposed on the weather[90]. If such a separation existed, it might at least justify a statistical version of Taylor's hypothesis in which the large scale velocity is considered statistically constant (i.e. stationary). Various statistical properties such as spatial and temporal energy spectra would be similar even though no detailed transformation of a given

[90] Zawadzki (1973) finds that from 5 to 40 minutes this version of Taylor's hypothesis is consistent with radar rain data, but that for longer times it is inconsistent. We suspect that his data may be much more consistent with the generalizations of Taylor's hypothesis discussed here. For a discussion of conventional Taylor hypotheses in rain, see Gupta & Waymire (1987).

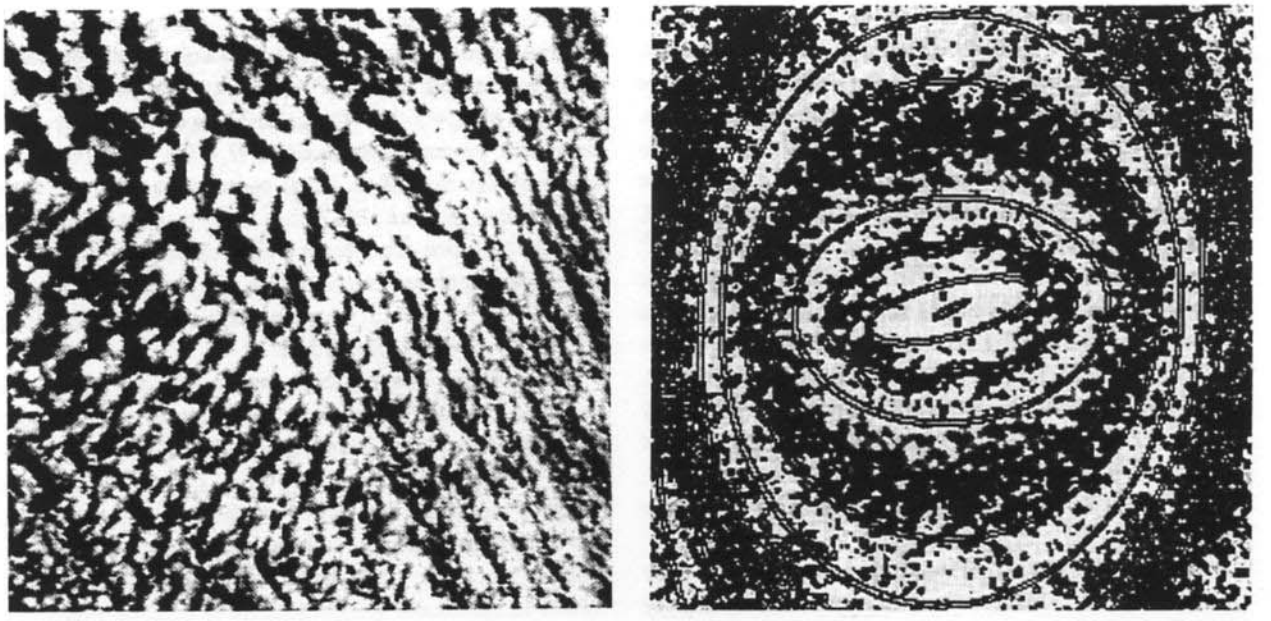

Fig. 35a Illustrations of the Monte Carlo differential rotation technique applied to NOAA satellite infra-red image of a field of Marine Stratocumulus clouds at 1.1 km resolution (256 × 256 points), the left is a grey scale rendition in real space, the right is the modulus squared of the fourier transform in Fourier space. The superposed ellipses are the best fits corresponding to a sphero-scale of 3.5 km,

$$\mathbf{G}=\begin{bmatrix}0.57 & -0.40\\ 0.40 & 1.43\end{bmatrix}$$

(in linear GSI, the Fourier space generator is the transpose of the real space generator). From Pflug *et al.* (1993).

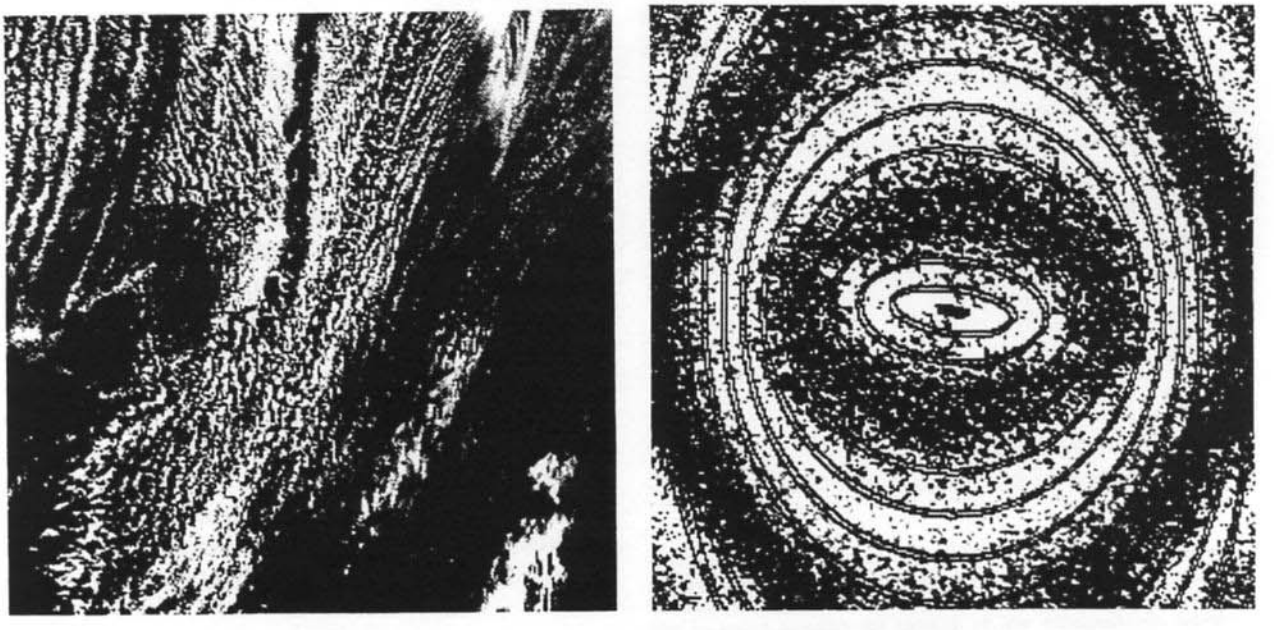

Fig. 35b Same as Fig. 35a except for cloud associated with a midlatitude cyclone, at visible wavelengths, 1.1 km resolution with 512 points on a side. The estimated generator, was

$$\mathbf{G}=\begin{bmatrix}0.68 & -0.18\\ 0.16 & 1.32\end{bmatrix}$$

the sphero-scale, 3.9 km. From Pflug *et al.* (1993).

time series to a particular spatial pattern would be possible. Only some kind of statistical equivalence would be possible.

However, as argued here, the scaling is likely to continue over most of the meteorologically significant range of scales. No large scale forcing velocity can be appealed to in order to transform from space to time; a turbulent velocity must be used (equation 5). Due to the multifractal nature of the wind, the exact scaling will depend on the $K(q)$ of the energy flux[91] (ε). For example, $<v_l> \approx l^{1/3-K(1/3)}$ according to Schmitt *et al.* (1992), in wind tunnel wind data, $C_1 \approx 0.25$, $\alpha \approx 1.3$, hence $-K(1/3) \approx 0.07$. Denoting this small intermittency correction by δ, we expect that rather than being scale independent, the space-time transformation has a scale dependent velocity $\langle v_l \rangle \approx l^H$ with $H_v = 1/3 + \delta$. The two geophysically relevant statistical Taylor's hypotheses therefore correspond to $H_v = 0$ or $H_v = 1/3 + \delta$ depending on the existence (or not) of the 'gap'.

The theoretical arguments mentioned above make it clear that the turbulent velocity is likely to be the relevant one for space-time transformations; this rules out the constant velocity ($H_v = 0$) hypothesis[92]. In fact, as discussed in Pflug *et al.* (1991, 1993), a good way to directly measure the series of 'balls' is to look for lines of constant energy density in Fourier space; Fig. 36 shows the result using vertically pointing radar data), the elliptical character of the (vertical) spatial wavenumber/frequency isolines, with eccentricity clearly varying with scale; this shows unambiguously that empirically (z, t) space is anistropic. Theoretically, with the help of in the formalism of Generalized Scale Invariance, we can understand this by deriving the space-time transformation from the (turbulent) value of $H_v (\approx 1/3)$. Consider (x, y, t) space, the space-time transformation can be simply expressed by statistical invariance with respect to the following transformation (generalized reduction in scale by factor λ): $x \Rightarrow \lambda x$, $y \Rightarrow \lambda y$, $t \Rightarrow \lambda^{1-H_v}$ or, using the notation $\mathbf{r} = (x, y, z, t)$, $\mathbf{r}_\lambda = T_\lambda \mathbf{r}_1$ with $T_\lambda = \lambda^{-G}$ and:

$$\mathbf{G} = \begin{bmatrix} 1 & 0 & 0 & \\ 0 & 1 & 0 & \\ 0 & 0 & 1 - H_v \end{bmatrix}$$

we therefore obtain Trace $\mathbf{G} = 3 - H_v$ i.e. by measuring d_{el} or H_v we can determine $\mathbf{G}$ (assuming that there are no off-diagonal elements corresponding to rotation between space and time, and ignoring differential rotation in the horizontal). The isotropic statistical Taylor's hypothesis is therefore expressed by $d_{el} = 3$ ($H_v = 0$), the anisotropic, turbulent scale-dependent Taylor's hypothesis is $H_v \approx 1/3$, $d_{el} \approx 8/3$. If we now consider the full (x, y, z, t) space, it has already been shown (Lovejoy *et al.*, 1987) that in (x, y, z) space $d_{el} = 2.22$ (i.e. the z direction contributes 0.22 to the trace of $\mathbf{G}$) for the corresponding transformation in (x, y, z) space for radar rain data, hence for the (x, y, x, t) process, the corresponding value is $d_{el} \approx 2 + 0.22 + 2/3 \approx 2.89$.

The generator of space/time transformations defines the operation required to go from large to small space/time structures. When it is coupled with the multifractal probability generator (characterized by H, C_1, α), it provides a complete statistical description of the space/time process, and hence – in principle – all the information necessary to produce stochastic predictions. Such predictions may be viewed as systematic generalizations of existing prediction techniques based on the 'stochastic memory' of the system. Work is currently in progress at McGill and the Météorologie Nationale to use this approach to improve nowcasting methods for extrapolating radar echoes and satellite estimated rain areas[93] (e.g. Bellon *et al.*, 1980). For any given set of data, they have the potential to provide the theoretically optimum prediction: all that is required is knowledge of the multifractal generators ($\mathbf{G}$, H, C_1, α).

Dynamical simulations of rainfall

In this section we indicate briefly how to exploit the universality (and the measured H, C_1, α parameters) to perform multifractal simulations. The first 'continuous'[94] multifractal models of this type were discussed in Schertzer & Lovejoy (1987a, b), and Wilson (1991). Wilson *et al.* (1991) gives a comprehensive discussion including many practical (numerical) details[95]. In particular, the latter describes the numerical simulation of clouds and topography, including how to iteratively 'zoom' in, calculating details to arbitrary resolution in selected regions. Although we will not repeat these details here, enough information has been given in the previous sections to understand how they work. First, for a conserved (stationary) multifractal process φ_λ we define the generator $\Gamma_\lambda = \log \varphi_\lambda$. To yield a multifractal φ_λ, Γ_λ must be exactly a $1/f$ noise, i.e. its spectrum[96] is $E(k) \approx k^{-1}$ (this is

[91] *A priori*, any of the statistics $\langle v_l^q \rangle^{1/q}$ could be used in space-time transformations; all that is required is a parameter with the dimensions of velocity. It is therefore possible that (due to the multiple scaling of v_l) that the relevant transformation will be different for different orders of rain singularities γ (indeed, in view of the different a values found in time and space, this is necessary). Here for simplicity, we ignore this possible complication and consider transformations of the low order singularities corresponding to $q \sim 1$.

[92] Using lidar data, Lovejoy & Schertzer (1991a) find the value ($H_v = 0.5 \pm 0.3$) which is not accurate enough to usefully estimate δ. A more accurate radar based estimate $H_v = 0.38 + 0.05$ was announced by Tsonis *et al.* (1990).

[93] For rain forecasts for up to six hours, such techniques are already the best available.

[94] 'Continuous' since it does not involve integer ratios between eddies and sub-eddies; it is continuous in scale, avoiding the artificial straight lines of the (discrete ratio) cascades.

[95] For a recent illustration, see Fig. 10 from Lovejoy & Schertzer (1991c).

[96] For $\alpha < 2$, the generator variance diverges, we use 'generalized' spectra – see Schertzer & Lovejoy (1987a), appendix C.

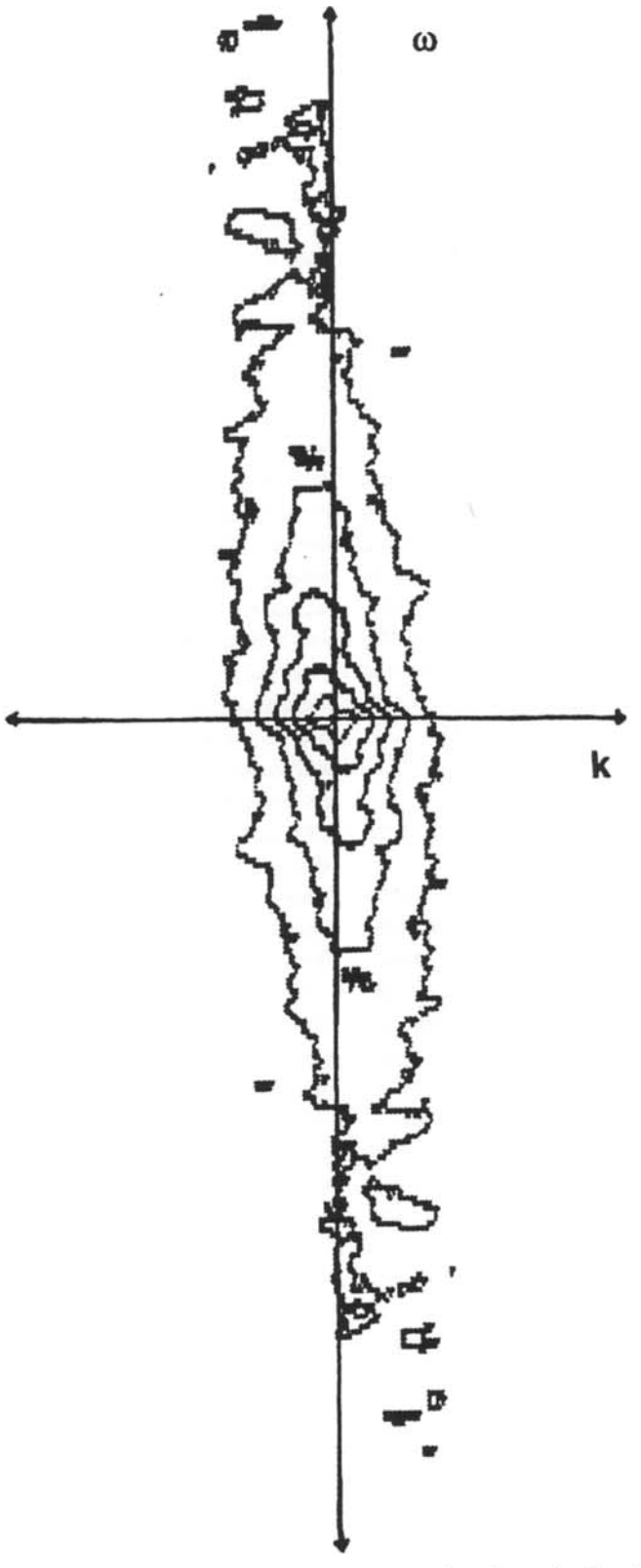

Fig. 36 We plot here the contours of the (two dimensional) energy spectrum from the vertically pointing radar reflectivities; 2 second temporal resolution, 21 m spatial resolution. The figure is the result of averaging the Fourier space energy density (modulus squared of the Fourier transform) over 20 consecutive (z, t) planes, each with 256×512 points (Fourier conjugate axes are k, ω respectively). Note the clear differential stratification. The rotation of the principle axes with respect to the (Fourier) axes seems not to be differential (hence due to a mean wind). From Tessier *et al.* (1993).

necessary to ensure the multiple scaling of the moments of φ_λ). To produce such a generator, we start with a stationary Gaussian or Lévy 'subgenerator'. The subgenerator is a noise consisting of independent random variables with either Gaussian ($\alpha = 2$) or extremal Lévy distributions (characterized by the Levy index α), whose amplitude (e.g. variance in the Gaussian case) is determined by C_1. The subgenerator is then fractionally integrated (power law filtered in Fourier space) to give a (generalized) k^{-1} spectrum. This generator is then exponentiated to give the conserved φ_λ which will thus depend on both C_1 and α. Finally, to obtain a nonconserved process with spectral slope β, the result is fractionally integrated by multiplying the Fourier transform by k^{-H}. The entire process involves two fractional integrations and hence four FFTs. 512×512 fields can easily be modeled on personal computers (they take about 3 minutes on a Mac II), and $256 \times 256 \times 256$ fields (e.g. space-time simulations of dynamically evolving multifractal clouds) have been produced on a Cray 2 (Brenier[97], 1990, Brenier *et al.*, 1990). We used the multifractal parameters estimated by the various methods described above, taking $H \approx 0.3$, $C_1 \approx 0.1$, $\alpha \approx 1.35$ in space to produce the simulation shown in Fig. 37.

CONCLUSIONS

For over ten years, scaling ideas have provided an exciting new perspective for dealing with rain and other dynamical processes occuring in the atmosphere and other geophysical systems; in this paper we have attempted to give a brief review of this mushrooming field. To maintain a focus, as indicated in the title, we have restricted our attention as much as possible to an account of the necessary multifractal formalism and to specific results on rain. Although multifractal notions are also relevant in stream flows, river basins and other areas of hydrology, we have omitted these from the discussion. We have only mentioned in passing the now burgeoning literature concerning scaling analyses and modeling of clouds and their associated radiative transfer. Finally we have only given a brief outline of the relation of our results to turbulence theory and to recent empirical turbulence results.

During the period covered by this review, scaling ideas were extended far beyond the restrictive bounds of the fractal geometry of sets to directly deal with the multifractal statistics (and dynamics) of fields. Multifractals are now increasingly understood as providing the natural framework for scale-invariant nonlinear dynamics. Furthermore, due to the existence of stable attractive multifractal generators they provide attractive physical models. This implies that many of the details of the dynamics are irrelevant (universal behaviour) and leads to new and powerful multifractal simulation and analysis techniques (many of which were discussed).

Scaling ideas have also been enriched by extensions in another quite different direction: scaling anisotropy. Recall that a scaling system is one in which small and large scale (statistical) properties are related by a scale changing operation involving only the scale ratio: there is no characteristic size. Until recently, this scale change was restricted to ordinary 'zooms' or magnifications. Since the 1950s, this isotropic self-similar scaling has provided the theoretical basis of the standard model of atmospheric dynamics: a large scale two dimensional turbulence and a small scale three dimensional turbulence. The only generalization of scaling beyond self-similarity was a slight variation called 'self-affinity' which combined the zoom with a (differential) 'squashing' along certain fixed directions (e.g. coordinate axes). While this extension is necessary to account for the observed atmospheric stratification (implying a single scaling, anisotropic turbulence), it is still very special. In particular, geophysical applications generally involve not only differential stratification but also differential rotation (e.g. due to the Coriolis force). The formalism developed to deal with scaling anisotropy is Generalized Scale Invariance (GSI). GSI goes far beyond self-affinity: not only does it involve both differential rotation and stratification, it allows both effects to vary from place to place in either deterministic or even random manners.

We have argued that due to the enormous quantities of rain data spanning many orders of magnitude in time and space, that rain has and will continue to play a leading role in testing and developing new ideas in scaling and nonlinear dynamics. The rapid progress of this field makes the task of reviewing difficult. In the first part, we have attempted to concentrate on results which most clearly demonstrate the scaling of rain; by combining many different measurement techniques although the exact limits are still not clear, we have seen that it is possible that rain is scaling over most of the meteorologically significant range of scales. In general, we did not attempt detailed intercomparisons of different empirical results, largely because many were derived from essentially experimental data analysis techniques (such as functional box-counting, area-perimeter relations etc.), which are now somewhat outdated and which in any event were often applied to quite different data sets. Nevertheless, the measurements presented here cover the entire range from ≈ 1 mm (blotting paper analysis of rain drop distributions), to ≈ 10000 km (the global rain network), and give us considerable confidence that the basic (multi) scaling holds reasonably well.

Whereas early analysis and modeling techniques were

[97] This paper describes how such clouds simulations were used to produce a video called 'Multifractal Dynamics'.

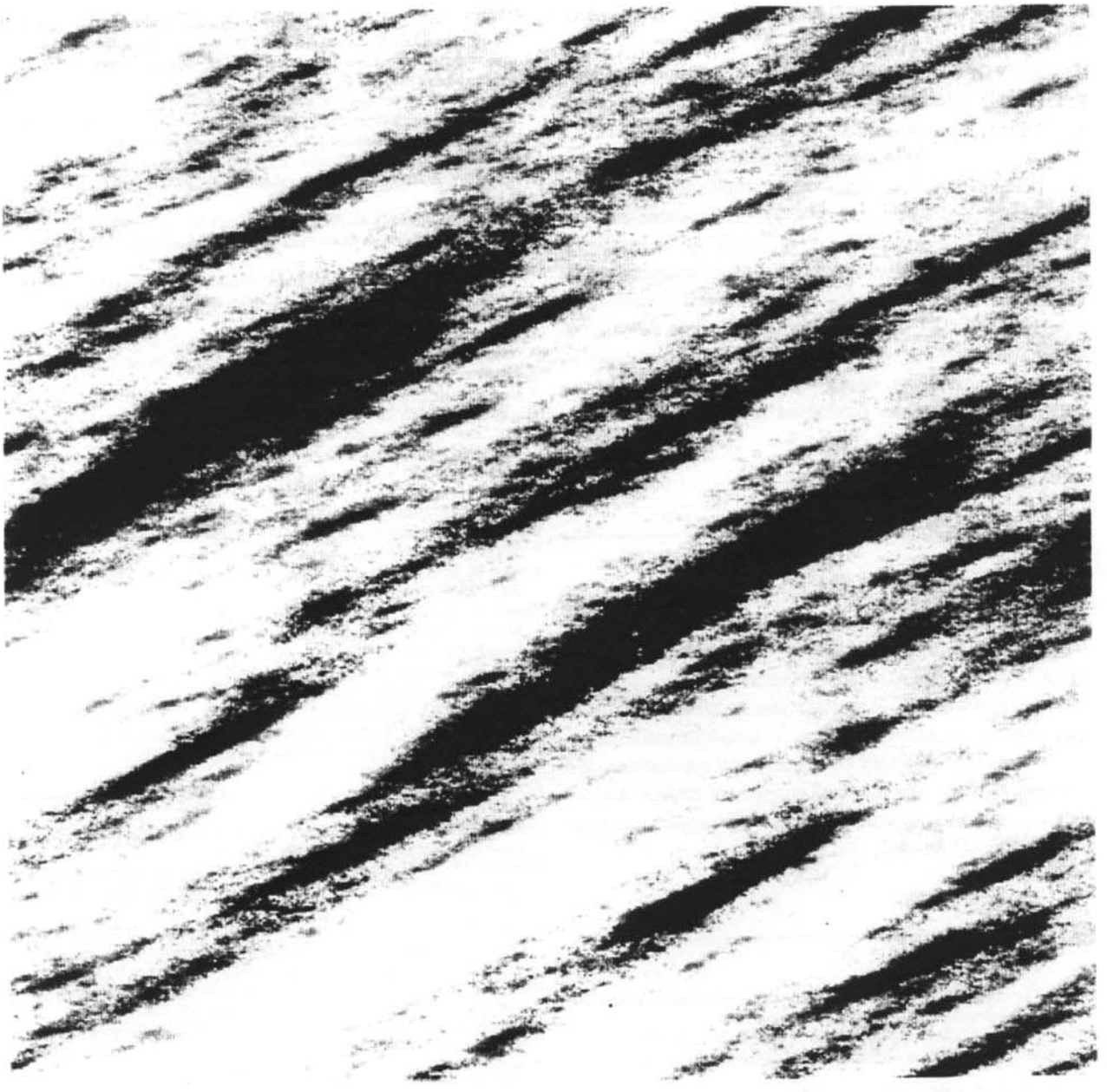

Fig. 37 Numerical simulation of a universal continuous cascade multifractal rain field on a 512×512 point gridwidth $\alpha = 1.3$, $C_1 = 0.1$, $H = 0.3$, G the same as empirically estimated in Fig. 35b. We thank S. Pechnold for help with the simulation.

based on *ad hoc* geometric notions relevant to fractal sets, the more mature multifractal framework outlined in the main part of the paper depended on two important breakthroughs. The first was the connection with the physics of rain processes via the problematic of passive scalar clouds, and the second, the continuous (cascade) modelling of the latter with the associated discovery of multifractal universality classes. Universality also provided the framework for the development of a new generation of 'specific' multifractal analysis methods that are analogous to parametric methods in standard statistics and are statistically quite robust. Indeed, the results of the Double Trace Moment technique are now providing consistent estimates of multifractal parameters in rainfall measured over wide ranges of scale in both time and space, as estimated from both rain gage and radar measurements (see Tables 3 and 4 for summaries). Although these results are quite recent, they suggest that the field is maturing, and that it is now the time for developing a variety of multifractal applications. Some have already been mentioned; the multifractal objective analysis problem, the

multifractal observers problem for radar data, the statistics of extreme rain events.

Other areas where work is only just beginning were also mentioned, in particular the problem of multifractal space/time transformations, scaling anisotropy, and stratification, as well as their modeling. These are areas where we may soon expect exciting new developments, especially for multifractal forecasting methods, and multifractal classification of storms, morphologies and textures. Finally, given increasing confidence in our multifractal parameter estimates, all these ideas can be tested on (dynamical) multifractal models which are thus likely to play an important role in helping to understand the larger problem of resolution dependence of remotely sensed data, including the relation between the radiance and rain fields (useful for improving satellite rain estimating algorithms).

AKNOWLEDGEMENTS

We thank A. Davis, N. Desaulniers-Soucy, M. Duncan, F. Fabry, C. Hooge, P. Hubert, P. Guerrido, P. Ladoy, C. Larnder, D. Lavallée, S. Pecknold, K. Pflug, F. Schmitt, Y. Tessier and B. Watson for helpful comments, discussions and technical assistance. F. Francis is thanked for helping us in the analysis of the satellites images, V. Sahakian and F. Begin are thanked for help with the multifractal simulations. We also acknowledge the financial support of DOE's Atmospheric Radiation Measurement (ARM) project, contract #DE-FG03-90ER61062.

REFERENCES

Armijo, L. (1966) Statistical properties of radar echo patterns and the radar echo process. *J. Atmos. Sci.*, **23**, 560–8.

Atmanspacher, H., Scheingraber, H. & Weidenmann, G. (1989) Determination of $f(a)$ for a limited random point set. *Phys. Rev.* A, **40**, 3954.

Bak, P., Tang, C. & Weissenfeld, K. (1987) Self-organized criticality: an explanation of 1/f noise. *Phys. Rev. Lett.*, **59**, 381–4.

Baryshnikova, Y. S., Zaslavskii, G. M., Lupyan, E. A., Moiseev, S. S. & Sharkov, E. A. (1989) Fractal dimensionality of cloudiness IR images and turbulent atmospheric properties. *Akad. Nauk USSR, Issledovanii Zemli, iz Kosmos*, **1** (in Russian), 17–26.

Bell, T. L. (1987) A space-time stochastic model of rainfall for satellite remote sensing studies. *J. Geophys. Res.*, **92**, 9631–44.

Bellon, A., Lovejoy, S. & Austin, G. L. (1980) A short-term precipitation forecasting procedure using combined radar and satellite data. *Mon. Wea. Rev.*, **108**, 1554–66.

Benzi, R., Paladin, G., Parisi, G. & Vulpiani, A. (1984) *J. Phys.* A, **17**, 3521.

Bialas, A. & Peschanski, R. (1986) Moments of rapidity distributions as a measure of short-range fluctuations in high-energy collisions. *Nucl. Phys. B*, **273**, 703–18.

Biondini, R. (1976) Cloud motion and rainfall statistics, *J. Appl. Meteor.*, **15**, 205–24.

Blanchard, D. C. (1953) Raindrop size-distribution in Hawaiian rains. *J. Meteor.*, **10**, 457–73.

Bochi Kebe, G. & Howes, K. (1990) *Determination of the three dimensional spatial distribution and of the fractal dimension of passive scalar fields using stereoscopic techniques*, 3rd year honours lab project report, 46pp, McGill Physics dept.

Bouquillon, C. & Moussa, R. (1991) Caracterisation fractale d'une serie chronologique d'intensité de pluie. *Proceedings of Rencontres Hydrologiques Franco-Roumaines, Ecoles des Mines*, 3–6 Sept. 1991, 6pp.

Bras, R. L. & Rodriguez-Iturbe, I. (1976) Rainfall generation: a nonstationary time varying multidimensional model. *Wat. Resour. Res.*, **12**, 450–6.

Brax, P. & Pechanski, R. (1991) Levy stable law description of intermittent behaviour and quark-gluon phase transitions, *Phys. Lett.* B, 225–30.

Brenier, P. (1990) *Simulations dynamiques multifractale des nuages*, Master's Thesis. Ecole Normale Superieure des Sciences et Techniques Avancées, Paris, France.

Brenier, P., Schertzer, D., Sarma, G., Wilson, J. & Lovejoy S. (1990) Continuous Multiplicative cascade models of passive scalar clouds. *Annales Geophys.*, **8** (Special Issue), 320.

Cahalan, R. F. (1991) Landsat Observations of Fractal Cloud Structure. *Scaling, fractals and non-linear variability in geophysics*, D. Schertzer & S. Lovejoy (eds.), pp. 281–96, Kluwer.

Cole, J. W. (1964) *Statistics related to the shape and scale of pattern elements*. Final Report, Contract Cwb-10709, Travelers Research Center Hartford, Conn.

Come, J. M. (1988) *Caractérisation fractale des relations Pèrimetre/Surface des précipitations en zone soudano-sahélienne*. MSc. thesis, Ecole Nationale Supérieure des Mines de Paris, 102pp.

Crane, R. K.(1990) Space-time structure of rain rate fields. *J. Geophy. Res.*, **95**, 2011–20.

Davis, A., Lovejoy, S., Gabriel, P., Schertzer, D. & Austin, G. L. (1990) Discrete Angle Radiative Transfer. Part III: numerical results on homogeneous and fractal clouds. *J. Geophys. Res.*, **95**, 11729–42.

Davis, A., Lovejoy, S. & Schertzer, D. (1991a) Radiative transfer in multifractal clouds. *Scaling, fractals and non-linear variability in geophysics*, D. Schertzer & S. Lovejoy (eds.), pp. 303–18, Kluwer.

Davis, A., Lovejoy, S. & Schertzer, D. (1991b) Discrete Angle Radiative transfer in a multifractal medium, *SPIE proceedings 1558*, pp. 37–59, San Diego, 21–26 July.

Detwiller, A. (1990) Analysis of cloud imagery using box-counting. *Inter. J. of Remote Sensing*, **11**, 887–98.

Drufuca, G. (1977) Radar derived statistics on the structure of precipitation patterns. *J. Appl. Met.*, **16**, 1029–35.

Duncan, M. (1993) Universal multifractal analysis and simulation of radar reflectivity of rain, Ph.D. dissertation, McGill University, 230pp.

Duncan, M., Lovejoy, S., Fabry, F. & Schertzer, D. (1992) Fluctuating radar cross-section of a multifractal distribution of scatterers. Proc. 11th Internat. Conf. on Precipitation and Clouds, pp. 997–1000.

Duroure, C. & Guillemet, B. (1990) Analyse des Hétérogénéités spatiales daes stratocumuls et cumulus. *Atmos. Res.*, **25**, 331–50.

Eagleson, P. S., Fennessey, N. M., Qinlang, W. & Rodriguez-Iturbe, I. (1987) Application of spatial poisson models to air mass thunderstorm rainfall. *J. Geophys. Res.*, **92**, 9661–78.

Fan A. H. (1989) Chaos additif et multiplicatif de Levy. *C. R. Acad. Sci. Paris*, I **308**, 151–4.

Fraedrich, K. & Larnder, C. (1993) Scaling regimes of composite rainfall time series. *Tellus*, **45A**, 289–98.

Frisch U. P., Sulem P. L. & Nelkin M. (1978) A simple dynamical model of intermittency in fully developed turbulence. *J. Fluid Mech.*, **87**, 719–24.

Gabriel, P., Lovejoy, S., Davis, A., Schertzer, D. & Austin, G. L. (1990) Discrete Angle Radiative Transfer. Part II: renormalization approach to scaling clouds. *J. Geophys. Res.*, **95**, 11717–28.

Gabriel, P., Lovejoy, S., Schertzer, D. & Austin, G. L. (1988) Multifractal analysis of satellite resolution dependence. *Geophys. Res. Lett.*, pp. 1373–6.

Giraud, R., Montariol, F., Schertzer, D. & Lovejoy, S. (1986) The codimension function of sparse surface networks and intermittent fields. Astract vol., *Nonlinear Variability in Geophysics*, 35–6, McGill University, Montreal, Canada.

Ghilardi, P. (1990) A search for chaotic behaviour in storm rainfall events. *Annales Geophys.* (special issue), p. 313.

Grassberger, P. (1983) Generalized dimensions of strange attractors. *Phys. Lett.* A **97**, 227.

Gupta, V. & Waymire, E. (1987) On Taylor's hypothesis and dissipation in rainfall. *J. Geophys. Res.*, **92**, 9657–60.

Gupta, V. & Waymire, E. (1990) Multiscaling properties of spatial rainfall and river flow distributions. *J. Geophys. Res.*, **95**, 1999–2010.

Halsey, T. C., Jensen, M. H., Kadanoff, L. P., Procaccia, I. & Shraiman, B. (1986) Fractal measures and their singularities: the characterization of strange sets. *Phys. Rev.* A **33**, 1141–51.

Harris, D. & Lewis, G. (1991) *Determination of fractal distribution of precipitation using laser scattering*. 3rd year honours project report, 47pp, McGill Physics dept.

Hentschel, H. G. E. & Proccacia, I. (1983) The infinite number of generalized dimensions of fractals and strange attractors. *Physica* **8D**, 435–44.

Houze, R. A. & Chee-Pong Cheng (1977) Radar characteristics of tropical convection observed during GATE: mean properties and trends over the summer season. *Mon. Wea. Rev.*, **105**, 964–80.

Hubert, P. (1991) Analyse multifractale de champs temporels d'intensités des precipitations. *Proceedings of Rencontres Hydrologiques Franco-Roumaines, Ecoles des Mines*, 3–6 Sept. 1991, 6pp.

Hubert, P. & Carbonnel, J. P. (1988) Caractérisation fractale de la variabilité et de l'anisotropie des précipitations intertropicales. *C. R. Acad. Sci. Paris*, **307**, 909–14.

Hubert, P. & Carbonnel, J. P. (1989) Dimensions fractales de l'occurence de pluie en climat soudano-sahelien. *Hydro. Continent.*, **4**, 3–10.

Hubert, P. & Carbonnel, J. P. (1991) Fractal characterization of intertropical precipation variability. *Scaling, fractals and non-linear variability in geophysics*, D. Schertzer & S. Lovejoy (eds)., pp. 209–13, Kluwer.

Hubert P., Tessier, Y., Ladoy, P., Lovejoy, S., Schertzer, D., Carbonnel, J. P., Violette, S., Desurosne, I. & Schmitt, F. (1993) Multifractals and extreme rainfall events, *Geophs. Res. Lett.*, **20**, 931–4.

Hurst, H. E. (1951) Long-term storage capacity of reservoirs. *Trans. of the Amer. Soc. of Civil Engin.*, **116**, 770–808.

Jennings, A. H. (1950) *Mon. Wea. Rev.*, **78**, 4–5.

Kida, S. (1991) Log stable distribution and intermittency of turbulence. *J. Phys. Soc. of Japan*, **60**, 5–8.

Keddem, B. & Chiu, L. S. (1987) Are rain rate processes self-similar? *Wat. Resour. Res.*, **23**, 1816–18.

Koleshnikova, V. N. & Monin, A. S. (1965) Spectra of meteorological field fluctuations. *Izv. Atmos. Oceanic Physics*, **1**, 653–69.

Kolmogorov, A. N. (1940) Wienersche spiralen and einige andere interessante kurven in Hilbertschen Raum. *C. R. (Doklady) Acad. Sci. URSS (N.S.)*, **26**, 115–18.

Kolmogorov, A. N. (1962) A refinement of previous hypotheses concerning the local structure of turbulence in viscous incompressible fluid at high Reynolds number. *J. Fluid Mech.*, **83**, 349.

Konrad, T. G. (1978) Statistical models of summer rainshowers derived from fine-scale radar observations. *J. Appl. Meteor.*, **17**, 171–88.

Kumar, P. & Foufoula-Georgiou, E. (1993) A new look at rainfall fluctuations and scaling properties of spatial rainfall using orthogonal wavelets. *J. Appl. Meteor.*, **32**, 209–22.

Ladoy, P., Schertzer, D. & Lovejoy, S. (1986) Une étude d'invariance locale-regionale des temperatures. *La Météorologie*, **7**, 23–34.

Ladoy, P., Marquet, O., Piriou, J. M., Lovejoy, S. & Schertzer, D. (1987) Inhomogeneity of geophysical networks, calibration of remotely sensed data and multiple fractal dimensions. *Terra Cognita*, **7**, 2–3.

Ladoy, P., Lovejoy, S. & Schertzer, D. (1991) Extreme fluctuations and intermittency in climatological temperatures and precipitation. *Scaling, fractals and non-linear variability in geophysics*, D. Schertzer & S. Lovejoy (eds)., pp. 241–50, Kluwer.

Ladoy, P., Schmitt, F., Schertzer, D. & Lovejoy, S. (1993) Variabilité temporelle des observations pluviometriques à Nimes, *C. R. Acad. des Sci.*, **317**, II, 775–82.

Lamperti, J. (1962) Semi-stable stochastic processes. *Trans. Am. Math. Soc.*, **104**, 62–78.

Larnder, C., Desaulniers-Soucy, N., Lovejoy, S., Schertzer, D., Braun, C. & Lavallée, D. (1992) Evidence for universal multifractal behaviour in human speech. *Chaos and Bifurcation*, **2**, 715–19.

Lavallée, D. (1991) *Multifractal analysis and simulation techniques and turbulent fields*, 142pp, PhD. thesis, McGill University.

Lavallée, D., Schertzer, D. & Lovejoy, S. (1991a) On the determination of the co-dimension function. *Scaling, fractals and non-linear variability in geophysics*, D. Schertzer & S. Lovejoy (eds)., pp. 99–110, Kluwer.

Lavallée, D., Lovejoy, S. & Schertzer, D. (1991b) Universal multifractal theory and observations of land and ocean surfaces, and of clouds, *SPIE proceedings 1558*, San Diego, 21–26 July.

Lavallée, D., Lovejoy, S., Schertzer, D. & Ladoy, P. (1993) Nonlinear variability and Landscape topography: analysis and simulation. *Fractals in Geography*, L. De Cola & N. Lam (eds.), Prentice Hall, 158–92.

Levich, E. & Tzvetkov, E. (1985) *Phys. Rep.*, **120**, 1–45.

Lopez, R. E. (1976) Radar characteristics of the cloud populations of tropoical disturbances in the northwest Atlantic. *Mon. Wea. Rev.*, **194**, 269–83.

Lopez, R. E. (1977a) Some properties of convective plume and small fair-weather cumulus fields as measured by acoustic and lidar sounders. *J. Appl. Meteor.*, **16**, 861–5.

Lopez, R. E. (1977b) The log-normal distribution and cumulus cloud populations. *Mon. Wea. Rev.*, **105**, 865–72.

Lovejoy, S. (1981) *Analysis of rain areas in terms of fractals, 20th conf. on radar meteorology*, pp. 476–84, AMS Boston.

Lovejoy, S. (1982) The area-perimeter relations for rain and cloud areas. *Science*, **216**, 185–7.

Lovejoy, S. (1983) La geometrie fractale des regions de pluie et les simulations aleatoires. *Houille Blanche*, **516**, 431–6.

Lovejoy, S., Tardieu, J. & Monceau, G. (1983) Etude d'une situation frontale: analyse meteorologique et fractale. *La Météorologie*, **6**, 111–18.

Lovejoy, S. & Schertzer, D. (1985a) Generalised scale invariance and fractal models of rain. *Wat. Resour. Res.*, **21**, 1233–50.

Lovejoy, S. & Schertzer, D. (1985b) Rainfronts, fractals and rainfall simulations. Hydro. Appl. of Remote sensing and data trans., *Proc. of the Hamburg symposium*, IAHS publ. no. 145, pp. 323–34.

Lovejoy, S. & Mandelbrot, B. (1985) Fractal properties of rain and a fractal model. *Tellus*, **37A**, 209–32.

Lovejoy S. & Schertzer, D. (1986a) Scale invariance, symmetries, fractals and stochastic simulations of atmospheric phenomena, *Bulletin of the AMS*, **67**, 21–32.

Lovejoy, S. & Schertzer, D. (1986b) Scale invariance in climatological temperatures and the spectral plateau. *Annales Geophys.*, **4B**, 401–10.

Lovejoy, S., Schertzer, D. & Ladoy, P. (1986) Fractal characterization of inhomogeneous measuring networks. *Nature*, **319**, 43–4.

Lovejoy, S., Schertzer, D. & Tsonis, A. A. (1987) Functional box-counting and multiple elliptical dimensions in rain. *Science*, **235**, 1036–8.

Lovejoy, S. & Schertzer, D. (1988) Extreme variability, scaling and fractals in remote sensing: analysis and simulation, *Digital image processing in Remote Sensing*, J. P. Muller (ed.), pp. 177–212, Francis and Taylor.

Lovejoy, S. & Schertzer, D. (1989) Comments on 'Are rain rate processes self-similar?' *Wat. Resour. Res.*, **25**, 577–9.

Lovejoy, S. & Schertzer, D. (1990a) Multifractals, universality classes, satellite and radar measurements of clouds and rain. *J. Geophys. Res.*, **95**, 2021–34.

Lovejoy, S. & Schertzer, D. (1990b) Our multifractal atmosphere: a unique laboratory for nonlinear dynamics. *Physics in Canada*, **46**, 62–71.

Lovejoy, S. & Schertzer, D. (1990c) Fractals, rain drops and resolution dependence of rain measurements. *J. Appl. Meteor.*, **29**, 1167–70.

Lovejoy, S., Gabriel, P., Davis, A., Schertzer, D. & Austin, G. L. (1990) Discrete Angle Radiative Transfer. Part I: scaling and similarity, universality and diffusion. *J. Geophys. Res.*, **95**, 11699–715.

Lovejoy, S. & Schertzer, D. (1991a) Multifractal analysis techniques and rain and cloud fields from 10^3 to 10^6m. *Scaling, fractals and non-linear variability in geophysics*, D. Schertzer & S. Lovejoy (eds.), pp. 111–44, Kluwer.

Lovejoy, S. & Schertzer, D. (1991b) Universal Multifractal temperature simulations. *EOS*, **72**, 1–2.

Lovejoy, S. & Schertzer, D. (1993) Scale invariance and multifractals in the atmosphere. *Encyclopedia of the Environment*, Pergamon, 527–32.

Mandelbrot, B & Van Ness, J. W. (1968) Fractional Brownian motions, fractional noises and applications. *SIAM Review*, **10**, 422–50.

Mandelbrot, B. & Wallis, J. R. (1968) Noah, Joseph and operational hydrology. *Wat. Resour. Res.*, **4**, 909–18.

Mandelbrot, B. & Wallis, J. R. (1969) Some long-run properties of geophysical records. *Wat. Resour. Res.*, **5**, 228.

Mandelbrot, B. (1974) Intermittent turbulence in self-similar cascades: divergence of high moments and dimension of the carrier. *J. Fluid Mech.*, **62**, 331–50.

Mandelbrot, B. (1983) *The Fractal Geometry of Nature*. Freeman, San Francisco, 318pp.

Mandelbrot, B. (1984) Fractals in physics: squig clusters, diffusions, fractal measures and the unicity of fractal dimensionality. *J. Stat. Phys.*, **34**, 895–930.

Mandelbrot, B. (1989) Fractal geometry: what is it and what does it do? *Fractals in the Natural Sciences*, M. Fleischman, D. J. Tildesley & R. C. Ball, pp. 3–16, Princeton University Press.

Marquet, O. & Piriou, J. P. (1987) *Modélisations et analyses multifractales de la pluie*. Thèse Ingenieur des travaux, Ecole Nationale de la Météorologie Nationale, Toulouse.

Marshall, J. S. & Palmer, W. M. (1948) The distribution of raindrops with size. *J. Meteor.*, **5**, 165–6.

Marshall, J. S. & Hitschfeld, W. (1953) Interpretation of fluctuating echoes from randomly distributed scatters, part I. *Can. J. Phys.*, **31**, 962–94.

Meneveau, C. & Sreenivasan, K. R. (1987) Simple multifractal cascade model for fully developed turbulence. *Phys. Rev. Lett.*, **59** (13), 1424–7.

Meneveau, C. & Sreenivasan, K. R. (1991) The multifractal nature of turbulent energy dissipation. *J. Fluid Mech.*, **224**, 429–84.

Montariol, F. & Giraud, R. (1986) *Dimensions et multidimensions des réseaux de mesure et des précipitations*. Thèse Ingenieur des travaux, Ecole Nationale de la Météorologie Nationale, Toulouse.

Novikov, E. A. & Stewart, R. (1964) Intermittency of turbulence and spectrum of fluctuations in energy-dissipation. *Izv. Akad. Nauk. SSSR. Ser. Geofiz.*, **3**, 408–12.

Obhukhov, A. (1962) Some specific features of atmospheric turbulence. *J. of Geophys. Res.*, **67**, 3011.

Olsson, J., Niemczynowicz, J., Berndtsson, B. & Larson, M. (1990) Fractal properties of rainfall time series. *Annales Geophys.* (special issue), p. 142.

Osborne, A. R. & Provenzale, A. (1989) Finite correlation dimension for stochastic systems with power-law spectra. *Physica* D, **35**, 357–81.

Paladin, G. & Vulpiani, A. (1987) *Phys. Rev. Lett.*, **156**, 147.

Parisi, G. & Frisch, U. (1985) A multifractal model of intermittency, *Turbulence and predictability in geophysical fluid dynamics and climate dynamics*, pp. 84–8, Ghil, Benzi & Parisi (eds.), North-Holland.

Paulhaus, J. L. H. (1965) *Mon. Wea. Rev.*, **93**, 331–5.

Pflug, K., Lovejoy, S. & Schertzer, D. (1991a) Generalized Scale Invariance, Differential Rotation and Cloud Texture. *Nonlinear Dynamics of Structures*, R. Z. Sagdeev, U. Frisch, F. Hussain, S. S. Moiseev & N. S. Erokhin (eds.), pp. 71–80, World Scientific.

Pflug, K., Lovejoy, S. & Schertzer, D. (1991b) Generalized Scale Invariance, Differential Rotation and Cloud Texture: analysis and simulation. *J. Atmos. Sci.* (in press).

Phan, T. D. & Miville, B. (1986) *Fractal dimension of rain drops distribution*. 3rd year honours lab report, 116pp, McGill physics dept.

Ratti, S. (1991) Universal multifractal analysis of multiparticle production in hadron-hadron collisions ar r(s) = 16.7GeV. *Proceedings of Hadron physics conf.*, China, Sept. 1991.

Ratti, S., Salvadori, G., Lovejoy, S. & Schertzer, D. (1991) Preprint FNT (in preparation).

Richardson, L. F. (1922) *Weather prediction by numerical process*. Republished by Dover, 1965.

Rémémeras, G. & Hubert, P. (1990) Article: *'Hydrologie' de l'Encyclopedia Universalis*, Paris, XI, pp. 796–806.

Rodriguez-Iturbe, I., Gupta, V. K. & Waymire, E. (1984) Scale considerations in the modelling of temporal rainfall. *Wat. Resour. Res.*, **20**, 1611–19.

Rodriguez-Iturbe, I., de Power, B. F. & Valdés, J. B. (1987) Rectangular pulses point process models for rainfall: analysis of empirical data. *J. Geophys. Res.*, **92**, 9645–56.

Rodriguez-Iturbe, I., de Power, B. F., Sharifi, M. B. & Georgakakos, K. P. (1989) Chaos in rainfall. *Wat. Resour. Res.*, **25**, 1667–75.

Rosso, R. & Burlando, P. (1990) Scale Invariance in temporal and spatial rainfall. *Annales Geophys.* (special issue), p.145.

Rhys, F. S. & Waldvogel, A. (1986) Fractal shape of hail clouds. *Phys. Rev. Lett.*, **56**, 784–7.

Schertzer, D. & Lovejoy, S. (1983a) The dimension of atmospheric motions, Preprints, *IUTAM Symp. on turbulence and chaotic phenomena in fluids*, pp. 141–4, Kyoto, Japan.

Schertzer, D. & Lovejoy, S. (1983b) Elliptical turbulence in the atmosphere. *Proceedings of the 4th symposium on turbulent shear flows*, 11.1–11.8, Karlsrhule, West Germany.

Schertzer, D. & Lovejoy, S. (1984) *Turbulence and chaotic phenomena in fluids*, T. Tatsumi (ed.), pp. 505–8, North-Holland.

Schertzer, D. & Lovejoy, S. (1985) The dimension and intermittency of atmospheric dynamics, *Turbulent Shear Flow*, **4**, 7–33, B. Launder (ed.), Springer.

Schertzer, D. & Lovejoy, S. (1985b) Generalised scale invariance in turbulent phenomena. *Physico-Chemical Hydrodynamics Journal*, **6**, 623–35.

Schertzer, D. & Lovejoy, S. (1986) Intermittency and singularities: generalised scale invariance in multiplicative cascade processes. *Abstract vol., Non-linear variability in Geophysics Workshop*, 14–15, McGill U., Montreal, Canada.

Schertzer, D. & Lovejoy, S. (1987a) Physically based rain and cloud modeling by anisotropic, multiplicative turbulent cascades. *J. Geophys. Res.*, **92**, 9692–714.

Schertzer, D. & Lovejoy, S. (1987b) Singularités anisotropes, et divergence de moments en cascades multiplicatifs. *Annales Math. du Que.*, **11**, 139–81.

Schertzer, D., Lovejoy, S., Visvanthan, R., Lavallée, D. & Wilson, J. (1988) Multifractal analysis techniques and rain and cloud fields. *Fractal Aspects of Materials: Disordered Systems*, D. A. Weitz, L. M. Sander & B. B. Mandelbrot (eds.), pp. 267–70, Materials Research Society, Pittsburg.

Schertzer, D. & Lovejoy, S. (1989a) Nonlinear variability in geophysics: multifractal analysis and simulations. *Fractals: Their physical origins and properties*, Pietronero (ed.), pp. 49–79, Plenum Press, New York.

Schertzer, D. & Lovejoy, S. (1989b) Generalized scale invariance and multiplicative processes in the atmosphere. *Pageoph*, **130**, 57–81.

Schertzer, D. & Lovejoy, S. (1992) Hard vs. soft multifractal processes, *Physica* A, **185**, 187–94.

Schertzer, D. & Lovejoy, S. (1991b) Nonlinear geodynamical variability: Multiple singularities, universality and observables. *Scaling, fractals and non-linear variability in geophysics*, D. Schertzer & S. Lovejoy (eds.), pp. 41–82, Kluwer.

Schertzer, D., Lovejoy, S., Lavallée, D. & Schmitt, F. (1991) Universal hard multifractal turbulence, theory and observations. Nonlinear Dynamics of Structures. R. Z. Sagdeev, U. Frisch, F. Hussain, S. S. Moiseev, N. S. Erokhin (eds.), pp. 213–35, World Scientific.

Schertzer, D., Lovejoy, S. & Lavallée, D. (1993) Generic multifractal phase transitions and self-organized criticality. In: *Cellular Automata: Prospects in Astrophysical Applications*, Pendang, J. M. & Lejeune, A. (eds.), World Scientific, 216–27.

Schertzer, D., Lovejoy, S., Schmitt, F. & Lavallée, D. (1991c) Multifractal analysis and simulations of nonlinear geophysical signals and images. *Proceedings, 13th GRETSI Colloqium*, Juan-Les-Pins, 16–20 Sept. 1991, pp. 1313–25.

Schertzer, D. & Lovejoy, S. (1994) Multifractal generation of self-organized criticality. In: *Fractals in the Natural and Applied Sciences*. Novak, M. M. (ed.), Elsevier, 325–39.

Schmitt, F., Lavallée, D., Schertzer, D. & Lovejoy, S. (1992) Empirical determination of universal multifractal exponents in turbulent velocity fields. *Phys. Rev. Lett.*, **68**, 305–8.

Seed, A. (1989) *Statistical problems in measuring convective rainfall*. PhD. Thesis, McGill University, 141pp.

Segal, B (1979) High-Intensity rainfall statistics for Canada. *Comm. Res. Centre, Dept. of Communications, Canada, report CRC 1329-E*, Ottawa, Canada.

Sèze, G. & Smith, L. (1990) On the dimension of a cloud's boundary. Preprint vol., *7th conf. on Atmos. Rad.*, AMS, Boston, pp. 47–57.

Taylor, G. I. (1938) The spectrum of turbulence. *Proc. R. Soc. Lond.* A, **164**, 476–90.

Tessier, Y. (1993) Multifractal objective analysis: rain and clouds, Ph.D. thesis, McGill University, 143pp.

Tessier, Y., Lovejoy, S. & Schertzer, D. (1993) Universal multifractals in rain and clouds: theory and observations. *J. Appl. Meteor.*, **32**, 223–50.

Tessier, Y., Lovejoy, S. & Schertzer, D. (1994) The multifractal global rain gauge network: analysis and simulation. *J. Appl. Meteor.*, **33**, 1572–86.

Tsonis, A. A. & Elsner, J. B. (1989) Chaos, Strange Attractors and Weather. *Bull. Amer. Meteor. Soc.*, **70**, 14–23.

Tsonis, A. A., Elsner, J. B., Lovejoy, S. & Schertzer, D. (1990) The space/time fractal structure of rain and Taylor's hypothesis. *EOS*, 466.

Visvanathan, R., Weber, C. & Gibart, P. (1991) The stochastic coherence and the dynamics of global climate models and data. *Scaling,*

fractals and non-linear variability in geophysics, D. Schertzer & S. Lovejoy (eds.), pp. 269–78, Kluwer.

Wallace, P. R. (1953) Interpretation of fluctuating echoes from randomly distributed scatters, part II. *Can. J. Phys.*, **31**, 995–1009.

Warner, C. & Austin, G. L. (1978) Statistics of radar echoes on day 261 of GATE. *Mon. Wea. Rev.*, **106**, 983–94.

Waymire, E. (1985) Scaling limits and self-similarity in precipitation fields. *Wat. Resour. Res.*, **21**, 1271–81.

Weisnagel, J. & Powell, A. (1987) *Lidar detection of rain drops*. 3rd year honor project report, 47pp, McGill Physics Dept.

Welch, R. M., Kuo, K. S., Wielicki, B. A., Sengupta, S. K. & Parker, L. (1988) Marine stratocumulus cloud fields off the coast of Southern California observed by LANDSAT imagery, part I: Structural characteristics. *J. Appl. Meteor.*, **27**, 341–62.

Wilson, J. (1991) *Physically based stochastic modelling of rain and cloudfields*. MSc. thesis, McGill University, 97pp.

Wilson, J., Lovejoy, S. & Schertzer, D. (1986) An intermittent wave packet model of rain and clouds. *2nd conf. on satellite meteor. and remote sensing*, AMS Boston, pp. 233–6.

Wilson, J., Lovejoy, S. & Schertzer, D. (1991) Physically based cloud modelling by scaling multiplicative cascade processes. *Scaling, fractals and non-linear variability in geophysics*, D. Schertzer & S. Lovejoy (eds.), pp. 185–208, Kluwer.

Yaglom, A. M. (1966) The influence of the fluctuation in energy dissipation on the shape of turbulent characteristics in the inertial interval. *Sov. Phys. Dokl.*, **2**, 26–30.

Yano, J.-I. & Takeuchi, Y. (1988) Fractal dimension analysis of horizontal cloud pattern in the intertropical convergence zone. *Scaling, fractals and non-linear variability in geophysics*, D. Schertzer & S. Lovejoy (eds.), pp. 297–302, Kluwer.

Zawadzki, I (1973) Statistical properties of precipitation patterns. *J. Appl. Meteor.*, **12**, 459–72.

Zawadzki, I (1987) Fractal versus correlation structure in rain. *J. Geophys. Res.*, **92**, 9683–93.